The Role of Scleraxis in Inducing Vascular Stiffness

A Thesis Submitted to the Faculty of Graduate Studies of
The University of Manitoba

In Partial Fulfillment of the Requirements of the Degree of

Doctor of Philosophy

By

Danah Sufian Al Hattab

Department of Physiology and Pathophysiology,
Max Rady College of Medicine,
Rady Faculty of Health Sciences,
University of Manitoba,
Winnipeg,
Canada.

ACKNOWLEDGEMENTS

The completion of this thesis would have never been possible without the support and encouragement of all the people surrounding me. Firstly, I would like to express my sincere gratitude to my supervisor Dr. Michael Czubryt for being a phenomenal mentor to me throughout my MSc. and my Ph.D. studies, for the continuous support, patience, motivation, and immense knowledge. His guidance has been fundamental for my success in science as well as my growth as an individual. I could not have imagined having a better advisor and mentor.

I would like to extend my sincere appreciation to my thesis committee: Dr. Jeff Wigle, Dr. Grant Pierce, and Dr. Elissavet Kardami, for their insightful comments, encouragement, and constructive feedback. Their expertise and support were instrumental in shaping the direction and quality of this work.

From the bottom of my heart, I would like to say a big thank you to my current and past lab mates for their energy, understanding, and help throughout my project, Teri Moffatt, Allison Ledingham, Dr. Kim O'Hara, Dr. Nina Aroutiounova, Dr. Raghu Nagalingam, Sikta Chattopadhyaya, and Khoung Le without your help and wise guidance this project would have not been the same!

Also, I want to extend my sincere gratitude to all the ICS members and Department of Physiology and Pathophysiology members who have helped me and supported me during this program, especially Ejlal Abu-Al Rub and Karen Swanson for the great friendship and our extended lovely chats.

My sincere thanks also go to Dr. Hope Anderson who gave me access to her lab and use the pressure myography equipment. Dr. Crystal Acosta and Dr. Danielle Lee for training me to use the pressure myograph, technical guidance, and problem-solving ideas. Without their precious support, it would not be possible to conduct this research.

I want to recognize all the R.O. Burrell lab members, especially Sheri Bage and Rob Mazur for their amazing efforts in maintaining my animal studies and working with me on such a challenging study.

I am deeply grateful to St. Boniface Hospital Research Foundation, Institute of Cardiovascular Sciences, University of Manitoba, Heart and Stroke Research Foundation of Canada, and Bank of Montreal Fellowship, for their generous funding, scholarships, and fellowships during my program.

Last but not the least, I would like to thank my family: my parents Sufian and Nadwa, and my siblings Ehab, Eyad, Lina, and Dina for their continuous prayers and for believing in me. I also want to thank my brothers-in-law who have been generous with their love and encouragement. Finally, I am grateful to my lovely family; Sami for being an amazing friend and a great companion, for my kids Sama, Hala, and Sanad, for the love, support, entertainment, and help to get me through many stressful times in the most positive way.

DEDICATION

I dedicate this thesis to,

My dear husband

Sami Abu Nawwas

For his unconditional love, support, and patience

and to our lovely kids,

Sama, Hala, and Sanad

Thank you for making the journey of this life fun and exciting every day!

TABLE OF CONTENTS

LIST OF TABLES

LIST OF ABBREVIATIONS

Abbreviations	Definitions
ACE	Angiotensin Converting Enzyme
AFM	Atomic Force Microscopy
AGT	Angiotensinogen
AHA	American Heart Association
ANOVA	Analysis of Variance
ApoE-	Apolipoprotein E deficient mouse
AT1 receptor	Angiotensin type 1 receptor
ATP	Adenosine Triphosphate
bHLH	basic helix-loop-helix

BP	Blood Pressure
CCK8	Cell Counting Kit-8
CO	Corn Oil gavage
CSA	Cross Sectional Area
DAPI	4',6-Diamidino-2-Phenylindole
DNA	Deoxyribonucleic acid
DOCA	Deoxycorticosterone acetate
ECM	Extracellular Matrix
EDTA	Ethylenediaminetetraacetic acid
EGF	Epidermal growth factor
EGTA	Ethylene Glycol-Bis (β-aminoethyl ether)-N,N,N′,N′-Tetra acetic acid
EM	Elastic Modulus
EMT	Epithelial to Mesenchymal Transition
eNOS	Endothelial Nitric Oxide Synthase
ERK1/2	Extracellular signal-regulated kinase 1/2
ESH	European Society of Hypertension
FGF	Fibroblast Growth Factor
GAPDH	Glyceraldehyde 3-phosphate dehydrogenase
GFP	Green Fluorescent Protein
cGMP	Cyclic guanosine monophosphate
GTP	Guanosine triphosphate
HAOSMC	Human Aortic Smooth Muscle Cell
HCM	Hypertrophic cardiomyopathy
I-MEMA	Interlamellar Mucoid Extracellular Matrix Accumulation
IMT	Intima–Media Thickness
IP	Intraluminal Pressure
JNK	c-Jun N-terminal kinase
LDLR	Low Density Lipoprotein Receptor
MAP	Mean Arterial Pressure
MAPK	Mitogen-Activated Protein Kinase
MLCK	Myosin Light Chain Kinase
MMP	Matrix metalloproteinases
MOI	Multiplicity of Infection
MRBP	Mouse and Rat Tail Cuff Blood Pressure
MT	Masson’s Trichrome
MW	Media Width
MYH	Myosin Heavy Chain 11
NSAID	Non-Steroidal Anti-Inflammatory Drug
PBS	Phosphate-Buffered Saline
PCNA	Proliferating Cell Nuclear Antigen
PDGF	Platelet-Derived Growth Factor

PI3K	Phosphatidylinositol 3-kinase
PKG	Protein Kinase G
PR	Picrosirius Red
PVDF	Polyvinylidene difluoride
PWV	Pulse Wave Velocity
qPCR	Quantitative Polymerase Chain Reaction
RAAS	Renin-Angiotensin-Aldosterone System
RAS	Renin-Angiotensin System
RNA	Ribonucleic Acid
ScxKO	Scleraxis Knock-Out
Scx^{TG}	Transgenic Scleraxis
Scx^{WT}	Wild Type Scleraxis
SD	Standard Deviation
SDS-PAGE	Sodium Dodecyl Sulfate-Polyacrylamide Gel Electrophoresis
SHR	Spontaneous Hypertensive Rat
SMA	Smooth Muscle Actin
SMC	Smooth Muscle Cell
SMMHC	Smooth Muscle Myosin Heavy Chain
SNP	Sodium Nitroprusside
TAC	Transverse Aortic Constriction
TAM	Tamoxifen
TBST	Tris-buffered saline with 0.1% Tween® 20 detergent
TCF21	Transcription factor 21
TGFβ1	Transforming Growth Factor β 1
TPR	Total Peripheral Resistance
VSMC	Vascular Smooth Muscle Cell
VVG	Verhoeff-Van Gieson
WB	Western Blot
WT^{CO}	Wild Type Mice with Corn Oil Gavage
WT^{TAM}	Wild Type Mice with Tamoxifen Gavage
αSMA	Alpha Smooth Muscle Actin

TABLE OF FIGURES

ABSTRACT

Arterial stiffness occurs when structural changes in the arterial wall, such as increased extracellular matrix (ECM) proteins or vascular smooth muscle cells (VSMCs), or cellular dysfunction disrupt the arteries' ability to adapt to changes in blood pressure or flow. This condition is linked to cardiovascular diseases and increased risks of adverse outcomes. Angiotensin II (AngII) contributes to arterial stiffness by constricting blood vessels, promoting VSMC proliferation, and enhancing ECM protein production. Scleraxis transcription factor contributes to cardiac fibrosis by upregulating ECM genes and activating fibroblasts to myofibroblasts. Scleraxis expression is upregulated in the high-pressure side of the aorta wall in the transverse aortic constriction (TAC) mouse model.

In this project, we hypothesized that overexpression of scleraxis in fibroblasts or VSMCs using TCF21iCre or Myh11Cre approaches, respectively, would increase vascular stiffness in mesenteric arteries and aortas. We assessed mesenteric artery stiffness and function using pressure myography and performed immunohistology staining and gene expression analysis on harvested aortas. *In vitro*, we increased scleraxis expression in human aortic smooth muscle cells (HAOSMCs) and assessed proliferation capacity.

Our findings showed that scleraxis upregulation in VSMCs decreased compliance in mesenteric arteries without altering the structure or function in these arteries. Scleraxis upregulation in HAOSMCs induced cell proliferation and a switch from a synthetic phenotype toward the proliferative phenotype.

Mice with both scleraxis upregulation and AngII infusion exhibited stiffer mesenteric arteries. This was accompanied by a decrease in vascular lumen diameter, an increase in smooth

muscle cell (SMC) contractility and impaired relaxation. Unexpectedly, the combination of scleraxis with AngII reduced ECM expression, suggesting arterial remodelling was occurring. HAOSMCs treated with AngII and scleraxis demonstrated a decrease in proliferation, and an increased expression of contractile genes, indicating a contractile VSMC phenotype.

In summary, our findings suggest that upregulation of scleraxis expression in VSMCs alone induces vascular stiffness by promoting SMC proliferation. However, when combined with AngII, vascular stiffness is exacerbated by inducing a ' contractile' phenotype in SMCs. These findings highlight the complex and context-dependent role of scleraxis in vascular stiffness, emphasizing the importance of considering specific pathological conditions and factors when studying its effects on vascular function.

CHAPTER 1: INTRODUCTION

Considering scleraxis' established role in upregulating extracellular matrix (ECM) proteins within the cardiac tissue, consequently inducing cardiac fibrosis, our study aims to investigate the potential involvement of scleraxis in vascular physiology and pathology.

A. Background & Literature Review

Vascular diseases are a group of medical conditions that arise from the dysfunction of blood vessels in the body. Some of the most common diseases related to vascular dysfunction include atherosclerosis, hypertension, and aneurysms. To understand these diseases, it is essential to have a basic understanding of the normal structure and function of blood vessels. Arteries are one of the main components in the circulatory system that are responsible for delivering oxygen and nutrients to organs and tissues. Therefore, when arteries become damaged or diseased, they can no longer perform their function properly, leading to multiple cardiovascular problems. It is important to understand the normal structure and function of arteries, and how the dysfunction of arteries can lead to vascular diseases, in order to develop novel approaches to target these diseases and manage their progression.

1. Arterial System

Systemic arteries play a key role in nourishing organs throughout the body. They are hollow tubes that extend away from the heart carrying oxygenated blood and nutrients to distribute to different tissues while pulmonary arteries carry deoxygenated blood to the lungs for oxygenation. Arteries can accommodate large changes in blood pressure resulting from the pumping action of the heart due to their unique structure and characteristics.

1.1 Anatomy

Anatomically, arteries can be easily distinguished from veins as they have a thicker layer of VSMCs. Veins have thinner walls compared to arteries, contain valves that help prevent the backflow of blood, and have highly elastic walls to facilitate large changes in capacity. Veins play an important role in returning blood to the heart and maintaining cardiac output.

Arteries are composed of 3 layers (Fig. 1), [1]:

-Tunica intima: composed of a single layer of endothelial cells lining the inner surface of arteries.

-Tunica Media: the major layer in arteries composed of a circular arrangement of vascular smooth muscle cells along with elastic fibers which regulate the internal diameter of the vessel. This layer is more prominent in arteries than in veins.

-Tunica Adventitia: the outer layer of the arteries composed of ECM proteins that shape the vessel and provide structural support. Fibroblasts are found in this layer.

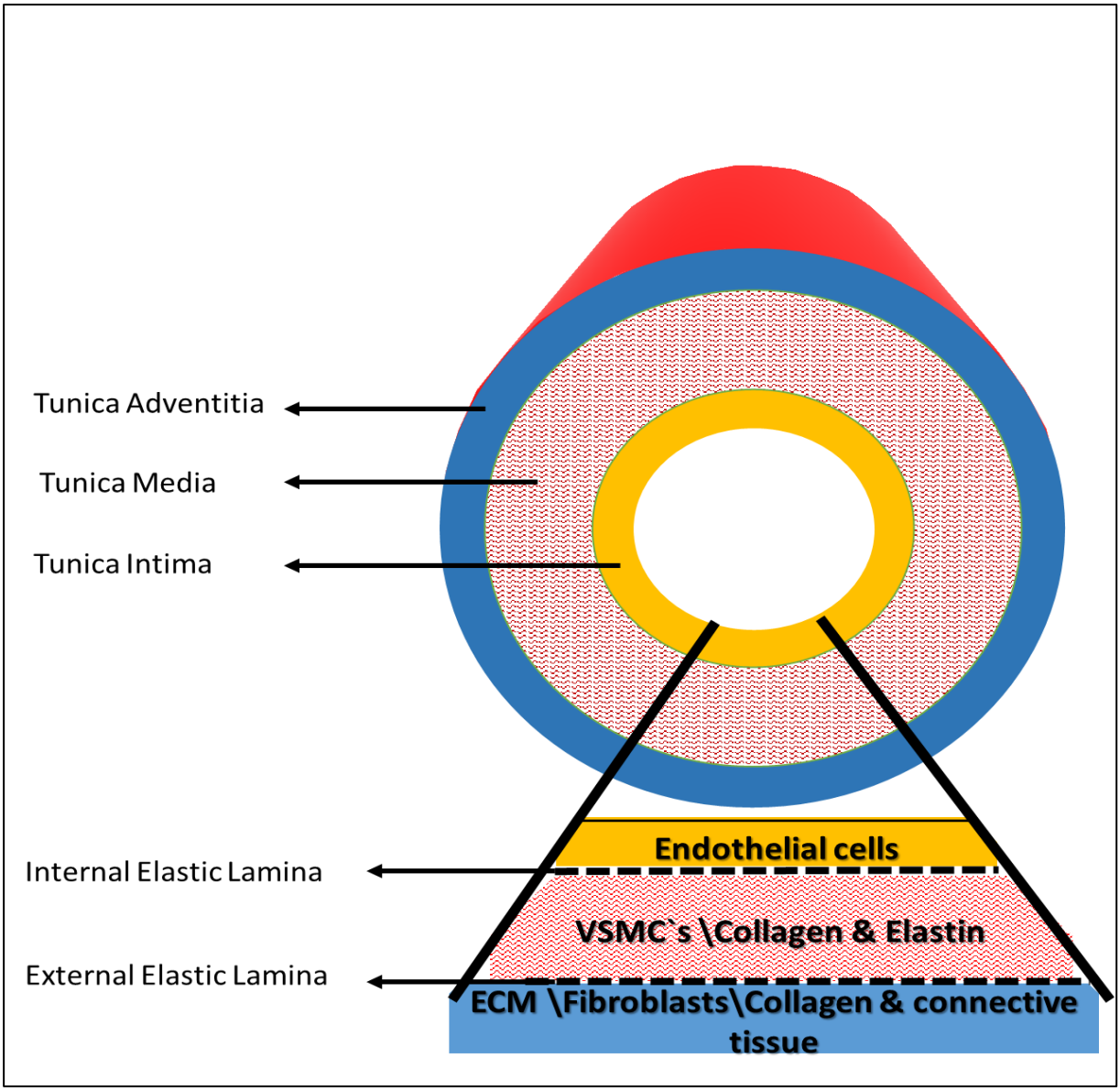

Figure 1. Arterial anatomy.

The arterial structure anatomy diagram illustrates the different layers of the artery. The innermost layer is the tunica intima which includes endothelial cells; the middle layer is the tunica media which includes VSMCs, collagens and elastin; and the outermost layer is the tunica adventitia which includes ECM proteins such as collagen, fibroblasts, and other connective tissue components.

1.2 Types of Arteries

The amount of muscular tissue, collagen and elastin fibers varies within each arterial layer depending on the size and location of the artery within the body. For example, larger arteries, such as the aorta, classified as conductance arteries, have a thicker tunica media with more elastic fibers. Conversely, smaller arteries and arterioles, known as resistance arteries, possess relatively thicker tunica adventitia layers with more collagen fibers.

The structure and composition of the artery walls can differ between different species of animals. For example, the aortas of larger animals such as horses and pigs have more elastin fibers than those of smaller animals, which helps them withstand the increased blood pressure produced by their larger hearts [2].

Arteries are classified into 3 types based on their composition:

1) Elastic arteries are the largest arteries in terms of diameter. The diameter of the human aorta can vary depending on the individual and their age, but typically ranges from 2-3 cm. The diameter of the mouse aorta is much smaller, typically ranging from 0.5-1.5 mm [3, 4]. Elastic arteries include the aorta and pulmonary arteries. Each of these vessels receives blood directly from the heart, so the elastic tissue is abundant in the tunica media to accommodate the high pressures that result from each heartbeat and to maintain a relatively constant pressure gradient while blood is pushed through the arterial tree.

2) Muscular arteries move blood from the elastic arteries through the body. Muscular arteries range from 0.3-1.0 cm in diameter in humans, and from 10-300 μm in diameter in mice [5, 6]. Muscular arteries contain more smooth muscle cells in the tunica media layer than the elastic

arteries so they can actively expand and contract to regulate changes in blood volume and flow. The femoral and coronary arteries are examples of muscular arteries.

3) Arterioles, also called small resistance arteries, are the smallest type of arteries. They are 10-300 μm in diameter in humans and 10-50 μm in mice [7], and play a key role in regulating blood flow into the capillaries (see below).

All classes of arteries are comprised of the three vascular layers (tunica intima, media, and adventitia). However, the smallest arterioles that lead to capillaries have only a single vascular smooth muscle layer surrounding the endothelial layer [1, 8].

1.3 Resistance Arteries and Total Peripheral Resistance

Mean arterial pressure (MAP) is defined as the average pressure in the arteries during one cardiac cycle, including both systole and diastole. As the blood flows from the arteries to the veins, MAP decreases, with the steepest drop in pressure taking place between arteries and arterioles, from approximately ~100 mmHg to ~40 mmHg (Fig. 2). Small resistance arteries exhibit high resistance due to their small diameter, which causes a dramatic drop in MAP [9]. Therefore, arterioles are the major contributors to total peripheral resistance (TPR) in the arterial tree. Changes in cardiac output and TPR can alter MAP.

TPR is identified as the amount of resistance exerted on the blood by the arterial walls to push the blood through the entire systemic circulatory system and generate blood pressure (BP) [10].TPR is an important factor that determines blood pressure and cardiac output, based on the equation:

$$\mathrm{TPR} = \frac{\mathrm{MAP}}{\mathrm{Cardiac\ output}}$$

Because TPR is inversely proportional to cardiac output, high TPR can increase the workload on the heart, leading to hypertension and other cardiovascular diseases. Conversely, low TPR can cause inadequate blood flow to the tissues, leading to hypotension and poor perfusion. The hallmark of high blood pressure is increased peripheral resistance in resistance arteries. Thus, increased peripheral resistance plays an important role in the pathogenesis of hypertension.

Another important concept to understand is Poiseuille's equation or law, which is a mathematical formula that describes the relationship between blood pressure, flow rate, and resistance of the blood in an artery as a single tube. Poiseuille's equation describes the factors that affect blood flow through the arteries, including the viscosity of blood, vessel radius, and vessel length. Poiseuille's law helps to explain how the diameter of the blood vessels and the viscosity of the blood affect blood flow and resistance. Since blood flow is proportional to the fourth power of the vessel radius, even a small increase in lumen diameter through vasodilation can result in a significant increase in blood flow.

$$F = \frac{\Delta P \pi r^4}{8 \eta l}$$

- Flow rate (F), pressure difference between two ends (ΔP), internal lumen radius (r), blood viscosity (η), length of artery (l).

Overall, Poiseuille's equation highlights the importance of vessel radius in determining blood flow.

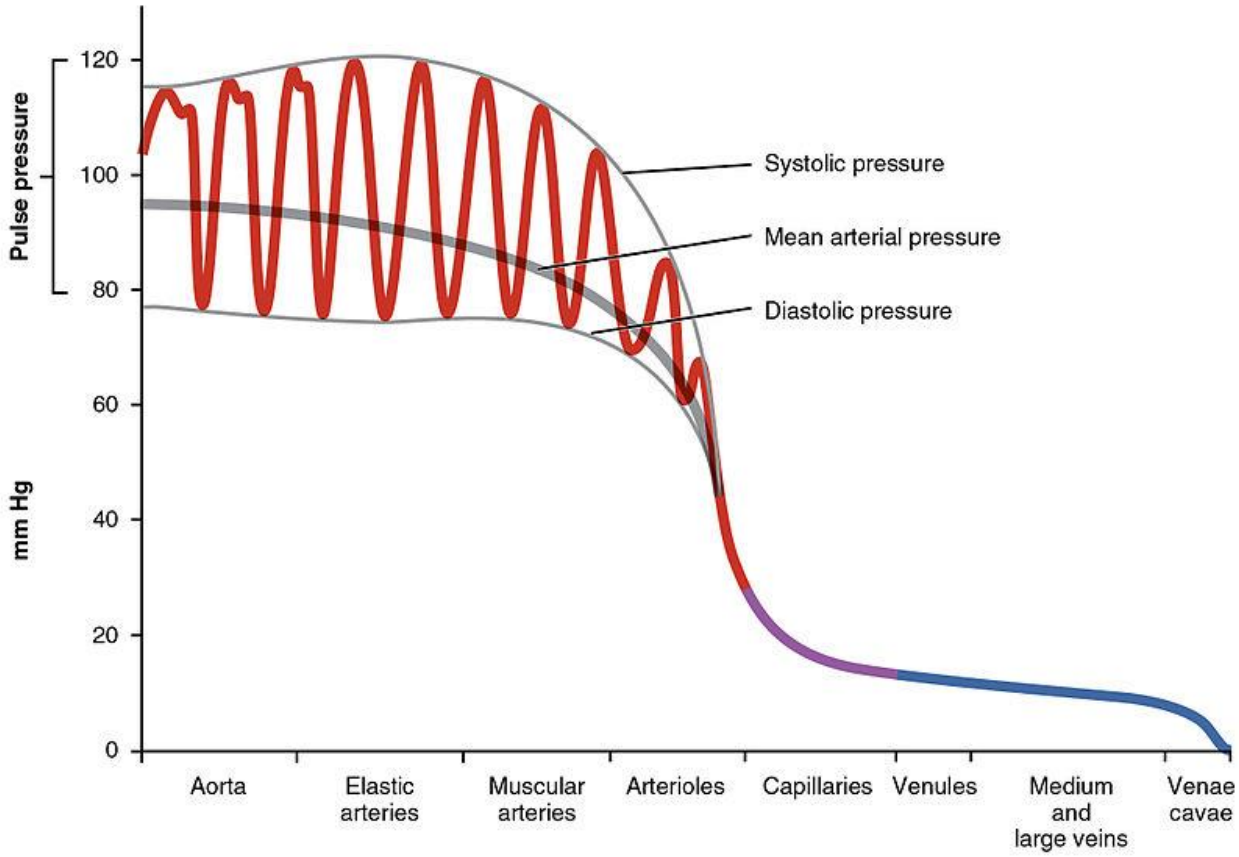

Figure 2. Schematic of systolic and diastolic blood pressure changes in different blood vessels within the circulatory system.

The arterial tree shows the greatest drop in pressure in arterioles to the range of 40-50 mmHg.

Adopted from 2109 Systemic Blood Pressure by OpenStax College, is available under CC BY 3.0 Unported from Wikimedia. Anatomy & Physiology, Connexions Website.

http://cnx.org/content/col11496/1.6/, Jun 19, 2013.

1.4 Elastic and Resistance Arteries at the Molecular Level

As mentioned above, elastic arteries such as the aorta accommodate the high stress generated from the heart pumping by buffering the heart's pulsatile flow to a nearly steady flow in peripheral vessels via a unique phenomenon called the “Windkessel effect.” The Windkessel effect refers to the expansion of the aorta's conduit section when it receives a significant bolus of blood during systole. This expansion is then followed by an elastic recoil which pushes the blood through the arterial tree during diastole. Thus, the aortic elasticity serves in effect as a secondary pump that pushes blood forward, decreasing the load on the heart, reducing the systolic flow, and increasing diastolic flow in the resistance arteries [11, 12].

In contrast, if the aortic wall becomes stiff and loses its elasticity, it can lead to pathological consequences. When the aorta is less distensible, it becomes less capable of accommodating the increased blood volume that occurs during systolic contraction, which can lead to higher blood pressure and altered cardiac muscle function. Additionally, when the aortic wall is stiff, the pulsatile pressure wave generated by the heart's contractions can be transmitted with greater intensity into the peripheral arteries, including the smaller arteries and arterioles, which are less able to tolerate these large pressure fluctuations. This increased pressure transmission can lead to endothelial dysfunction, inflammation, oxidative stress, and other changes that increase the risk of atherosclerosis and other cardiovascular diseases [13].

Overall, any modifications in aortic elasticity or increased stiffness that impair aortic distention can have significant pathological consequences that alter cardiac muscle function, blood pressure, and increase the risk of cardiovascular diseases and atherosclerosis [14]. This unique property of the aorta depends on its geometry as described above and the proportion of its structural micro-components.

The aortic media is the thickest among all arteries, and is composed of VSMCs, elastin, collagen, and a non-fibrous matrix. Early studies showed that the static mechanical properties of the media are attributed mainly to its elastin and collagen components, as these mechanical properties were not altered after eliminating smooth muscle function by treating aortic segments with potassium thiocyanate [15]. Subsequent research has examined the physical interaction between the elastic lamina and VSMCs in the developing aorta of mice [16]. This study showed that this interaction helps VSMCs to maintain a well-organized cytoskeletal structure in the medial layer of the aortic wall, in turn allowing VSMCs to respond to mechanical strain. The elastic lamellar units in the aortic wall are responsible for this synchronization, as they contain alternating elastic fibers and VSMCs that form "contractile elastic" units. This unique arrangement of the lamellar units enables the aortic wall to effectively transmit the mechanical force generated during blood pumping, thus pushing blood forward.

On the other hand, in the media of resistance arteries, VSMCs are the key players in regulating the vasomotor function of arterioles, and in contrast to elastic arteries, elastin contribution is relatively low at lower intraluminal pressures when compared to distensible collagen at higher pressures [11, 17]. Other findings have indicated that focal adhesion sites between VSMCs and these fibers represent critical interaction sites in transmitting micromechanical forces in response to externally applied forces [18]. Additionally, recent studies have demonstrated complex interactions between the collagen and elastin networks within each layer in response to changes in luminal pressure [19, 20]. These studies demonstrated that the arrangement of ECM proteins within the walls of resistance arteries, particularly at the microvascular level, affects the transmission of mechanical forces throughout the arterial wall.

1.5 Arterial Cell Physiology and Function

1.5.1 Endothelial Cells

Endothelial cells play an important role in regulating vascular tone in the tunica intima because they generate vasoactive molecules that may regulate VSMC tone and growth. For instance, endothelial cells can secrete either vasorelaxant agents such as nitric oxide (NO), bradykinin, and prostacyclin or vasoconstrictor agents such as endothelin -1. The secretion of vasoconstrictive or vasorelaxant agents results in significant changes in blood flow and peripheral resistance. In vessel injury, endothelial cells provide a surface for the adhesion of platelets and leukocytes and produce substances involved in blood coagulation such as von Willebrand factor, plasminogen activators, and plasminogen activator inhibitor type 1 [21]. Therefore, any abnormality in the functioning of endothelial cells, such as a loss of NO synthesis, can disrupt the normal functions of the vascular system, leading to various cardiovascular diseases including atherosclerosis, hypertension, and thrombosis [22].

Acetylcholine (Ach) is a well-known inducer of vasorelaxation. An important finding by Furchgott and Zawadzki showed that Ach can only induce arterial smooth muscle relaxation when the vascular endothelial layer is intact [23]. Subsequent studies demonstrated that Ach directly interacts with the muscarinic receptors on the endothelial cells, stimulating the production and release of NO that diffuses into the tunica media and causes vascular smooth muscle relaxation [24].

1.5.2 Vascular Smooth Muscle Cells (VSMCs)

VSMCs are the primary components of the arterial media layer and play a crucial role in maintaining the integrity of the arterial wall. VSMCs are characterized by their unique fusiform shape, which features a large central nucleus surrounded by a substantial endoplasmic reticulum and

Golgi apparatus. At their ends, they narrow to allow an end-to-end mechanical junction coupling with the surrounding smooth muscle cells. The plasma membrane of VSMCs contains numerous invaginations called caveolae, which increase the surface area for both mechanical tight junctions and electrical coupling via gap junctions. These caveolae are involved in clustering the ion channels and receptors for cellular signal transduction [25] .

The contraction of VSMCs is attributed to the presence of contractile actomyosin filaments within each cell, coupled with Ca^{2+} influx. VSMC contraction is regulated by phosphorylation of the myosin light chain by Ca^{2+}-calmodulin-dependent myosin light chain kinase (MLCK). The MLCK enzyme is activated by the binding of Ca^{2+} to a protein called calmodulin (CaM), activated MLCK facilitates actin-myosin interaction and cross-bridge cycling, resulting in the shortening of the smooth muscle cell and contraction [25].

VSMCs play a crucial role in regulating vascular activity and myogenic tone. Vascular tone is the partial contraction of VSMCs that facilitates rapid increases or decreases in vessel diameter. Specifically, the tone in resistance arteries maintains a resting level of contraction, reducing the internal diameter to 50-80% of its maximum passive diameter and allowing these vessels to dilate or contract, thereby altering vascular resistance and blood flow [26]. Myogenic tone is defined as the ability of the VSMC layer in arteries to contract in response to stretch in the vessel or an increase in the transmural pressure. Myogenic VSMC contraction is distinct from other triggers, such as neural, metabolic, and hormonal factors, and is critical for regulating blood flow and maintaining vascular resistance [26].

The phenotypic plasticity of VSMCs plays a vital role in vascular homeostasis (Fig. 3). VSMC plasticity is defined as the changes in VSMC characteristics, including morphology, function, structure, and molecular gene expression, in response to changes in the surrounding

environment and functional requirements. This is referred to as "phenotype switching" or "phenotype transition" [27]. Phenotype switching is commonly associated with the transition from the 'contractile' to the 'synthetic' phenotype. In normal physiological conditions, VSMCs are quiescent, non-proliferative, and are in a contractile phenotype. This phenotype is characterized by the expression of genes that encode proteins involved in maintaining myofilament structure and function, including calponin, transgelin (SM22α), α-smooth muscle actin (αSMA) and SM-myosin heavy chain (SMMHC) [28].

Each of these contractile genes plays an important role in the mechanical function of the VSMC. For example, calponin regulates smooth muscle cell contraction by modulating actin-myosin interaction. calponin is a Ca^{2+} binding protein that binds intracellularly to actin filaments, inhibiting actomyosin ATPase and actin filament motility. Therefore, when calponin is phosphorylated, the affinity of calponin binding to actin is reduced, which reduces its ability to inhibit actomyosin ATPase and stimulate myosin-actin interaction, leading to the contractile phenotype [29]. Similarly, SM22α is an actin binding protein that belongs to the calponin family and modulates VSMC contraction. However, studies suggest that VSMC contraction induced by SM22α is independent of the $Ca^{2+/}$MLCK phosphorylation pathway [30].

SMMHC is one of the main contractile proteins that stimulates VSMC contraction through hydrolysis of ATP to generate mechanical force and muscle contraction. SMMHC is the most definitive marker of smooth muscle cells during embryogenesis [31]. Additionally, αSMA is a cytoskeletal contractile protein that forms actin microfilaments and is present in all smooth muscle cells, interacting with myosin proteins to induce cell contraction [32].

In contrast, under pathological conditions, VSMCs undergo phenotypic modulation as they switch from the contractile phenotype to the synthetic phenotype. The synthetic phenotype is

characterized by a loss of contractile filaments and associated molecules, and increased cellular proliferation and growth [26]. For example, vascular remodeling in atherosclerosis is associated with pathological intimal thickening occurring as a result of VSMCs switching to the synthetic phenotype and hyperplasia [33]. Although the transition from a contractile to a synthetic phenotype is a common scenario in some diseases or injuries, it is not always the case in some chronic severe pathological conditions where VSMCs modulate to adapt to the exaggerated stresses. For example, in a study involving stroke-prone Spontaneously Hypertensive Rats (SHR), it was found that VSMCs in aortas and coronary arteries maintained a contractile phenotype that reduced the damaging consequences resulting from severe hypertension [34]. Subsequent studies suggested that the increase of VSMC stiffness in the aorta of SHR was associated with the expression of contractile genes. Moreover, when inhibitors for the contractile markers were used, the measured stiffness of VSMCs was reduced [35].

Sodium nitroprusside (SNP) is a pharmaceutical agent used as a fast-acting vasodilator antihypertensive drug. SNP is composed of a ferrous iron complexed with NO and five cyanide ions. When SNP reacts with sulfhydryl groups on cell surfaces, NO is produced, which then diffuses across the endothelial cells and binds to guanylate cyclase (GC) in VSMCs. This binding stimulates the conversion of guanosine triphosphate (GTP) to cyclic guanosine monophosphate (cGMP), which activates protein kinase G (PKG) and leads to the relaxation of VSMCs, vasodilation of arteries, and a decrease in blood pressure [36-38].

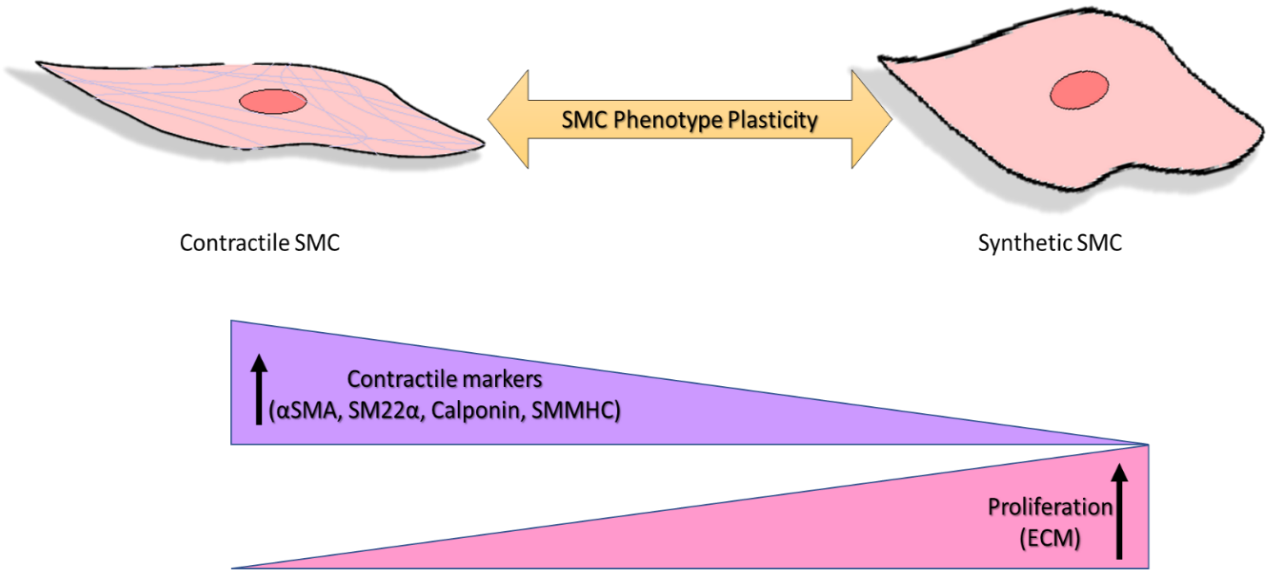

Figure 3. Physiological vascular smooth muscle cell plasticity.

This schematic shows VSMCs which normally exhibit a quiescent, non-migratory contractile phenotype (left). The contractile phenotype is characterized by an elongated spindle-shaped morphology and elevated expression of contractile markers including alpha smooth muscle actin (αSMA), smooth muscle protein 22 alpha or transgelin (SM22α), calponin and smooth muscle myosin heavy chain (SMMHC). Following vascular injury, VSMCs are induced to differentiate into a proliferative, migratory synthetic phenotype (right), which is characterized by reduced expression of contractile markers and increased expression of ECM proteins. This phenotypic transition is associated with a change in cell morphology from an elongated spindle shape to a more cobblestone-like morphology.

1.5.3 Vasa Vasorum Physiology in Large Arteries

The vasa vasorum constitutes a network of microvasculature that delivers nutrition and oxygenation to the adventitia and outer layer of the medial layers of large arteries and veins, thereby supporting their structure and function [39, 40]. Vasa vasorum comprises of various small blood vessels, including arterioles, capillaries, and venules. Studies indicate that the blood flow within the vasa vasorum can be modulated by neural regulation, involving both sympathetic stimulation-induced contraction and baroreceptor-controlled relaxation in dogs [41]. Furthermore, research suggests that the release of vasoactive substances such as nitric oxide and endothelin in dogs can alter blood flow regulation within the vasa vasorum [42]. Dysfunction of vasa vasorum has been associated with the development of multiple cardiovascular diseases, including atherosclerosis, aortic dissection, hypertension, and deep vein thrombosis [43].

The established concept in atherosclerosis suggests that endothelial dysfunction marks the initial stage of the disease progression. However, some evidence indicates that the dysfunction of vasa vasorum within the adventitia of major arteries may also play a pivotal role in the development of this condition. A study suggests that artificially obstructing blood flow in the vasa vasorum of canine abdominal aorta can lead to the initiating of intimal thickening and smooth muscle proliferation, followed by lipid deposition and hypertrophy of the neointima [44].

Further investigations have revealed an increase in microvessel density derived from adventitial vasa vasorum in atherosclerotic coronary arteries, suggesting a role for neovascularization surrounding plaques in the pathogenesis of atherosclerosis [45]. In atherosclerosis, it is proposed that hypoxia in the adventitial wall and decreased oxygenation may trigger neovascularization of the vasa vasorum. These microvessels then penetrate the media and intima of large blood vessel walls, providing nourishment and stability to developing plaques by

delivering growth factors and hormones. This hypothesis is supported by studies utilizing immunohistochemical and confocal microscopy techniques to examine microvessels in human coronary arteries [46]. These studies revealed the presence of microvessels within thickened intima and atherosclerotic plaques, with their abundance directly correlated to plaque size and inversely related to lumen diameter. The observed neovascularization could be traced from the adventitial vasa vasorum through the media, primarily situated at the plaque`s base adjacent to the normal intima.

While these newly formed microvessels provide a notable boost in nutrient blood supply to the thickened artery wall, several studies suggest that these vessels are fragile and prone to rupture. Consequently, these microvessels may contribute to intraplaque haemorrhage, plaque rupture and thrombus formation. In summary, vasa vasorum contribute to atherosclerosis by facilitating inflammatory cell infiltration, intimal thickening, intraplaque hemorrhage, and subsequent atherothrombosis, ultimately leading to conditions such as stroke or myocardial infarction that results in stroke or myocardial infarction [47].

1.6 Arterial Functional and Mechanical Terms

The terminology used to describe the mechanical properties of arteries is crucial in bridging the gap between clinical practice and basic research findings. To facilitate communication, it is helpful to use common terms that are recognized by both clinical and basic scientists. Arterial mechanics can be understood by idealizing the blood vessel as a cylindrical hollow tube and applying the laws of physics accordingly.

Blood flow inside arteries exerts internal forces known as 'intraluminal pressure' that push radially outward against the vessel wall, and these forces are distributed along the arterial path. Intraluminal pressure (IP) is generated by the force exerted by the heart as it pumps blood through

the circulatory system, and it varies depending on different factors, including blood vessel diameter, blood viscosity, and blood vessel elasticity [48].

To study arterial mechanics, we investigate how the arteries respond to changes in intraluminal pressure by measuring changes in the internal lumen diameter and the thickness of the artery wall under different pressures. Based on the internal lumen diameter and wall thickness, we can measure the mechanical properties of the artery, such as elasticity and stiffness.

The cross-sectional area (CSA) of an artery is an important parameter in arterial mechanics and represents the area encompassing both the media and intima CSA and can be calculated using the vessel radius. To determine the total arterial CSA, the radius value can be applied to the formula for the area of a circle (πr^2), since blood vessels are cylindrical in shape. Additionally, the media CSA can be calculated by subtracting the area of the inner circle (using the internal lumen radius) from that of the outer circle (using the vessel external radius). The media CSA refers to the total area occupied by the media layer of the vessel when viewed in cross-section [49].

The media CSA plays a vital role in determining the resistance of the arterial wall to blood flow. When the resistance of the vessel increases, the blood flow decreases, and *vice versa* (see above). An increase in the media CSA of a blood vessel contributes to arterial stiffness and reduced compliance, leading to an increase in the resistance to blood flow and a subsequent decrease in blood flow. For example, in hypertensive patients, the media CSA of the common carotid artery has been found to be increased compared to normotensive individuals, and hypertensive patients with increased media CSA have an increased risk of atherosclerosis and other cardiovascular events Overall, the media CSA is an important parameter to consider in the pathophysiology of hypertension and its associated complications [50, 51].

Blood vessels walls are designed to withstand different stresses or forces. These stresses can be identified based on the direction of the force applied to the vessel wall. For example, the circumferential wall stress (σ-c) is defined as the tensile radial force applied on the vessel wall from the blood pressure and is perpendicular to the long axis of the vessel wall (Fig. 4). When the blood flows through the blood vessel, it exerts a force on the vessel wall, creating an internal pressure. The vessel wall resists this pressure, and this resistance generates a circumferential stress on the wall. This stress is generated by the vessel wall to resist the bursting effect from the internal pressure applied by the blood flow [52].

The process of vascular remodeling in response to changes in blood flow and pressure is an example of the law of Laplace, which states that circumferential stress is directly proportional to internal pressure and vessel radius and inversely proportional to vessel wall thickness. Blood vessels have the ability to adapt to changes in pressure by adjusting their diameter and wall thickness, thus altering the circumferential stress, to maintain their structural integrity and functionality [53, 54]. If the intraluminal pressure in a blood vessel becomes too high, it can lead to excessive circumferential stress on the vessel wall, causing the vessel to rupture or leak, or damage the cells of the vessel wall, particularly endothelial cells. This can lead to various cardiovascular diseases, such as hypertension, atherosclerosis, and aneurysms. Therefore, understanding the mechanics of circumferential stress is important in the diagnosis and treatment of these diseases [55-57].

Another major internal stress that is applied on the blood vessel wall is shear stress (σ-s). Shear stress is defined as the frictional parallel force caused by blood flow across the endothelial surface of the blood vessel (Fig. 4). Moderate levels of shear stress are important for maintaining the health of the endothelium, promoting the release of nitric oxide and other vasodilators that help

regulate blood pressure. However, an increase in shear stress as a result of an increase in blood viscosity or an increase in the intraluminal pressure may damage the intima, particularly causing endothelial dysfunction, which can contribute to the development of atherosclerosis [58-60].

However, blood vessels are flexible in structure, and can undergo deformation in response to changes in blood pressure. The strain is defined as the amount of deformation or change in the vessel wall diameter when a certain force is applied [35, 57]. Furthermore, the Elastic Modulus (EM) is a measure of how much stress is required to produce a given amount of strain in the vessel wall and calculated based on the change in the slope of the strain-stress curve. The EM is often used to describe the mechanical properties of blood vessels, as it provides information about how well the vessels can accommodate changes in blood pressure and flow. Thus, the stiffer the vessel is, the steeper is the slope, and the greater is the EM. This term indicates the elasticity or stiffness of the vessel wall to resist deformation, which is determined by vascular geometry and vascular wall composition [52].

The EM of blood vessels varies depending on the type of vessel and the location in the body. For example, arteries tend to be stiffer than veins due to differences in the composition and structure of their walls. The EM also changes with age and in response to various diseases, such as atherosclerosis, which can cause the vessel walls to become stiffer and less elastic [61, 62]. The EM vs. stress curve indicates vascular stiffness based on the quantity and quality of the vascular wall components including collagens, elastin fibers, and VSMC. In contrast to increased stiffness, vessel compliance is another term that is commonly used to describe the vessel's capacity to distend and adapt to pressure changes [63, 64].

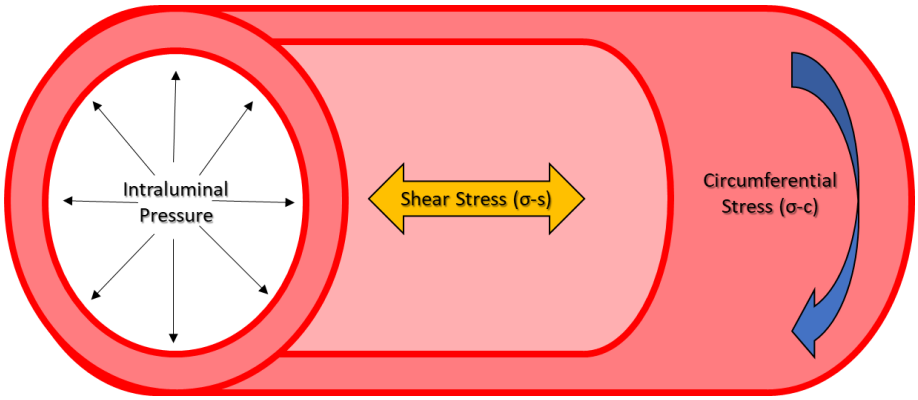

Figure 4. A schematic representation showing the mechanical forces affecting blood vessels.

The shear stress is due to the blood circulation that causes stress on the endothelial layer at the interior surface of the vessel wall. The shear stress depends on the flow rate (F), the blood viscosity (η), and the vessel radius (r). The intraluminal pressure causes perpendicular stress on the full-thickness of the vessel wall, leading to circumferential stress.

2. Arterial Stiffness

2.1 Pathophysiological Mechanisms that Can Induce Arterial Stiffness

Arterial stiffness is defined as the decreased vessel compliance that alters arterial pressure and blood flow, thereby impacting cardiac function and overall perfusion. Arterial stiffness is strongly associated with the development of cardiovascular diseases such as atherosclerosis, hypertension, and heart failure [65]. Multiple factors contribute to the development of arterial stiffness, including an increase in smooth muscle cell stiffness, fibrosis (by increasing the collagen content), cross-linking of elastin or collagen, calcification of the media, reactive oxygen species-induced inflammation, and endothelial dysfunction [66].

2.2 Measurements of Arterial Stiffness in Animal and Human Models

Arterial stiffness is a highly clinically relevant and independent prognostic biomarker for the development and progression of cardiovascular diseases [67]. Therefore, it is crucial to be able to measure the level of stiffness within blood vessels.

The gold standard for measuring aortic stiffness in humans is through carotid-femoral pulse wave velocity (PWV). This method was recommended by the 2013 guidelines for the management of arterial hypertension of the European Society of Cardiology and the European Society of Hypertension (ESH), as well as the 2015 American Heart Association (AHA) for improving and standardizing vascular research on arterial stiffness [59, 68-71]. PWV is a widely accepted non-invasive clinical measurement that involves obtaining waveforms through the skin at the right common carotid artery and the right femoral artery (i.e., "carotid-femoral" PWV) and measuring the time delay (Δt or transit time) between the two waveforms. PWV is calculated as PWV = Distance (meters)/Δt (seconds) and is used to evaluate the extent of arterial damage and to assess cardiovascular risks [72]. When arteries are stiffer, blood flows through them at a faster rate because a stiffer artery does not expand as much in response to a pressure wave, and thus the kinetic energy of the blood causes it to travel at a faster rate than it would in a more compliant, healthy arterial wall [68]. Thus, increased PWV indicates a stiffer artery. In clinical practice, other reproducible methods can also be used to measure PWV, including brachial-ankle pulse wave velocity (baPWV) and the Cardio-Ankle Vascular Index, to evaluate arterial stiffness [69]. Another common method used to measure arterial stiffness is the pulsation model, which uses imaging techniques such as ultrasound or magnetic resonance imaging. These image-based techniques enable direct measurement of the physical properties of the arterial wall by analyzing the pulsatile

changes in the arterial wall and accurately determine the mechanical properties of the vessel, including its elasticity and compliance [73].

In both *in vivo* and *in vitro* animal studies, various measurements can be used to evaluate arterial stiffness. A common *in vivo* measurement for evaluating arterial stiffness in animals, as in humans, is PWV. *In vitro* studies use histological methods to quantify the structure and geometry of vessels, which can help explain changes in vascular stiffness. Two other methods used to evaluate arterial stiffness is using isolated vessel pressure myography or sectioned vascular rings in wire myography. The main difference between these two methods is that the pressure myograph uses a uniform, standard intraluminal pressure applied to the inner wall of the vessel, while the wire myography technique normalizes the pressure to the size of the vessel [69].

2.2.1 Wire Myography

Wire myography is a technique employed to measure the functional responses of isolated blood vessels by assessing the reactivity of smooth muscle and endothelial cells. It is used to measure isometric contractions/relaxations of blood vessels, among several other in vitro bioassays. Wire myography allows the study of a wide range of vessel diameters, ranging from 300 μm to 3 mm. Commonly investigated vessels in wire myography studies include conduit arteries such as the aorta, carotid, and pulmonary arteries, as well as resistance arteries like the mesenteric and cerebral arteries [74, 75].

This method involves preparing vessel sections as ring segments and mounting them onto wires known as jaws, or steel pins. One jaw is connected to a micrometer, allowing control of vessel diameter, while the other jaw is linked to a force transducer that measures the tension produced by the vessel. The measured force is adjusted according to the vessel size. The vessel segment is then

immersed in a perfusion chamber containing a physiological buffer solution. During experiments, the vessel diameter is maintained constant while the tension of the vessel is measured. Active pharmacological agents are introduced to stimulate vessel contraction or relaxation from a pre-contracted state [75]. Wire myography offers several advantages: it is simple to set up and maintain, it can be applied to study vessels of different sizes, and it is a cost-effective approach for evaluating vascular function.

2.2.2 Pressure Myography

Pressure myography provides a more accurate representation of physiological conditions compared to wire myography because blood vessels in the body are naturally subjected to pressure rather than being stretched between wires. In pressure myography, the blood vessel is cannulated at one or both ends where the intraluminal pressure is controlled to achieve a value that is physiologically relevant. By adjusting the intraluminal pressure, the myogenic response can be studied, allowing for a better understanding of vascular function [7].

Moreover, pressure myography provides the capability to manipulate intraluminal flow and shear stress, which play a vital role in regulating vascular contractility. By adjusting the pressure difference between the inflow and outflow cannula, the flow and shear stress can be increased without altering the intraluminal pressure. This allows researchers to create the appropriate shear stress levels (ranging from 3-20 dyn/cm^2) for investigating their effects on vascular function.

Pressure myography is preferred over wire myography for studying vascular function, as pressure myography is considered a more accurate representation of the vessels physiological state, improving the study of its function as the natural shape and diameter are better preserved. Pressure myography allows the study of small resistance arteries, which play a crucial role in determining

vascular resistance, whereas wire myography is primarily limited to larger conduit arteries. One significant advantage of pressure myography is the reduced risk of damaging the endothelium, as there is no need to pass wires through the vessel lumen. Therefore, when studying endothelial function, pressure myography provides a more reliable approach compared to wire myography [76-78].

3. Hypertension

Hypertension, commonly called "high blood pressure," is a common outcome of arterial stiffness. BP is the force that blood exerts against the walls of arteries, and is considered high when it reaches 135/85 mmHg or above [79]. Systolic BP is the pressure in the artery during heart contraction, while diastolic BP is the pressure in the artery when the heart relaxes after contraction. Hypertension affects more than one billion adults worldwide, and approximately 22.7% of Canadian adults over 20 years old are living with diagnosed hypertension, although its prevalence is likely higher as many cases are undiagnosed [80, 81].

Blood pressure is categorized based on the American College of Cardiology and the American Heart Association 2017 guidelines into four stages [69]. These are:

1) Normal BP (below 120/80 mmHg).
2) Elevated risk of developing hypertension (systolic pressure between 120 and 129 mmHg and diastolic pressure less than 80 mmHg); associated with a 2.5 times greater risk of cardiovascular diseases in women and a 1.6 times greater risk of cardiovascular diseases in men.
3) Stage I hypertension (130–139 mmHg systolic or 80–89 mmHg diastolic).
4) Stage II hypertension (systolic pressure of 140 mmHg or higher or a diastolic pressure of 90 mmHg or higher).

The higher the blood pressure, the higher the risk of developing peripheral vascular diseases, heart attack, and stroke.

3.1 Classification of Hypertension

3.1.1 Essential Hypertension

Essential (primary) hypertension occurs in 95% of hypertensive people, and is described as heterogeneous because it can occur due to diverse factors including age, sex, race, socioeconomic status, and geographic patterns [82]. Essential hypertension can be caused by a combination of factors that increase BP and contributes to the development of multiple cardiovascular diseases, including myocardial ischemia, cardiac hypertrophy, and heart failure [37, 83].

Due to the variable symptoms of hypertension, the exact etiology is not well described, and in many cases is considered to be idiopathic. However, one of the main mechanisms that contributes to the pathophysiology of hypertension is increased dietary salt consumption. Increased salt consumption increases water retention and reabsorption, which expands the blood volume and impairs the Renin-Angiotensin-Aldosterone System (RAAS) response, thus increasing sympathetic nervous system activation. These changes together increase total peripheral resistance and afterload, which in turn leads to the development of hypertension [37]

3.1.2 Secondary Hypertension

Secondary hypertension is defined as elevated blood pressure that is secondary to an identified underlying cause [37]. It accounts for a small fraction (about 5-10%) of cases in patients with hypertension and can involve:

1. Renal Parenchymal Disease which includes different renal disorders such as diabetic nephropathy, glomerulonephritis, interstitial renal parenchymal diseases, and polycystic kidney disease.

2. Endocrine Disorders which include primary aldosteronism, pheochromocytoma, and Cushing`s syndrome.

3. Renovascular Disorders which are mainly due to stenosis of renal arteries, either bilateral or unilateral.

4. Vascular Disorders, such as coarctation of the aorta.

5. Miscellaneous conditions such as obstructive sleep apnea, polycystic ovarian syndrome, preeclampsia, or the use of certain drugs like antidepressants, NSAIDs, sodium-containing antacids.

3.2 Renin-Angiotensin-Aldosterone System (RAAS)

RAAS is a critical regulator of chronic blood pressure changes. It involves renin, Angiotensin, and aldosterone, each of which is increased in response to renal arterial pressure reduction, and which act to elevate or restore renal arterial pressure (Fig. 5). The RAAS acts by modulating blood volume through sodium reabsorption, potassium secretion, water retention, and increasing resistance through modulating vascular tone [37]. A decrease in arterial pressure to the kidneys triggers renin secretion into the blood. Renin cleaves angiotensinogen to angiotensin I (an inactive form of AngII) [84]. An enzyme secreted from the vascular endothelium in the lungs and kidneys, called angiotensin-converting enzyme (ACE), then catalyzes the conversion of angiotensin I to AngII [85].

AngII mediates a fast-acting response to low arterial blood pressure by binding to AngII type 1 (AT1) receptors in the kidneys, adrenal cortex, and arterioles. This binding causes

vasoconstriction, which increases blood pressure, and stimulates the release of aldosterone from the adrenal cortex. AngII also promotes sodium reabsorption in the kidneys, which increases blood volume and arterial blood pressure.

Aldosterone mediates a slower response to low arterial blood pressure by binding to mineralocorticoid receptors in the kidneys. This binding causes the late distal tubule and the collecting duct of nephrons in the kidneys to retain sodium, excrete potassium, and increase reabsorption of water, thus increasing the blood volume and the blood pressure over time. Overall, AngII mediates a fast-acting response to low arterial blood pressure, while aldosterone mediates a slower response [50, 86].

3.2.1 Angiotensin II Overview

Angiotensin II exerts its effects through two main receptors: AT1 receptors and AT2 receptors. These receptors are G-protein-coupled proteins primarily located in vascular smooth muscle cells, adrenal cortex, heart, kidney, and brain. AT1 receptors mediate most of Ang II's known physiological actions, which include vasoconstriction, aldosterone release, sodium retention, and cellular proliferation. In contrast, AT2 receptors are less thoroughly understood but may oppose the actions of AT1 receptors in certain situations, promoting vasodilation, apoptosis, and antiproliferative effects.

AngII induces vasoconstriction of arterioles by binding to and stimulating AT1 receptor (AT1R), leading to a series of intracellular signaling cascades. As a result, Ca^{2+} is released within the smooth muscle cell, initiating MLCK phosphorylation and stimulating VSMCs to contract, as mentioned above. In general, AngII activates potent arteriolar vasoconstriction, which increases total peripheral resistance, causing an increase in blood pressure [87, 88].

AngII can be used to treat hypotension resulting from septic or other forms of distributive shock. AngII is marketed under the brand name Giapreza. In 2017, AngII was approved to treat dangerously low blood pressure resulting from septic shock [89]. Moreover, AngII contributes to VSMC growth by activating both proliferative and hypertrophic pathways. Several studies implicate AngII as having a role in VSMC hyperplasia (replication of DNA followed by cell division) or hypertrophy (increase in cell size and content without cell division), depending on tissue type and growth factors [90, 91]. Activation of AT1R by AngII leads to activation of downstream signaling pathways such as the extracellular signal-regulated kinase (ERK1/2), c-Jun N-terminal kinase (JNK), and p38 mitogen-activated protein kinase (MAPK) pathways, which are involved in VSMC proliferation and hypertrophy [92-94]. Furthermore, AngII-induced VSMC hyperplasia and growth is associated with the activation of the phosphatidylinositol 3-kinase (PI3K)/Akt pathway. Akt mediates the hypertrophic response of VSMCs to AngII by promoting protein synthesis and inhibiting protein degradation [95, 96].

It is noteworthy that in whichever tissues contain AT1R, AngII can bind to these receptors and modulate the responses of these tissues. AT1R can be found in various tissues including VSMCs, cardiac monocytes, fibroblasts, macrophages, and endothelial cells [97].

Elevated AngII was observed to be a key component in endothelial dysfunction, acting through AT1R [98]. NO is the primary endothelial-derived relaxing factor, which is synthesized by the endothelial nitric oxide synthase (eNOS). Exposure to AngII reduces eNOS activity and NO production, which results in impaired endothelial relaxation and causes endothelial dysfunction [99].

Most studies suggest that AT2R activation elicits a protective response in the heart. AT2R stimulation triggers defensive mechanisms in the heart, including cardiac regeneration, vasodilation

of coronary microvessels, and compensatory hypertrophy of cardiac myocytes [100]. Several studies propose that the AT2R stimulation following MI provides cardioprotection. Research employing genetically modified mice has demonstrated that upregulation of AT2R offers protective effects against post-infarction left ventricular remodelling and improves cardiac function in the later stages post MI [101, 102]. On other hand, in AT2R KO mice, the recovery from acute MI is significantly reduced compared to the wild-type mice. Additionally, AT2R KO mice exhibit exaggerated neointima formation and smooth muscle cell proliferation after vascular injury [103]. These findings suggest that AT2R exerts anti-proliferative and pro-apoptotic effects on vascular smooth muscle cells.

Moreover, AT2 receptors contribute to regulating blood pressure by modulating vascular tone through vasodilation. Current research suggests a correlation between AT2R and bradykinin B2 receptors in NO production during vasodilation. When stimulated by angiotensin II, AT2R activation elevates levels of cGMP through a mechanism involving bradykinin B2 receptors, thereby promoting the release of NO [104]. Furthermore, AT2R activation promotes the generation of bradykinin by activating kininogenases [105]. In summary, these findings underscore the diverse actions of Angiotensin II through its receptors.

3.2.2 Transgenic Mice Models Used for AngII Modulation

Transgenic mice models have been widely used to study the role of AngII in various physiological and pathological conditions [106] (Table1). These transgenic mice have been developed to manipulate the expression of genes within the RAAS pathway, either through overexpression or gene knockout. The aim of these manipulations is to effectively control the expression of AngII.

Overall, these transgenic mice models have provided valuable insights into the role of AngII in various physiological and pathological conditions and have helped to identify potential therapeutic targets for the treatment of diseases associated with AngII.

Table 1: Commonly used transgenic mice models in AngII research.

Transgenic Mouse Model	Gene Modulation	Uses
1. Angiotensinogen (AGT) Transgenic Mice	These mice either overexpress or knockout the AGT gene under the control of various promoters.	They have been used to investigate the effects of AngII levels in various tissues and organs [107, 108].
2. Renin Transgenic Mice	These mice can either overexpress or knockout renin, leading to altered production of AngII.	They have been used to study the role of the renin-angiotensin system in various physiological processes [109, 110].
3. AT1 Receptor Transgenic Mice	These mice can either overexpress or knockout the AT1R gene, leading to modulating sensitivity to AngII.	They have been used to investigate the effects of AngII-mediated signaling in various tissues and organs [111, 112].
4. ACE Transgenic Mice	These mice can either overexpress or knockout the ACE gene as ACE modulates the conversion of AngI to AngII.	ACE transgenic mice have been used to study the effects of AngII levels on cardiovascular and renal function [113, 114]

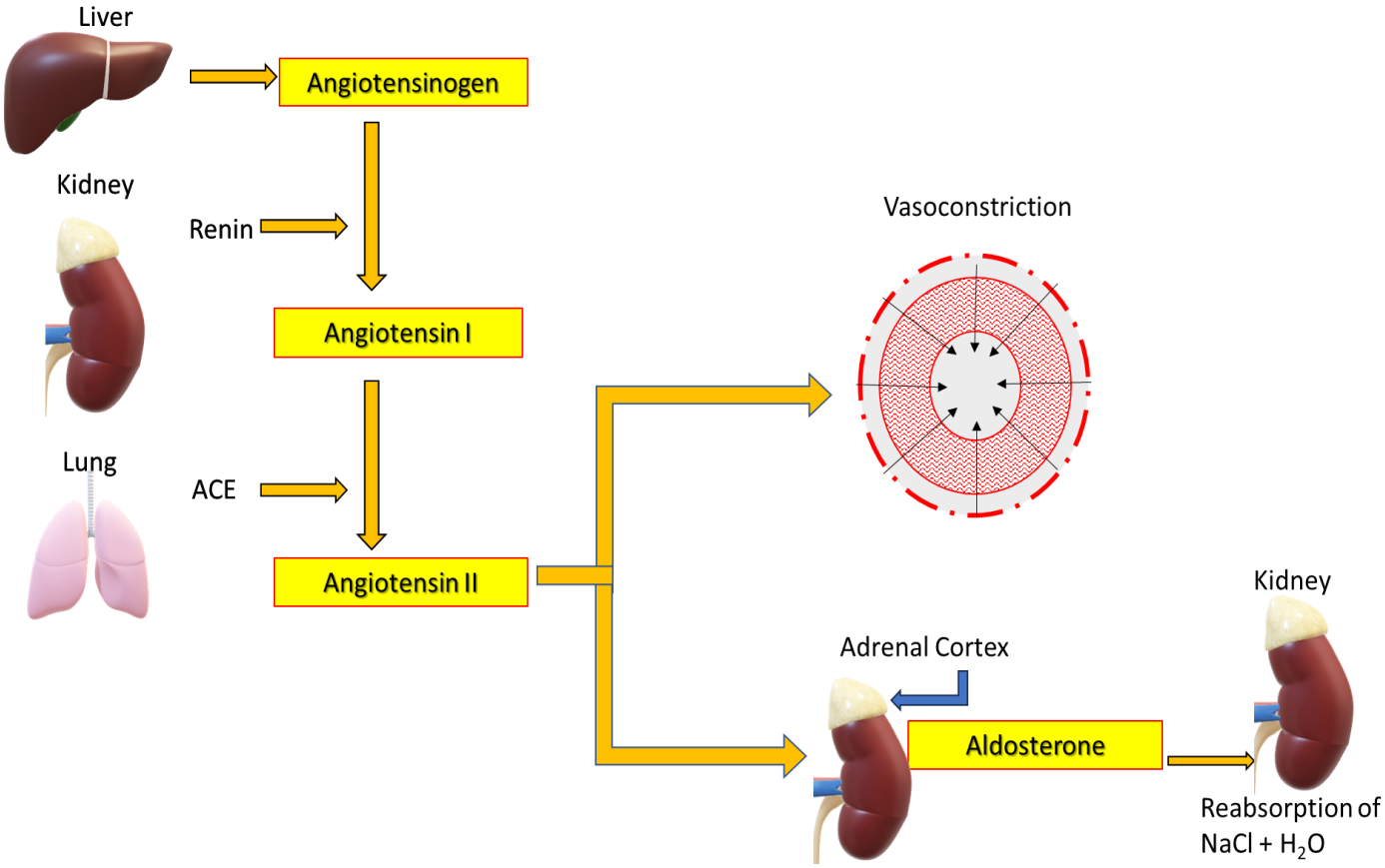

Figure 5. A schematic diagram of the Renin-Angiotensin-Aldosterone System (RAAS).

The RAAS regulates arterial pressure through the participation of its components, including angiotensinogen, which is released from the liver and cleaved into angiotensin I via the action of renin, which is excreted from the kidneys. The lungs produce Angiotensin-Converting Enzyme (ACE) to convert angiotensin I to its activated form, AngII. AngII increases blood pressure by acting on resistance blood vessels, causing vasoconstriction. Moreover, AngII acts on the adrenal cortex to release aldosterone, which acts in the kidney, causing reabsorption of salt and water, thus increasing the volume of blood and maintaining blood pressure.

***All images in this diagram were generated from 3D Model, or drawn by Microsoft PowerPoint (Version 2402 Build 16.0.17328.20124).*

3.3 Hypertensive Vascular Remodelling\Stiffness in Small and Large Arteries and Outcomes

Both small and large artery remodeling contribute to the development and complications of hypertension. Vascular abnormalities involve modifications altering vascular geometry or vascular mechanics which affect the pathogenesis and prognosis of hypertensive patients. Vascular remodeling occurs as an adaptive mechanism to minimize vascular wall damage triggered by persistent hemodynamic stress.

3.3.1 Vascular Geometry

The main components when measuring vascular geometry are lumen diameter, arterial wall thickness, and the media-cross sectional area (CSA). For example, any reduction in lumen diameter could significantly interfere with blood flow and increase arterial resistance as mentioned above.

Hypertensive resistance arteries undergo either one or a combination of two major forms of structural remodelling (Fig. 6) [115]:

(1) Inward eutrophic remodeling occurs via rearrangement or apoptosis of arterial wall components, and is characterized by reduction in the lumen diameter, and increased media/lumen ratio while the media cross-sectional area is unchanged. This type of remodeling is found in patients with mild essential hypertension and spontaneously hypertensive rats (SHR) [116, 117].

(2) Hypertrophic remodeling is characterized by hypertrophy or hyperplasia of VSMCs, where the media becomes thicker, pushing into the lumen and resulting in increased media cross-sectional area and media/lumen ratio. This type of remodeling is associated with severe hypertension, such as in patients with secondary hypertension and in the deoxycorticosterone acetate (DOCA) rat model [118, 119].

In large arteries such as the aorta and other elastic arteries, changes in vascular cross-sectional geometry are less critical than in resistance arteries, as large arteries have a higher capacity for adapting to hemodynamic changes due to their inherent elasticity, as mentioned above. However, in essential hypertension, large artery remodeling is characterized by an increase in intima-media thickness (IMT) and an enlargement in the lumen. This change compensates for the rise in BP, which tends to normalize circumferential wall stress [120]. The reason is attributed to impairment in the load-bearing elastin fibers in response to the cyclic strain and pulsatile tensile stress. Additionally, the stiffness of large arteries due to VSMC growth and changes in their phenotype could be a contributing factor and a pathological hallmark in essential hypertension [121].

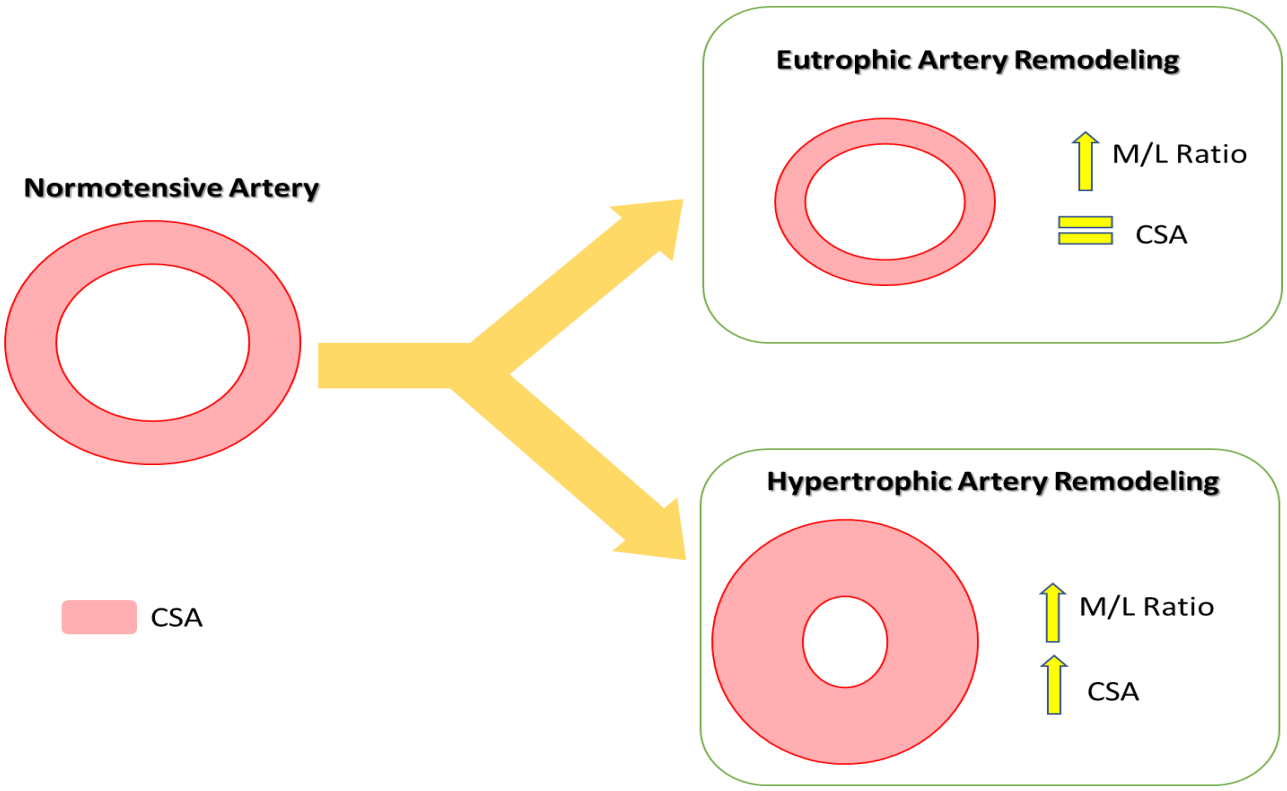

Figure 6. Structural remodeling in resistance arteries with hypertension.

Normotensive vessels may undergo structural modifications, including eutrophic growth, hypertrophic remodeling, or a combination of both. Hypertrophic remodeling is characterized by an increase in both the cross-sectional area (CSA) and the media-to-lumen ratio (M/L). Eutrophic remodeling, on the other hand, involves an unchanged media CSA and an increased M/L.

3.3.2 Vascular Mechanics

Small artery dysfunction is a hallmark of essential hypertension and is characterized by an impairment in the vasodilatory reserve, which is defined as the ability of a blood vessel to increase blood flow via maximal vasodilation [122]. Some studies suggest that chronic vasoconstriction in hypertensive patients can stimulate the development of eutrophic remodeling, resulting in a smaller lumen diameter and reduced arterial distensibility [123]. The Folkow group first observed this phenomenon using plethysmography to measure forearm blood flow under conditions of maximal vasodilation, from which they derived the concept of minimal flow resistance. They found that flow resistance is abnormally high in hypertensive patients due to structural alterations that contribute to increasing systemic resistance [124].

Reduced distensibility of resistance arteries can be attributed to either structural geometry or cellular responses within the vessel wall. A human study involving small arteries dissected from gluteal skin biopsies of essential hypertensive patients found that these resistance vessels exhibited eutrophic remodeling and an altered VSMC relaxation response [125]. VSMC dysfunction has been associated with the development and progression of hypertension due to increased smooth muscle contractility. Different studies have reported the increased contractile effect is due to the increase in VSMC plasma membrane permeability to Ca^{2+}, which has been demonstrated in VSMCs isolated from animal models of hypertension and coronary vasospasm [126, 127].

Conversely, multiple studies have identified the role of endothelial dysfunction in increased peripheral resistance in essential hypertension [128]. Endothelial dysfunction enhances vasoconstriction, structural remodeling, and increased myogenic tone through the production of multiple factors including renin-angiotensin system (RAS) components, endothelin-1,

catecholamines, and growth factors leading ultimately to increased vascular remodeling and peripheral resistance [129-131].

Reduced distensibility in large arteries is associated with an increased risk of cardiovascular events. Elastic artery stiffening is more commonly associated with aging, and is accelerated in the presence of hypertension, especially in the elderly with isolated systolic hypertension. Elastic artery stiffening results from the breakdown of elastic fibers, the accumulation of collagen fibers, and the deposition of more calcium due to increased blood flow turbulence. These alterations lead to a wider artery lumen, greater wall degeneration, and increased tension in the aorta [132, 133].

A recent study found that patients with isolated systolic hypertension had increased aortic stiffness and endothelial dysfunction when compared with patients of similar age [134]. Other studies showed that untreated hypertension may accelerate the rate of large artery stiffness and induce further progression in hypertension adverse outcomes [135].

3.4 Animal Models Used in Hypertension Research

The most frequent animal models used for hypertension studies are small animal models (i.e. mice, and rats). Small animals are commonly used due to their low cost, short life span, and small size which requires lower doses of drugs where hypertension is induced pharmacologically or through surgical interventions [136].

Pharmacological induction of hypertension typically involves the infusion of AngII, glucocorticoids, or DOCA (with or without a high-salt diet) [137]. Surgical interventions may include the constriction of the aorta using an extravascular band or the implantation of adjustable occluding devices in the suprarenal aorta or renal arteries, or intravascular devices in the renal

arteries [138]. These methods are commonly used in research because of their simplicity and reliability in inducing chronic hypertension.

4. Scleraxis Transcription Factor

4.1 Scleraxis Overview

The Scleraxis protein is a member of the basic helix-loop-helix (bHLH) superfamily of transcription factors that regulate cellular growth, proliferation, and differentiation of various cell types. During embryogenesis, scleraxis is initially expressed at high levels within mesenchymal precursors of the axial, appendicular, and cranial skeleton. Later, its expression becomes limited to regions where cartilage and connective tissue formation occurs. This indicates that scleraxis plays a crucial role in chondrogenesis [139]. Scleraxis is a transcription factor that regulates gene expression by binding to a specific hexanucleotide DNA sequence (CANNTG), known as an E-box, typically located in the promoter regions of target genes [140]. Structurally, scleraxis is characterized by a highly conserved domain containing a stretch of basic amino acids adjacent to two amphipathic α-helices separated by a loop [141].

4.2 Scleraxis Role in Cell Differentiation

Scleraxis is a master regulator of ECM formation and is important in the pathogenesis of cardiac fibrosis via regulating fibroblast to myofibroblast conversion [142]. Scleraxis directly transactivates the expression of various genes in the heart such as matrix metalloproteinases (MMPs) and numerous markers of the fibroblast and myofibroblast phenotype including fibronectin, vimentin, and fibrillar collagens col 1α1 and col 1α2 [143-145].

Previous findings from our lab indicate that scleraxis plays a crucial role in promoting Epithelial to Mesenchymal Transition (EMT) by increasing the expression of important

transcription factors Snai1 and Twist1, which are essential for both cancer metastasis and embryonic development [146]. Snai1 and Twist1 have been known to downregulate the expression of genes responsible for cell-cell adhesion, including E-Cadherin, which leads to the loss of epithelial properties and acquisition of mesenchymal characteristics, such as enhanced cell migration and metastasis. These changes are critical features in both cancer aggressiveness and embryonic differentiation [147, 148].

Scleraxis enhances gene expression during embryonic tendon development and maturation as well as in adult tendon healing [139]. Scleraxis expression starts from the early timepoints of development of tenocytes and is maintained in mature tenocytes [149]. Additional studies highlight the critical role of scleraxis in tendon cell differentiation [150, 151]. Overall, scleraxis has a crucial role in transactivating the genes that are required in cell differentiation in different scenarios whether it is through development or as an adaptive process for healing as a post-insult recovery such as in fibrosis.

Overexpression of scleraxis in various cell types has led to variable levels of gene expression, depending on the cell type and function. For instance, upregulation of scleraxis in cardiac fibroblasts enhances the expression of αSMA. On the other hand, upregulation of scleraxis in mesangial cells reduces the expression of αSMA in diabetic nephropathy, thus deactivating the mesangial cell phenotype under diabetic conditions [152]. Overall, this suggests that the modulation of gene expression by scleraxis is variable and is cell type specific.

Different studies have correlated physical mechanical stresses with scleraxis expression. Studies have investigated the role of mechanical stretch in inducing scleraxis expression and how this upregulates the genes responsible for fibrosis and the conversion of cardiac fibroblasts to myofibroblasts. In turn, these changes promote the progression of cardiac fibrosis and heart failure

[153]. Alternatively, other studies have shown that prolonged small loads on skeletal muscles decrease the expression of scleraxis. Since scleraxis plays a crucial role in tendon cell differentiation, this suggests that mechanical stimulation is necessary to trigger scleraxis gene expression and promote the development of the mature tendon phenotype [154].

4.3 Scleraxis Role in Vasculature

Although there is little direct evidence of scleraxis expression in the vasculature, recent transcriptomic studies using single-cell RNA sequencing indicate that scleraxis is expressed in both aortic and airway smooth muscle cells. These findings suggest that scleraxis may play a role in vascular homeostasis and function in these tissues [155].

A study investigated the effect of scleraxis upregulation in VSMCs in Klotho gene haplodeficiency mice [156]. The Klotho gene is an aging suppressor gene whose expression decreases with age. The study aimed to understand the mechanism by which the deficiency of Klotho gene induces arterial stiffness through scleraxis upregulation. The results showed that in haplodeficiency mice, scleraxis upregulation was associated with increased collagen and decreased elastin in the media of the aortas. Consequently, excessive collagen deposition within the aortas contributes to increased stiffness and decreased compliance, while the reduction in elastin impairs the arteries` ability to respond to blood pressure fluctuations by limiting their capacity to expand and recoil.

The involvement of scleraxis in maintaining vascular homeostasis and regulating arterial stiffness in Klotho gene haplodeficient aortas initiates ECM remodeling. This process involves the upregulation of MMP-2 and MMP-9 expression, leading to the degradation of ECM proteins like elastin. Consequently, this exacerbates arterial stiffening [143]. Additionally, scleraxis upregulation along with increased TGFβ1 levels, may promote the differentiation of fibroblasts into

myofibroblasts within the adventitia [142]. These myofibroblasts contribute to ECM deposition, particularly collagen, leading to tissue fibrosis [157]. To summarize, the upregulation of scleraxis contributes to arterial stiffness in a klotho-deficient mouse model. Scleraxis promotes collagen synthesis and fibroblasts differentiation, and its upregulation in klotho deficiency leads to increased collagen expression and fibrosis, contributing to arterial stiffening [156].

Another recent and interesting study revealed that in patients with Marfan syndrome, a genetic connective tissue disorder associated with aortic aneurysms, RNA-seq analysis of full-thickness aortic biopsies showed that scleraxis is one of the highly expressed genes. This finding suggests that scleraxis plays a significant in the pathophysiology of aortic tissues in Marfan syndrome patients [158].

4.4 Scleraxis Interaction with AngII Signaling

AngII plays a significant role in profibrotic signaling in the heart that in turn impairs cardiac function. AngII induces cardiomyocyte hypertrophy and cardiac fibroblast proliferation and activation. Also, AngII promotes ECM protein accumulation by activating scleraxis and other fibrotic mediators in the heart [159]. Moreover, it was reported that AngII induces vascular fibrosis via activation of the transcription factor Smad3 in aortic vascular smooth muscle cells [160]. Our lab has shown that Smad3 physically interacts with scleraxis and requires scleraxis to drive TGFβ/Smad fibrotic signaling in cardiac fibroblasts [157].

AngII is a vasoactive peptide that can have both systemic and local effects that alter heart function and increase blood pressure. Hypertrophic cardiomyopathy (HCM) is one of the primary causes of hypertension and is the leading cause of sudden death. One study employed the AngII receptor blocker losartan to reverse myocardial fibrosis in a transgenic mouse model of human hypertrophic cardiomyopathy, showing that AngII has a direct effect in inducing HCM [161].

Another study identified scleraxis upregulation as an important early prognostic biomarker for cardiac fibrosis in HCM patients [162]. Overall, this suggests that scleraxis upregulation and AngII are factors in HCM development and targets for treatment.

4.5 Scleraxis Knockout Mouse Model

Initial studies on scleraxis knockout mice demonstrated its critical role in early embryonic development, as knockout embryos died during the early stages of embryogenesis [163]. Subsequent studies reported that the initial phenotype associated with scleraxis knockout was primarily influenced by the presence of a neomycin-resistance cassette used to create the knockout, affecting the expression of neighboring genes [163]. To overcome this limitation, Schweitzer's group conducted conditional recombination experiments using a Cre/loxP approach to selectively remove the scleraxis coding region and excise the neomycin cassette [151]. The excision of the cassette allowed for the generation of full-term pups that exhibit a new loss-of-function scleraxis allele called scleraxis-null mice or scleraxis knockout mice (Scx^{KO}).

Scx^{KO} mice are characterized by a significant disruption in tendon differentiation represented by dorsal flexure of the forelimb paw, limited use of all paws, reduced function of the back muscles, and complete loss of tail movement [151]. Furthermore, Scx^{KO} mice showed alterations in tendon matrix production, characterized by a significant decrease of tendon matrix and disorganization at the cellular level [151]. Schweitzer's mouse model provided the first demonstration of a tendon differentiation phenotype and offered valuable insights into the function of scleraxis.

However, it was observed in the study that not all tendons in Scx^{KO} mice displayed defects in matrix production [151]. Specifically, force-transmitting tendons and those responsible

for transmitting muscle force to the skeleton were selectively affected, while tendons that primarily served as attachments for muscles without significant force development, such as those connecting intercostal muscles and ribs, remained mostly unaffected. These findings indicate that the loss or malformation of force-transmitting tendons in the absence of scleraxis suggests its crucial involvement in the normal development of tissues subjected to physical load [164]. Building upon these findings, another study was conducted to investigate the role of scleraxis in mechanical load-bearing tendons [154]. The study demonstrated that both cyclic and static mechanical loading induce the expression of scleraxis.

Subsequent investigations utilized Scx^{KO} mice to explore the role of scleraxis in various cell types beyond tendons. Specifically, previous research from our lab focused on the role of scleraxis in the phenotype conversion of cardiac fibroblasts to myofibroblasts [142]. The findings demonstrated a significant downregulation of ECM and fibroblast marker gene expression in the hearts of Scx^{KO} mice. However, the restoration of scleraxis expression rescued the function of scleraxis null cardiac fibroblasts, attenuating the impairment of myofibroblast function and increasing ECM gene expression [142]. These mice exhibited cardiac structured abnormalities such as altered valve structure, rounded ventricles, and involution of the apex. The absence of scleraxis resulted in a ~50% decrease in fibroblast number and a significant ~30% reduction in heart size. Despite the smaller size of the Scx^{KO} heart, echocardiography showed normal cardiac function, although capillary density was reduced by ~25%. The observed decrease in capillary density in the hearts of Scx^{KO} mice suggests that the absence of scleraxis may have an impact on either the components or numbers of blood vessels. This alteration in vasculature could potentially interfere with the adequate supply of nutrients and oxygen to the relatively smaller cardiac tissue. Despite no significant changes in the number of

cardiomyocytes, a noteworthy 29% reduction in cardiomyocyte cross-sectional area was observed indicating a potential role of scleraxis in the growth and size regulation of cardiomyocytes [142]. Overall, the reduced heart size in Scx^{KO} mice was primarily attributed to decreased myocyte volume. These findings suggest the diverse and important role of scleraxis in different cell types.

Another study explored the involvement of scleraxis in the various stages of valvulogenesis (heart valve formation) and its impact on adult heart valve function and structure [165]. The study focused on Scx^{KO} mice, which exhibited considerably thickened heart valve leaflets starting from embryonic day 17.5, characterized by increased ECM gene expression and the progression of pathological fibrosis leading to modest but not statistically significant impairment of cardiac function in Scx^{KO} mice compared to wild-type littermates, as confirmed through Echocardiography.

In conclusion, the role of scleraxis in different tissues is context-dependent, exhibiting varying effects. The utilization of Scx^{KO} mouse models has been instrumental in exploring the specific role of scleraxis in different tissue-specific contexts, including tendons and cardiac fibroblasts, providing a valuable insight into their development and functionality. Furthermore, the use of Scx^{KO} mice holds a promising potential for future research directions, allowing for the exploration of the role of scleraxis loss in other tissues.

5. Marfan Syndrome Overview and Correlation with Scleraxis Expression

Marfan syndrome is one of the most common inherited connective tissue disorders, leading to a wide range of manifestations across multiple organ systems, including ocular, cardiovascular, and musculoskeletal abnormalities. Additionally, it may impact the lungs, skin, and central

nervous system [166]. Marfan syndrome is caused by mutations in the fibrillin-1 gene, disrupting the synthesis or function of fibrillin-1, a crucial connective tissue protein [167].

Dysfunctional fibrillin-1 disrupts the structural integrity and elasticity of connective tissues by promoting an excessive release of sequestered TGFβ1 and increasing its activity. This leads to overexpression of MMP-2 and MMP-9 [168, 169]. Consequently, vascular remodeling occurs, impairing the ability of blood vessels and heart valves to withstand mechanical stress. This process results in cystic medial degeneration of the aorta, characterized by the accumulation of mucopolysaccharide cysts, leading to progressive dilation and eventual rupture of the aorta [170]. Patients with Marfan syndrome commonly present with cardiovascular manifestations, including aortic root dilation, aortic dissection, mitral valve prolapse, aneurysms and aortic regurgitation [167, 171]. Diagnosis involves clinical evaluation, assessment of family history assessment, genetic testing for fibrillin-1 mutations, and imaging studies such as echocardiography and MRI [166].

While there is no definitive cure for this syndrome, treatment strategies focus on symptom management and complication prevention. Theses may include using medications to regulate blood pressure and reduce aortic regurgitation, opting for surgical interventions to repair or replace affected heart valves or aortic segments, and implementing lifestyle modifications [172].

A recent intriguing study of patients with Marfan syndrome by RNA-seq analysis of full-thickness aortic biopsies unveiled scleraxis as one of the prominently expressed genes [158].

Marfan syndrome presents with a prominent mitral valve pathology, characterized by myxomatous degeneration featuring weakness and leakiness [173]. Heart valves, comprising collagen, proteoglycans, and elastin, undergo complex organization. Recent studies demonstrate a

notable upregulation of scleraxis expression in murine models with mutated fibrillin and human mitral valve cells from Marfan syndrome patients [174]. Elevated scleraxis levels in human mitral valve cells correlate with increased expression of proteoglycans such as aggrecan, biglycan, decorin, fibromodulin, and collagen types I and II, consistent with myxomatous valve phenotypes. [174]. Scleraxis is known to be integral in valvulogenesis, studies using scleraxis knockout mice demonstrate remodeled heart valves with decreased proteoglycan content [175]. These findings suggest a potential mechanism whereby scleraxis mediates myxomatous mitral valve disease pathogenesis in Marfan syndrome by upregulating proteoglycans, thereby providing a mechanistic link between fibrillin-1 mutations and mitral valve degeneration in this genetic disorder.

Previous findings from our laboratory have demonstrated that scleraxis regulates MMP-2 expression within cardiac myofibroblasts, with TGFβ-mediated MMP-2 expression depending on the presence of scleraxis [143]. In Marfan syndrome, dysfunction of fibrillin-1 leads to increased TGFβ expression, and MMPs which are suggested to be implicated in the degradation of elastic fibers in aortas. Consequently, the overproduction of these MMPs reduces connective tissue elasticity, resulting in the weakening of the aortic wall. The relationship between TGFβ levels and MMPs expression has been investigated in a Marfan mouse model, revealing that TGFβ upregulates mRNA expression of MMP-2 and MMP-9. This increased MMP-2 activity in the aortas subsequently induces ECM remodeling [176]. These findings suggest that scleraxis may play a potential role in the pathogenesis of Marfan syndrome.

B. **Research Aims & Objectives**

Vascular stiffness is a significant contributing factor to the development of cardiovascular diseases, especially hypertension. Scleraxis protein is known to induce cardiac stiffness and fibrosis, which can cause heart failure and eventually death. Scleraxis also activates cardiac fibroblasts and other cell types in response to injury or insult. Despite this knowledge, the impact of scleraxis on blood vessels is not well understood, and further research is necessary to determine the correlation between scleraxis and vascular dysfunction, especially when high blood pressure is present as an additional contributing factor in a pathological model. Different types of cells within the vascular wall layers, including endothelial cells in the tunica intima, smooth muscle cells in the tunica media, and fibroblasts in the tunica adventitia, contribute to the development and progression of vascular stiffness.

In this project, we hypothesize that scleraxis induces vascular stiffness, and its overexpression prompts and exacerbates, respectively, arterial stiffness in a hypertensive animal model.

This thesis characterizes the effect that scleraxis plays in inducing vascular changes of both small resistance arteries and aortas by assessing structure, mechanical behavior, and function. Our project consists of 2 major aims:

Aim 1.

Determine if scleraxis overexpression in either smooth muscle or adventitial fibroblasts is sufficient to induce vascular stiffness and impair vessel function in mice.

Aim 2.

In the AngII-induced hypertension mouse model, determine whether scleraxis overexpression exacerbates the vascular remodeling.

Objectives:

1. Characterise the structural remodelling, mechanics, and the vasodilatory functional responses of the cells in the mesenteric resistance arteries.

2. Characterise the structural changes of aortas in these models and changes in gene expression.

3. Characterise an *in vitro* model using VSMCs to determine the morphological, phenotypic, and gene expression changes resulting from scleraxis overexpression.

4. Characterise the structural remodelling, mechanics, and the vasodilatory functional responses of the cells within the mesenteric resistance arteries, alongside alterations in the aortas, utilizing an *in vivo* model featuring mice with scleraxis overexpression in an AngII-induced hypertensive model.

CHAPTER 2: MATERIALS AND METHODS

1. Animals

For the scleraxis knockout study, we used a strain of germline scleraxis null mice (strain $Scx^{tm1.1Stzr}$; MGI:3716564) that has been previously described in literature [151]. For scleraxis overexpression studies, we employed a Cre/lox system to up-regulate scleraxis expression in a cell-specific and temporally controlled manner. We crossed an established scleraxis transgenic mouse line with a floxed premature stop codon with tamoxifen-inducible Cre driver lines (Fig. 7). These Cre driver lines express Cre in either fibroblasts (the TCF21iCre (Tcf21tm3.1(cre/Esr1*) Eno) mouse line) or in vascular smooth muscle (the smooth muscle myosin heavy chain polypeptide 11 promoter (B6.FVB-Tg (Myh11-$CreER^{T2}$)1Soff/J) mouse line (from Jackson Laboratories) Myh11Cre).

Studies have developed the TCF21iCre mouse model, featuring a targeted insertion of tamoxifen-inducible Cre recombinase, MerCreMer, at the Tcf21 locus. This model enables inducible Cre recombinase expression specifically in Tcf21-expressing cells, most commonly in lungs, kidneys, gonads, spleen, and heart. By utilizing ROSA26 reporter mice, studies were able to demonstrate the precise and robust activation of Cre recombinase in multiple Tcf21-expressing tissues throughout embryonic and postnatal development [177].

Oslen and colleagues were the first to demonstrate the high specificity of Myh11 transcript expression in SMCs in both embryonic and adult mice [31]. This discovery identified Myh11 as the most specific marker for the smooth muscle lineage and the definitive marker of SMC differentiation. Subsequently, other research groups developed a transgenic mouse model

with an inducible Cre driven by the Myh11 gene, known as Myh11-CreER^{T2}, to investigate the role of SMC in vascular resistance in hypertension [178].

Although Cre will be expressed in all tissues in which the promoter is expressed, it will only be able to enter the nucleus to delete the premature floxed stop codon upon tamoxifen treatment, providing temporal control of scleraxis transgene expression. Scleraxis gene upregulation is initiated by daily gavage of tamoxifen in corn oil (186 mg/kg) once per day for five consecutive days to induce cell-specific scleraxis overexpression (Scx^{TG}), with wild type scleraxis controls (Scx^{WT}) treated with corn oil vehicle alone.

In all studies, we used young adult mice (8 weeks or older). For the first aim, we overexpressed scleraxis vs control, then sacrificed animals 8 weeks after tamoxifen gavage (Fig. 8A). For the second aim, to induce a pathological model of hypertension and vascular dysfunction (Fig. 8B), mini-osmotic infusion pumps (Alzet 1004) with a pumping rate 0.11 µl/hr, a working duration of 28 days, and a reservoir volume 100 µl were implanted subcutaneously to deliver 1 mg/kg/day of AngII, or saline as a control for 4 weeks. One week following implantation, mice received daily gavage of tamoxifen in corn oil (186 mg/kg) or corn oil control for 5 days similar to the first aim. Then animals were sacrificed 4 weeks after pump implantation. Animals were provided with food and water *ad libitum* and maintained on a 12/12 day/night cycle. Animal studies were conducted following the guidelines established by the Animal Care Committee of the University of Manitoba and the Canadian Council on Animal Care. All animals were euthanized in accordance with Canadian Council on Animal Care guidelines by administering a subcutaneous injection of ketamine/xylazine injection for anesthesia, followed by the removal of the heart. In the Myh11-CreER^{T2} mouse line, the Cre allele is inserted into the Y chromosome. Therefore, all the mice used in the study where we used the Myh11-Cre mouse model were males.

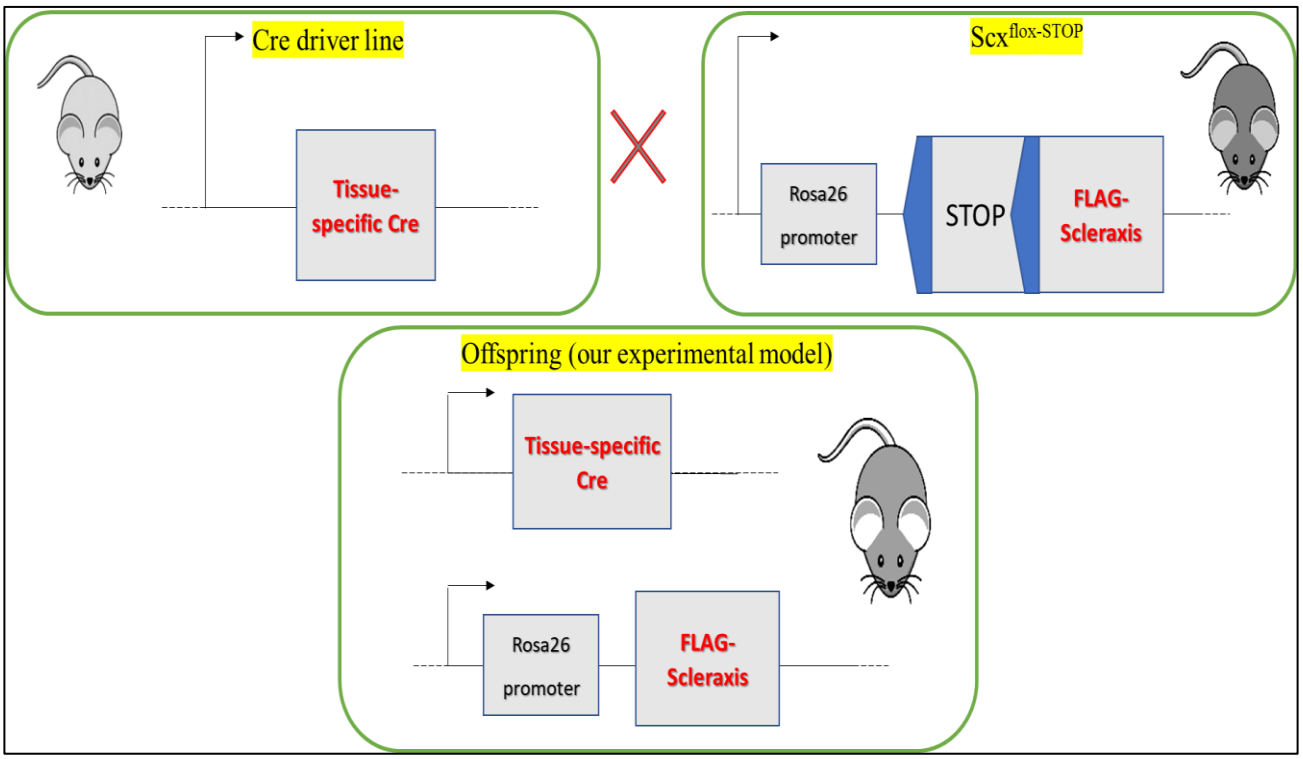

Figure 7: Schematic depicting the conditional scleraxis over-expression model.

A transgenic scleraxis mouse line under control of the Rosa26 promoter and containing a floxed premature stop codon was crossed to a Cre driver transgenic mouse line expressing Cre-recombinase under the control of a tissue-specific promoter, either Myh11Cre (vascular smooth muscle-specific expression) or TCF21iCre (fibroblast-specific expression). Tamoxifen is required for Cre to localize to the nucleus to enable the deletion of the stop codon. The resulting offspring will express scleraxis (lacking the premature stop codon) in all tissues where Cre is expressed.

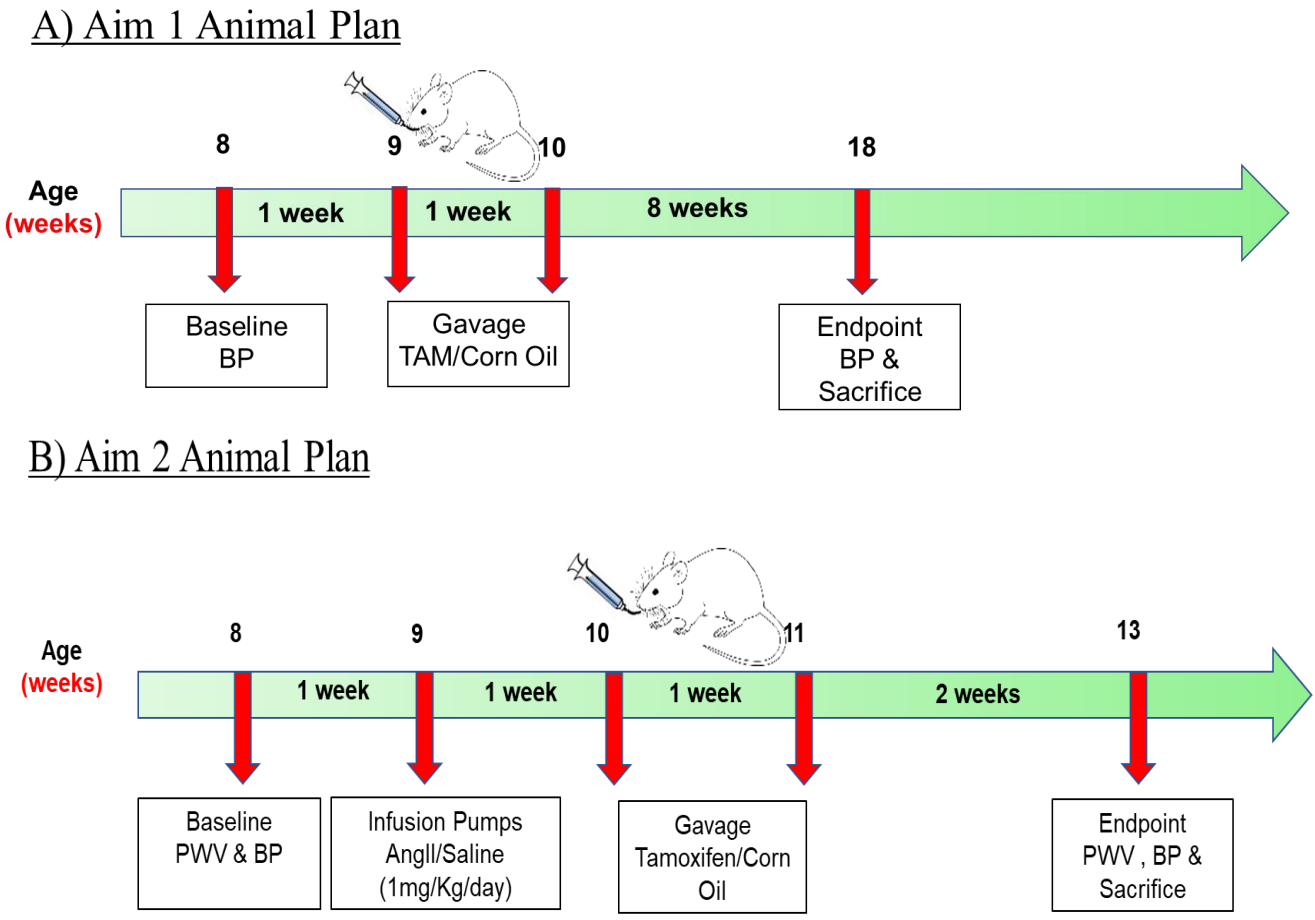

Figure 8. Timeline for the experimental animal models.

A) Timeline for animals for Aim 1. 8-week old mice underwent tail-cuff BP measurements initially, then were gavaged either with tamoxifen to induce Cre-expression or corn oil as a control. 8-weeks later, they underwent another BP measurement before sacrifice and tissue harvest. B) Timeline for animals in Aim 2. 8-week old animals were anesthetized and underwent baseline PWV measurement, followed by surgical implantation of a telemetry device. One week later, baseline BP was measured, and osmotic pumps were surgically implanted to deliver either AngII or saline control. One week later, animals were gavaged as described above and kept for

an additional 2 weeks. Endpoint PWV and BP were measured a few days before sacrifice and tissue harvest.

1.1 BP Measurements

For studies in the first aim, 8-week-old mice from each group were trained for 2 days to reduce the stress on mice that may alter the BP measurement. To achieve this training, the mice were habituated to the same experimental room and handled by the same technician. Additionally, they were conditioned to the blood pressure measurement procedure to minimize stress and anxiety. Actual BP measurements were recorded on the 3rd day using tail-cuff plethysmography (Mouse and Rat Tail Cuff BP (MRBP) System; IITC Life Science, Woodland Hills, CA). BP measurements were taken initially at the beginning of the study at the age of 8-9 weeks, and at the end of the study one day before sacrifice. At least 9 acceptable readings were obtained from each BP measurement and the average taken of all measurements to obtain the mean BP.

For studies involving osmotic pump-implanted mice, we used telemetry to measure BP. All telemetry hardware and software are HD-X10 Implants from Data Science International (MN, USA). Telemetry parameters recorded included, systolic, diastolic, mean arterial pressure, pulse pressure, activity and heart rate. Surgical implantation of the telemetry device was performed according to the manufacturer's instructions followed by a recovery period of at least 7 days. Animals were anesthetized, then the transmitter catheter was surgically placed in the left carotid and tunneled under the skin, with the device implanted into the ventral abdomen. All telemetry data were collected for a 24-h period in a designated quiet room where each mouse was singly housed and assigned to a specific receiver. Telemetry measurements were done for freely moving mice 3 times throughout the study: once at the beginning of the study, another in

the middle of the study one week after the gavage is completed, and once at the end of the study before sacrifice.

1.2 Pulse Wave Velocity Measurements

PWV of the femoral artery of anesthetized mice (in Aim 2) was measured at baseline (8 weeks of age) and endpoint (before sacrifice) with a 10-MHz electrocardiogram-traced Doppler probe (Indus Instruments, Houston, TX, USA). Three trace measurements were obtained per animal per time point. Analysis of the PWV data was performed in a blinded manner using the Doppler Signal Processing Workstation program (DSPW Version 1.624; Indus Instruments, Houston, TX, USA) to determine peak velocity, mean flow velocity, and minimum flow velocity.

2. Mesenteric Artery Isolation and Pressure Myography

Mesenteries were harvested and preserved in cold 1X Krebs buffer (118 mmol/L NaCl, 4.65 mmol/L KCl, 1.18 mmol/L $MgSO_4$, 1.18 mmol/L $KHPO_3$, 2.5 mmol/L $CaCl_2$, 25 mmol/L $NaHCO_3$, 5.5 mmol/L glucose, 0.026 mmol/L EDTA), (pH 7.4). 3rd order mesenteric arteries were isolated to maintain the consistency of all experiments. Arteries were mounted in a specialized pressure myograph chamber (Living Systems Instrumentation, Burlington, VT) containing Krebs buffer (pH 7.4). The pressure myograph system is characterized by being " a closed system to hold pressure" (i.e. one end was cannulated, and the other was occluded/tied off) as flow is not measured through this system (Fig. 9). Initially, one end of the vessel was cannulated and secured by a nylon tie onto a micro-cannula, then gently perfused from the intraluminal side with Krebs solution to remove the remaining luminal blood. Then, the other end of the vessel was occluded by being tied off on the micro-cannula without cannulation. The

artery was cannulated so that its walls were parallel and without stretch, similar to their normal physiological state.

Mouse small resistance mesenteric arteries were equilibrated for 30 minutes in aerated (20% O_2 and 5% CO_2) Krebs buffer (pH 7.4; 37°C) at a constant intraluminal pressure of 60 mm Hg. After equilibration, the internal vessel diameter was deemed the baseline diameter. To confirm the vessel`s viability, it was perfused with 125 mM KCl and considered viable if it constricted more than 30% of its baseline diameter in response. No change in intraluminal pressure during this process confirmed the vessel could hold pressure and that the ties were not leaking.

2.1 Mesenteric functional properties

Small resistance mesenteric arteries were equilibrated at 60 mm Hg and the diameter measured was taken as the diameter at equilibrium (Deq). Vessels were then pre-constricted by perfusing them with $1x10^{-6}$ M norepinephrine to reach maximal contraction (D0) just before adding a vasodilator. Vascular function was tested by perfusing the vessel with increasing concentrations of vasodilator drugs, either acetylcholine (10^{-9} M – 10^{-4} M), or sodium nitroprusside (10^{-9} M – 10^{-4} M) Both vasodilators were freshly prepared in Krebs solution supplemented with 10^{-6} M norepinephrine. Subsequently, changes in vessel diameters (Dx) were measured from the screen upon each distinct drug concentration applied. Functional responses were calculated at each increasing drug concentration as a percent diameter change using the following formula:

$$\%\ \boldsymbol{response} = (\boldsymbol{Dx} - \boldsymbol{D}0)/(\boldsymbol{Deq} - \boldsymbol{D}0) \times 100\%$$

- D0 is the diameter when pre-constricted

• Dx is the diameter when the vasodilator drug is applied

• Deq is the baseline diameter at 60 mm Hg

2.2 Mesenteric vascular geometry measurements

To remove the myogenic tone in mesenteries, they were deactivated by bath perfusion using Ca^{2+}-free Krebs solution (118 mmol/L NaCl, 4.65 mmol/L KCl, 1.18 mmol/L $MgSO_4$, 1.18 mmol/L $KHPO_3$, 25 mmol/L $NaHCO_3$, 5.5 mmol/L glucose, 0.026 mmol/L EDTA) containing a calcium chelator (1 mmol/L EGTA) for 30 - 60 minutes at 60 mm Hg intraluminal pressure. Therefore, measurements for passive arteriolar mechanics were applicable when the vessels were deactivated. Internal lumen diameter (Di) and the thickness of the vessel wall from the right and left sides were measured at three points along the length of the vessels at steady intraluminal pressure.

Other geometrical parameters were calculated based on the above measurements. This includes the Media to Lumen (M/L) ratio, which is calculated as the ratio of the media width from both sides of the wall (MW) to the internal lumen diameter (Di). The media Cross Sectional Area (CSA) is the measurement of the circumference of the vessel media when taking away the internal surface area by deduction of the internal CSA from the external CSA:

$$\boldsymbol{CSA} = \boldsymbol{\pi}(\boldsymbol{De^2} - \boldsymbol{Di^2})/4$$

***De** and **Di** are external and lumen diameters, respectively.

2.3 Mesenteric mechanical properties

Deactivated vessels were primed by gradually boosting the intraluminal pressure from 3 to 140 mm Hg. If any kink appeared in the vessel, the position of the cannula was modified to maintain parallel vessel walls. Vessel parameters including the internal lumen diameter and left

and right wall thicknesses were recorded while increasing the intraluminal pressure from 3 to 140 mm Hg.

At each point where intraluminal pressure was increased, the wall thickness and internal lumen diameter were measured, and from these measurements, stress and strain were calculated and plotted to represent the vessel compliance.

Media strain, which represents the amount of force that induces changes in vessel diameter, was calculated as:

$$\boldsymbol{\mathcal{E}} = (\boldsymbol{D} - \boldsymbol{D}0)/\boldsymbol{D}0$$

D is the lumen diameter at a specific intraluminal pressure and **D0** is the diameter at 3 mm Hg.

Circumferential stress, which reflects the amount of force that the vessel wall resists when applied, was determined by:

$$\boldsymbol{\sigma = PD/2M}$$

where P is the intraluminal pressure in dyn/cm^2 (1 mm Hg= 1.334 x 10^3 dyn/cm^2), D is the internal diameter and M is the media thickness.

The elastic modulus **EM** was calculated by measuring the change of the slope of the stress-strain data from the exponential equation **($y = ae^{bx}$)**:

$$\boldsymbol{EM} = \boldsymbol{\sigma}0\boldsymbol{e}^{\boldsymbol{\beta\mathcal{E}}}$$

σ 0 is stress at the baseline diameter of 3mm Hg and β is a constant related to the rate of increase in the stress-strain curve. The slope of the EM versus stress curve reflects the intrinsic stiffness of the wall components.

For a better understanding of the pressure myography procedural steps and the measurements that were followed, it is recommended to refer to this informative paper in the link below [7]:

https://doi.org/10.1152/ajpheart.01021.2020

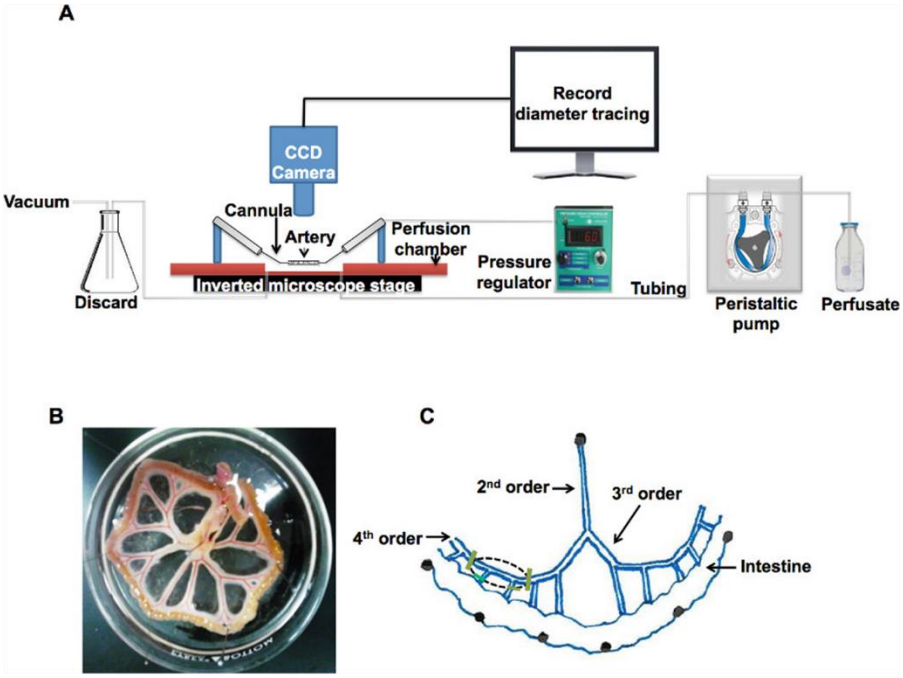

Figure 9. Illustration of the pressure myography chamber using mesenteric arteries.

A) Pressure myography system components contain a peristaltic pump to perfuse the vessel in the chamber, a pressure regulator to maintain the intraluminal pressure in the system, and a camera to record the changes in vessel geometrical parameters during the experiment. B) Mouse mesenteries were collected and pinned in a dissection dish. C) Schematic graph illustrating the 3rd order mesenteric artery location to be isolated.

This figure is adapted with permission from Jadeja, R. N., Rachakonda, V., Bagi, Z., Khurana, S. Assessing Myogenic Response and Vasoactivity in Resistance Mesenteric Arteries Using Pressure Myography. J. Vis. Exp. (101), e50997, doi:10.3791/50997 (2015) [179]

3. **Tissue fixation and staining**

Mice aortas were isolated and fixed in 10% buffered formalin, then embedded into paraffin blocks. Paraffin-embedded tissues were sectioned at 0.5 µm thickness, then tissue sections were processed accordingly.

3.1 Immunohistochemistry (IHC) staining

Tissue sections were stained with hematoxylin and eosin (H&E), Masson's trichrome (MT), or Picrosirius red (PR) for collagen fibers, or with Verhoeff-Van Gieson (VVG) staining for elastic fibers. Quantification of elastin vs. collagen ratio was done by comparing Black -VVG vs. Purple-MT surface area. These and other measurements including CSA and wall thickness were performed using Image-Pro Plus (Media Cybernetics, USA).

3.2 DAB staining

Paraffin-embedded tissue sections were deparaffinized on a heating-plate at 65°C for 20 mins. Then they were embedded in xylene for 10 mins and subsequently washed in 95% ethanol twice for 10 mins each. Next, the sections were incubated for 1 hour in blocking buffer (1% Bovine Serum Albumin, 0.3% Triton X100, 5% skim milk). The scleraxis primary antibody (diluted 1:50, Abcam ab58655) was prepared in 20% blocking buffer, then added to each section and incubated overnight at 4°C in a humidified chamber. The antibody solution was then washed three times with 1X PBS for 20 mins each. For the subsequent step, the secondary anti-rabbit Horseradish peroxidase conjugate (HRP) (dilution 1:50, Cell Signaling 7074S) was diluted in 20% blocking buffer in 1X PBS. It was added to each section and left to incubate for 3 hours at room temperature in a humidified chamber. The sections were then washed in 1X PBS for 20 mins. Finally, DAB chromogen was prepared using 1% of DAB Chromogen Concentrate in stable

peroxide substrate buffer (Cat. 1855910, Thermo Scientific). The mixture was well-mixed and subsequently added to each section. After 15 mins of incubation, the sections were monitored under microscope. For better staining, sections were incubated with the DAB overnight at 4°C in a humidified chamber. They were then washed twice with 1XPBS for 5 mins, followed by immersion in water. Hematoxylin (Sigma, HHS32) was applied for nuclear staining and incubated for 20 minutes at room temperature. Subsequently, the sections were washed with 2% sodium bicarbonate once to adjust the pH and achieve the bluish colour of the nuclei. Afterward, the sections were washed in ddH_2O, then in 95% ethanol twice for 10 mins, and finally in xylene once for 10 mins. They were subsequently dried and mounted on coverslips using a mounting medium consisting of 50% xylene (Fisher Scientific, Canada). Imaging was performed using an Olympus DP23 microscope, with cellSens standard software 4.1. The data were quantified by counting the dark brown stained cells, which were identified as scleraxis positive cells, within each square area. This analysis was conducted using four sections from each animal within each respective group.

3.3 Immunofluorescence to measure vascular cellularity

Sections were processed using a similar method as described above. Sections were incubated with the primary αSMA antibody (Sigma 92547) or Ki67 antibody (Abcam 92742) overnight at 4°C in a humidified chamber. Subsequently, the sections were incubated in secondary antibody, goat anti-mouse Alexa Fluor 594- red (ThermoFisher Scientific, Canada) for 3 hours at room temperature in a humidified chamber. To visualise the cell nuclei, sections were stained with chromosome counterstain 4′,6-diamidino-2-phenylindole (DAPI) (NovusBio 2-31156). Imaging was performed using an inverted fluorescence microscope (Olympus IX81). Cell counting was manually conducted using Olympus cellSens standard software. The cell counting involved identifying and quantifying the blue nuclear staining within the red stain of the αSMA-demarcated

area in the aorta. The quantification of the average of two merged images at 20X magnification per section per animal was performed.

The αSMA intensity was measured in images magnified at 10X to encompass the entire vessel area, employing ImageJ 1.54f software. The region of interest was focused on the aorta in the red-channel, and measurements were configured for area integrated density and mean grey value. Additionally, the background fluorescence was measured in an area without any fluorescence present. Using the following equation, the corrected total cell/tissue fluorescence was then determined:

Corrected Total Cell/ Tissue Fluorescence (CTCF) = Integrated Density – (Area of selected tissue X Mean fluorescence of background readings).

4. **Cell culture and *in vitro* studies**

Human Aortic Smooth Muscle Cells (HAOSMC) were purchased from Sigma Aldrich (C-12533) and cultured in a humidified incubator at 37°C and 5% CO_2 in Smooth Muscle Cell Growth Supplemented Medium (C-22062). Low passage HAOSMC (P4 to P8) were plated and grown to 60% confluency in culture dishes and then starved in basal medium without supplement for 24 hours to arrest all cells at similar cell cycle.

Cells were then infected with adenoviruses expressing either Scleraxis (AdScx) or Green Fluorescent Protein (AdGFP) at a multiplicity of infection of 10 in serum-free medium for 72 hours. In some experiments, cells were also treated with either 100 nM AngII (Sigma A9525) or saline for 24 hours post-infection.

4.1 CCK8 cell proliferation assay

Cell proliferation was analyzed using a Cell Counting Kit-8 (CCK-8) (CK04-011; Dojindo Laboratories, Rockville, MD, USA), according to the manufacturer's directions. Briefly, HAOSMC were plated in 96-well plates and infected with AdScx, AdGFP, or AdLacZ, or were uninfected, for 24, 48, or 72 h as above. CCK-8 solution was added to each well, except for 3 baseline control wells from each of the treated groups. Plates were incubated at 37 °C for 1 h, then the optical density at 450 nm was measured for each well using a microplate reader. Baseline mean was subtracted from each sample value, and the results were then normalized to untreated cells.

4.2 Flow cytometry (cell proliferation and cell cycle)

HAOSMC were starved for 24 hours, then infected by AdScx or AdGFP and treated with AngII or vehicle 24 hours post-infection as above. Click-iT™ Plus EdU Alexa Fluor™ 647 Flow Cytometry Assay Kit, (Invitrogen, C10635) was then used per the manufacturer`s instructions. Briefly, 72 hours post-infection, EdU was added to the culture medium at 10 μmol/L final concentration for 2 hours. Cells were then trypsinized and harvested. After centrifugation and washing the pellet, cells were fixed using Click-iT® fixative for 15 mins, then washed and permeabilized by 1X Click-iT® saponin-based permeabilization and wash reagent. Cells were incubated for 30 mins in a Click-iT cocktail reaction containing Alexa Fluor647. After washing, cells were incubated with DAPI to stain DNA and assess the cell cycle. Cells were then resuspended for flow cytometry analysis. Acquisition of cell samples was performed on a Beckman Coulter Cytoflex LX diginal flow cytometry analyzer (Beckman Coulter). DAPI was excited by 405nm violet laser, and its emission is filtered with 450/50 BP filter. Alexa647-EdU

was excited by 640nm red laser, and its emission was filtered with 660/20 BP filter. Data were analyzed with CytExpert (Beckman Coulter).

5. **Protein extraction & western blot**

Mice aortas were harvested and flash-frozen in liquid nitrogen. Tissues were weighed and freeze-crushed in tissue lysis buffer. All prep DNA/RNA/Protein Mini Kit (Cat. no. 80004, Qiagen) was used per the manufacturer's instructions, with both RNA and protein isolated from the same aorta.

For western blot analysis, 30 µg protein was diluted and denatured in 2x Laemmli sample buffer (Bio-Rad Laboratories). Samples were heated at 95°C for 5 min and then loaded onto Bio-Rad 4%–15% Mini-PROTEAN® TGX Stain-Free™ precast SDS-PAGE gels (Bio-Rad Laboratories). Gels were activated using the Bio-Rad ChemiDoc™ MP imager (Bio-Rad Laboratories) after electrophoresis, followed by semi-dry transfer onto methanol activated-PVDF membranes (Bio-Rad Laboratories) using the Bio-Rad Trans-Blot® Turbo™ transfer system (Bio-Rad Laboratories). Membranes were then blocked with 5% skim milk in Tris-buffered saline (pH 7.5) with 0.1% Tween® 20 (Sigma-Aldrich) (TBST) buffer for 1 h at room temperature. Blots were incubated overnight at 4°C with primary antibodies diluted in 1% skim milk in TBST buffer.

Antibodies used for immunoblotting were as follows: Ki67 (14-5698-82, Invitrogen;1:1000), Scleraxis (PA5-23943, Invitrogen;1:1000), PCNA (13-3900, Thermofisher,1:2000). Membranes were incubated in anti-rabbit secondary antibody conjugated to horseradish peroxidase (1:5000; 7074, Cell Signaling Technology) in 2% skim milk in TBST buffer for 1 h at room temperature and then washed for 10 min, 3 times, with TBST. Proteins were visualized using Clarity™ Western enhanced chemiluminescent substrate (Bio-Rad

Laboratories) and a Bio-Rad ChemiDoc™ MP imager (Bio-Rad Laboratories). Protein quantification was analyzed using Image Lab software (Bio-Rad Laboratories) with normalization to total protein loading and compared to the untreated cells as a control.

6. **Quantitative real-time PCR (Primer list)**

Mice aortas were processed as above using All Prep DNA/RNA/Protein Mini Kit (Cat. no. 80004, Qiagen) used per manufacturer's instructions for RNA isolation. cDNA was generated from 1000 ng RNA samples using an iScript cDNA Synthesis kit (Bio-Rad, USA). qPCR reactions were prepared using Advanced Universal SYBR Green Supermix (Bio-Rad, USA) and 1:6 diluted cDNA template along with 200 nM forward and reverse primers. Together, the total volume of forward and reverse primers used is 1µl per the total reaction mix volume of 10 µl . PCR amplification was performed in duplicate for each reaction on a CFX384 Touch Real-Time PCR (Bio-Rad, USA). The cycling conditions were as follows: 95°C (3 min), followed by 40 cycles of denaturation at 95°C (15 s), then 60°C (30s) annealing and extension at 72°C (30 s). After amplification, a continuous melt curve was generated from 60 to 95°C to confirm the generation of single amplicons. Relative gene expression was calculated using the $2^{-\Delta\Delta Ct}$ method with normalization to GAPDH (primer sequences as in the table below, listed 5' to 3'). Amplicon identity was confirmed by sequencing.

Table 2: qPCR Human Primers

Target	Forward	Reverse
Scleraxis	GTGAACACGGCCTTCACGG	CTGCGAATCGCTGTCTTTC
GAPDH	AGAAGGCTGGGGCTCATTTG	AGGGGCCATCCACAGTCTTC
Calponin	AGCTAAGAGAAGGGCGGAAC	CATCTGCAGGCTGACATTGA

Myh11	TGGAACTTCATCGACTTTGGG	ACAGCTTCTCCACGAAAGAC
SM22α	AACAGCCTGTACCCTGATGG	CGGTAGTGCCCATCATTCTT

Table 3: qPCR Mouse Primers

Target	Forward	Reverse
Scleraxis WT	ACAGATCTGCACCTTCTG	GCTCAGATCAGGTCCAA
Scleraxis Transgenic (TG)	ACAGATCTGCACCTTCTG	CTGATCAGCGAGCTCTAC
Col 1α1	TGCTCCTCTTAGGGGCCA	CGTCTCACCATTAGGGACCCT
Col 3α1	GGTTTCTTCTCACCCTGCTTC	GGTTCTGGCTTCCAGACATC
Elastin	GCTGCTGCTAAGGCTGCTAA	ACCATAGCCAGGAAAGCCAC
Fibronectin	CATTTGCTCCTGCACGTGTT	GGTGGGGCTGGAAAGATTACT
GAPDH	TCACCACCATGGAGAAGGC	GCTAAGCAGTTGGTGGTGCA

7. **Statistics and data analysis**

Results are expressed as mean ± SD. All analysis was performed using GraphPad Prism 9.5.0 (GraphPad Software Inc., CA, USA). Statistical differences were assessed using two-way analysis of variance (ANOVA) with multiple comparisons with Tukey`s post-hoc analysis. Mechanical properties were analyzed first by using either non-linear regression analysis if the plot was curved or linear regression if the plot was linear. Non-linear regression was performed using an exponential growth equation and the k-value was used to compare differences between values for using one-way ANOVA with multiple comparisons which is similar to the slope obtained using linear regression analysis. Functional responses were compared using non-linear

regression and then using two-way ANOVA with multiple comparisons. A value of $p<0.05$ was considered significant.

CHAPTER 3: RESULTS

1. Scleraxis upregulation in blood vessels of the TCF21iCre-Scx^{TG} mouse model (fibroblast overexpression).

Lineage tracing studies utilizing a tamoxifen-inducible Cre expressed from the TCF21 locus have revealed the commitment of TCF21-expressing epicardial cells to the cardiac fibroblast lineage through development. Moreover, it has been observed that TCF21 null hearts fail to generate cardiac fibroblasts. These findings identified the crucial role of the TCF21 transcription factor in the development of cardiac fibroblasts [177, 180]. In our laboratory, we have previously utilized the TCF21iCre mouse line to explore the involvement of scleraxis in cardiac fibroblasts using a TAC mouse model [181].

By crossing an established scleraxis transgenic mouse line with a floxed premature stop codon with tamoxifen-inducible fibroblast specific Cre driver lines, we generated TCF21iCre-Scx^{TG} mouse model that upregulates scleraxis expression specifically within the fibroblasts upon tamoxifen induction.

1.1 Scleraxis overexpression is specifically limited to the fibroblasts in the TCF21iCre-Scx^{TG} mouse model.

To validate the specific upregulation of scleraxis in the fibroblasts located within the adventitial layer surrounding the aorta in the TCF21iCre-Scx^{TG} mouse model, we conducted immunohistochemistry staining using a scleraxis antibody on aortic sections from TCF21iCre-Scx^{TG} and TCF21iCre-Scx^{WT} mice. The DAB immunohistochemistry images clearly display

positive brown precipitate staining for TCF21iCre-Scx^{TG} within the adventitia in images either with hematoxylin (Fig. 10A) or without hematoxylin (Fig. 10B). This positive staining confirms the upregulation of scleraxis expression, specifically in the fibroblasts within the adventitial layer, with no scleraxis in the medial or intimal layers.

In DAB immunohistochemistry, hematoxylin is used to visualize the cell nuclei. Given that the scleraxis antibody targets the localization of scleraxis within the nucleus, we performed staining both with and without hematoxylin. This approach allows for a clear and distinct visualization of the scleraxis antibody staining within the nucleus and ensures that there is no interference of overlapping signals, preventing masking of the weak nuclear signal from the scleraxis by the counterstain from hematoxylin.

A.

TCF21iCre-Scx^{WT}

TCF21iCre-Scx^{TG}

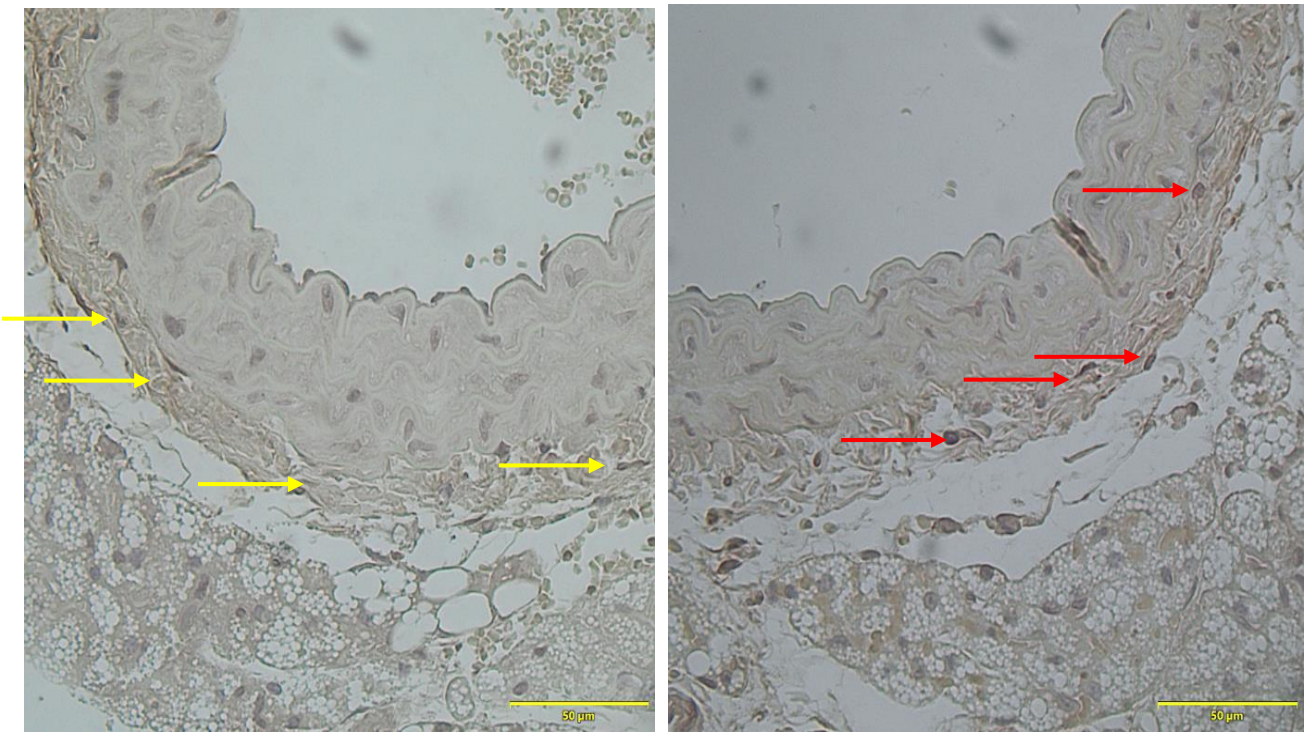

B.

TCF21iCre-Scx^{WT}

TC21iCre-Scx^{TG}

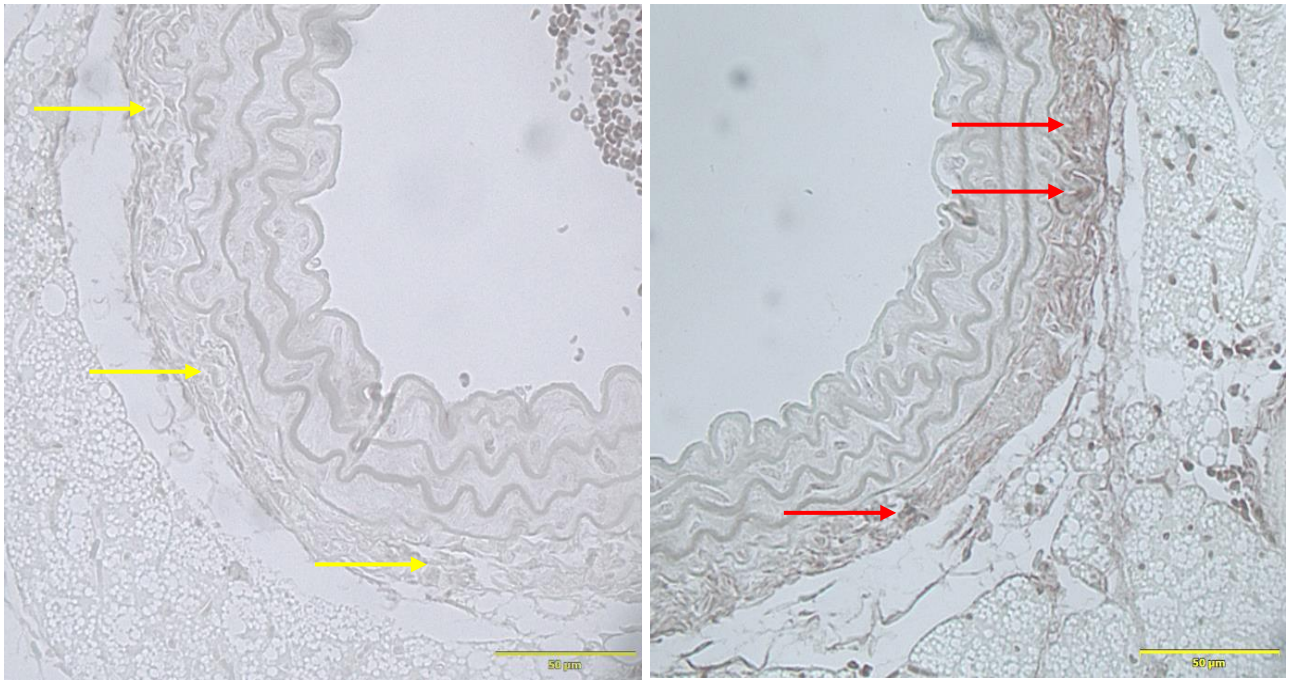

Figure 10. Specific upregulation of scleraxis expression in fibroblasts of aortas in TCF21iCre-Scx^{TG} mice.

DAB immunohistochemistry was performed on aortic sections from mice in two groups: TCF21iCre-Scx^{TG}, where scleraxis overexpression in fibroblasts was induced by tamoxifen, and TCF21iCre-Scx^{WT}, which is the control group that received corn oil. The images demonstrate DAB immunohistochemistry staining in these sections to verify that scleraxis upregulation is specific to the fibroblasts within the aortic tissues.

(A) These images indicate DAB immunohistochemistry results, with nuclei stained using counterstain hematoxylin. The darker brown precipitate observed in the adventitia (marked by red arrows) indicates positive staining, indicating the upregulation of scleraxis expression in fibroblasts within the TCF21iCre-Scx^{TG} aortic sections. In contrast, the control samples from TCF21iCre-Scx^{WT} (yellow arrows) show that scleraxis upregulation is absent. (B) DAB images without the counterstain hematoxylin. Images from TCF21iCre-Scx^{TG} aortic sections (marked by red arrows), show a positive darker brown precipitate that is unmasked from hematoxylin staining, indicating the upregulation of scleraxis expression that is absent in control sections of TCF21iCre-Scx^{WT} mice (yellow arrows). Scale bar =50 μm, representative of n =2.

1.2 Scleraxis upregulation in arterial fibroblasts does not alter the blood pressure in TCF21iCre-Scx^{TG} mice.

Tail cuff blood pressure measurements were conducted by the animal husbandry team at baseline before gavage, and at the endpoint of the study just before animal sacrifice, for all animals in both groups TCF2iCre-Scx^{WT} and TCF21iCre-Scx^{TG}. The blood pressure parameters assessed include systolic, diastolic, and mean blood pressure.

Our data show no significant differences in any of the blood pressure parameters between baseline and endpoint in either control (TCF21iCre-Scx^{WT}) or fibroblast-targeted scleraxis over-expression (TCF21iCre-Scx^{TG}) mice (Fig. 11). These results suggest that upregulating scleraxis alone in fibroblasts for 8 weeks is not sufficient to alter blood pressure in mice.

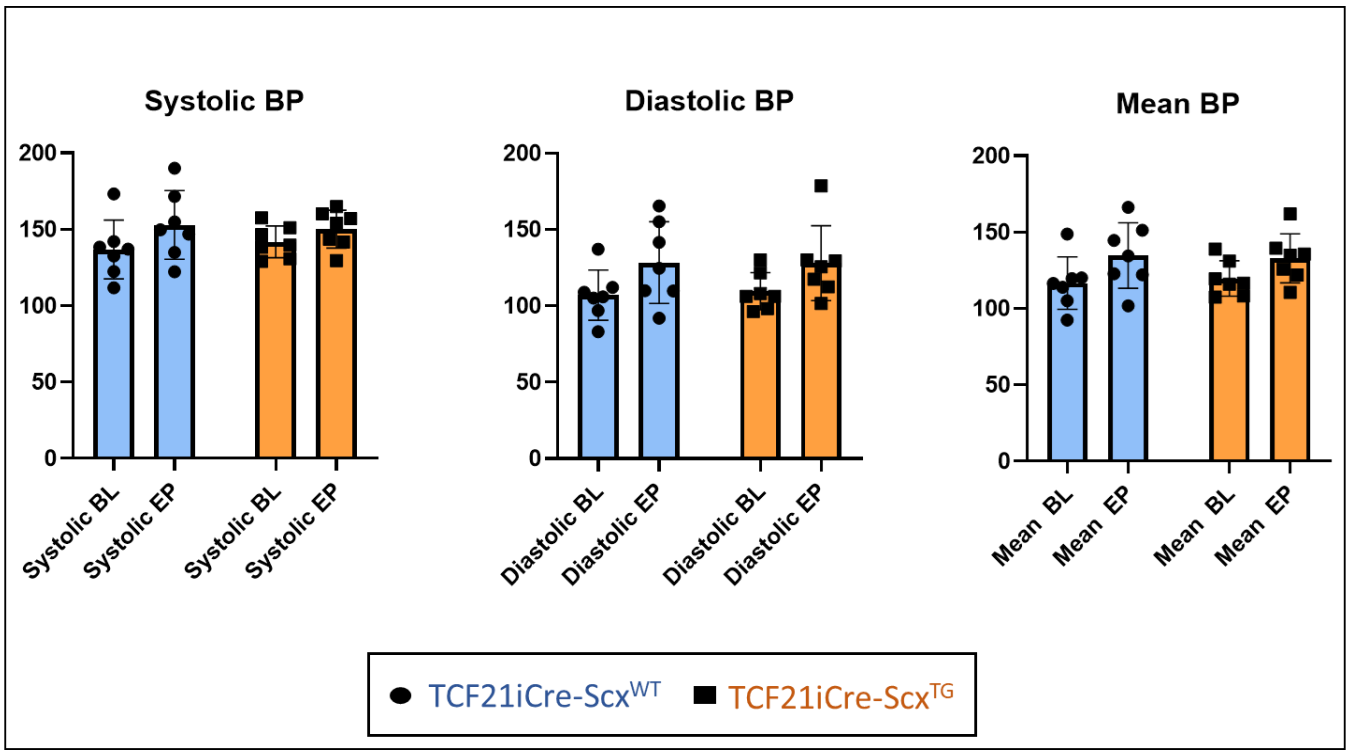

Figure 11. Blood pressure measurement in TCF21iCre-Scx^{WT} and TCF21iCre-Scx^{TG} mice.

Blood pressure was measured using tail-cuff plethysmography at baseline at the age of 8 weeks and at endpoint before sacrificing at the age of 17-18 weeks. There is no change in blood pressure parameters in TCF21iCre-Scx^{TG} scleraxis overexpressing mice compared to control mice TCF21iCre-Scx^{WT}. Data are shown as mean ± SD (n=7).

1.3 Scleraxis upregulation in fibroblasts does not alter aortic structural and molecular components.

1.3.1 Scleraxis upregulation in aortic fibroblasts does not cause structural changes in TCF21iCre-Scx^{TG} aortas.

Aortic sections of TCF21iCre-Scx^{WT} and TCF21iCre-Scx^{TG} mice were stained to investigate if scleraxis upregulation in fibroblasts could alter the structure of large conduit vessels. Aortic sections were stained using various stains, including hematoxylin and eosin (H&E) for overall assessment of aortic structure, Verhoeff-Van Gieson (VVG) staining to visualize elastin fibers and Picrosirius Red (PR), or Masson's trichrome (MT) for collagen visualisation.

Our findings reveal no notable difference between TCF21iCre-Scx^{TG} aortas compared to control TCF21iCre-Scx^{WT} as observed by different stains (Fig. 12). Additionally, no detectable alterations were noted in the quantity of collagen and elastin fibers, and there were no observed changes in the thickness of the vascular wall or the diameter of the lumen. In summary, these findings collectively suggest that the over-expression of scleraxis in fibroblasts does not induce structural modifications in the gross anatomy of the aorta.

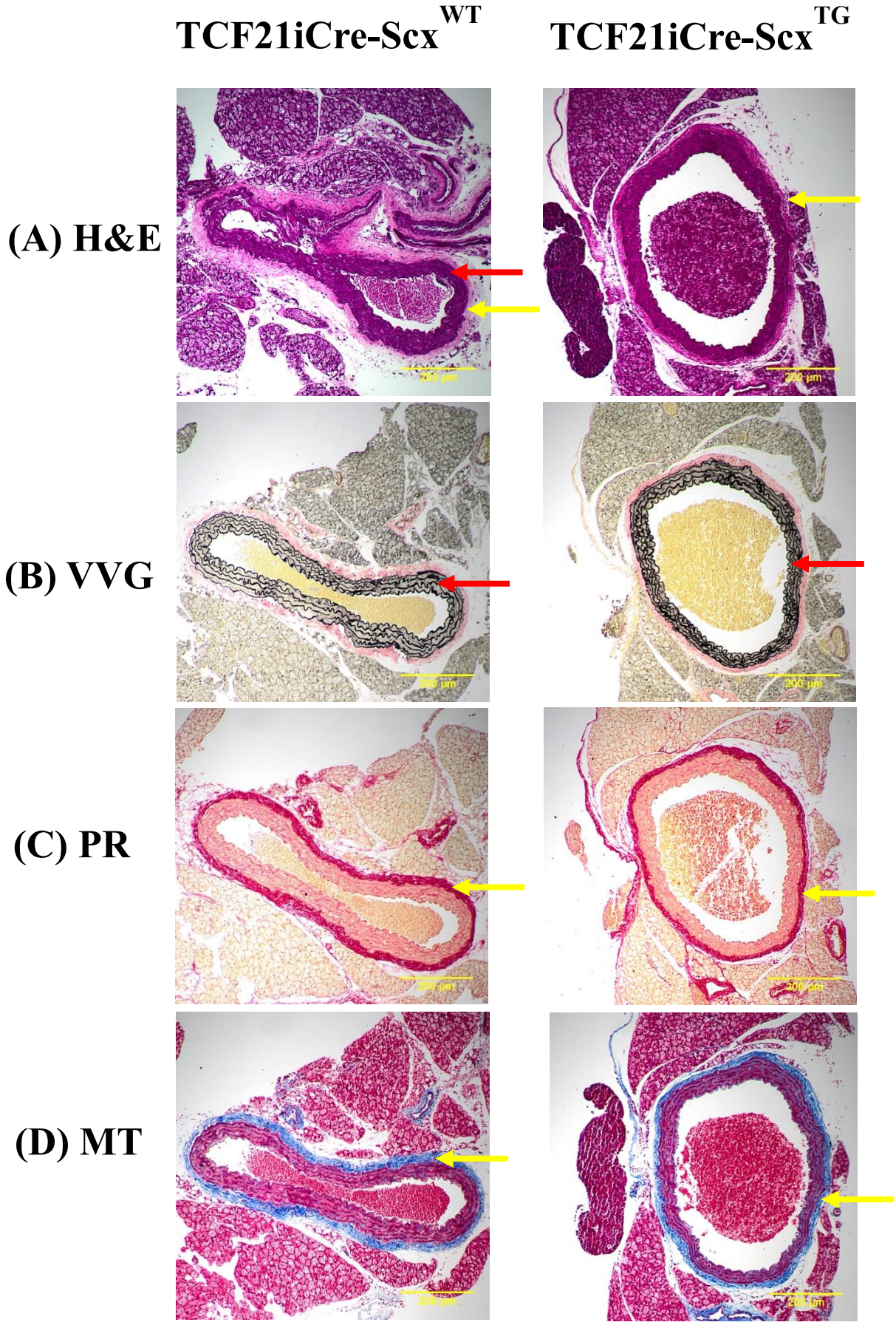
TCF21iCre-Scx^WT
TCF21iCre-Scx^TG
(A) H&E
(B) VVG
(C) PR
(D) MT

Figure 12. Representative images of histological sections to assess structural changes from TCF21iCre-Scx^{TG} mice aortas.

Immunohistochemical images of aortic sections stained with (A) hematoxylin and eosin (H&E) for the overall assessment of aortic structure, where hematoxylin stains the cell nuclei dark purple, and eosin stains the overall structure with colours varying from purple to pink, in this context, the media appears purple (red arrow), and the adventitia appears pink (yellow arrow) (B) Verhoeff-Van Gieson (VVG) staining is used to visualize elastin content, which is represented by black fibers within the media (red arrow) (C) Picrosirius Red (PR) and (D) Masson's trichrome (MT) staining are employed for collagen visualization. In PR staining, collagen is represented by the red color mainly in the adventitia (yellow arrow) (C), while MT staining presents collagen in a bluish color (yellow arrow) (D). No obvious structural changes were identified following scleraxis over-expression in fibroblasts in aorta sections from TCF21iCre-Scx^{TG} compared to aorta sections from control TCF21iCre-Scx^{WT}. Scale bar = 200 µm, (n= 4 animals , with 3 sections per animal).

1.3.2 No changes in the molecular components of aortas of TCF21iCre-Scx^{TG} mice were induced by scleraxis over-expression.

To confirm that scleraxis is upregulated at the mRNA level and to assess the effect of scleraxis over-expression on the expression of the pro-fibrotic genes, qPCR analysis was performed.

Our findings show that transgenic scleraxis mRNA levels are significantly increased in TCF21iCre-Scx^{TG} aortas ($P<0.05$). In contrast, the level of wild type scleraxis mRNA shows a non-significant trend towards a decrease, which may suggest the possibility that transgenic scleraxis could modulate the expression of wild type scleraxis, however, further experimental evidence is needed to confirm this hypothesis. Transgenic scleraxis overexpression is not sufficient to upregulate the expression of other ECM genes including Col 3α1, Col 1α1, fibronectin, and elastin in the aorta (Fig. 13). This data indicates that, in sharp contrast to its role in cardiac fibroblasts and myofibroblasts, scleraxis overexpression doesn't upregulate pro-fibrotic genes in the aorta and does not alter the vascular adventitia.

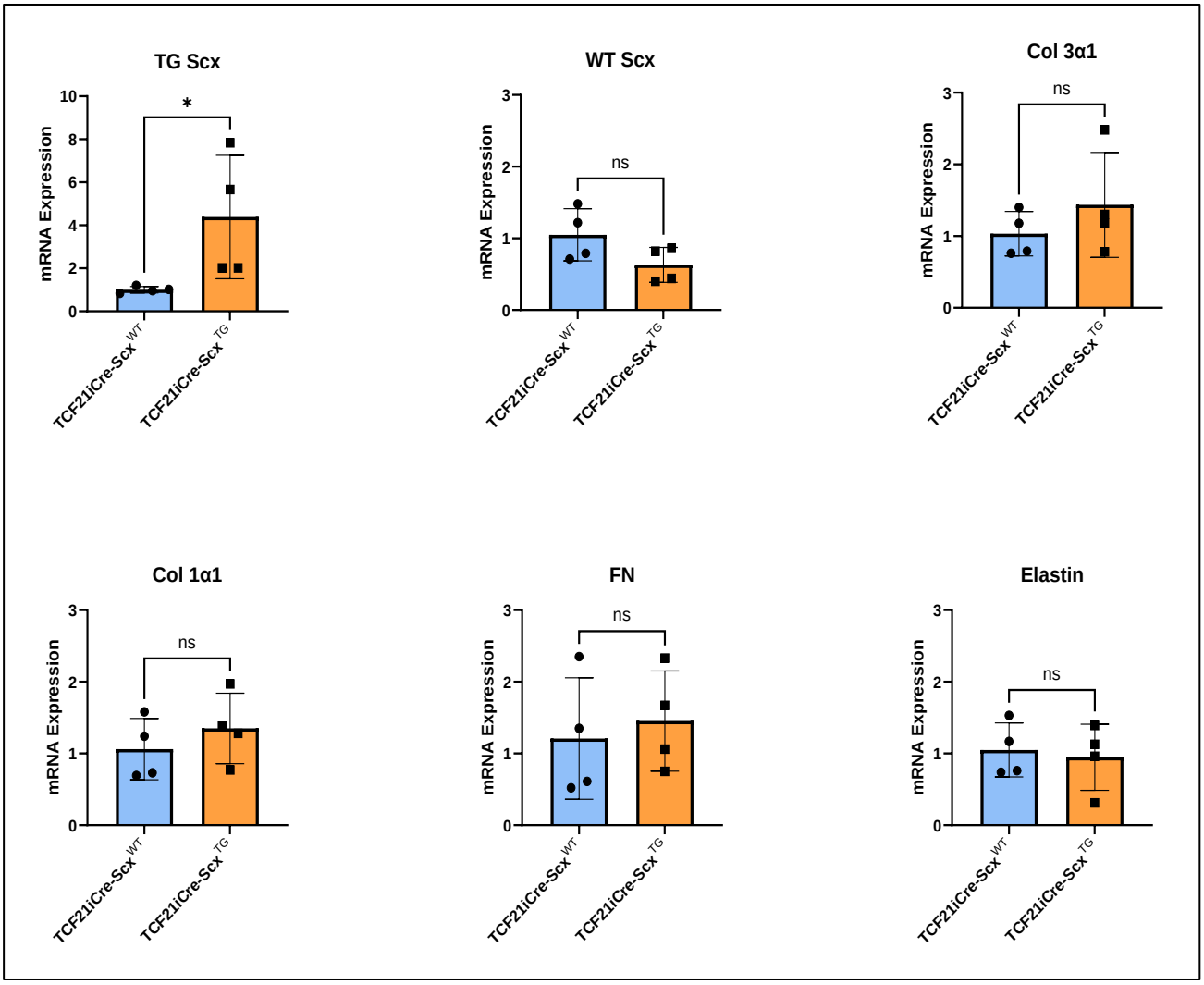

Figure 13. Gene expression of pro-fibrotic markers from aortas of scleraxis upregulated TCF21iCre-Scx^{TG} mice.

Transgenic scleraxis (TG Scx) is significantly upregulated in TCF21iCre-Scx^{TG} aortas vs. control (*P<0.05). Wildtype scleraxis (WT Scx) shows a trend towards a decrease but is not significant in TCF21iCre-Scx^{TG} aortas vs. controls. mRNA gene expression of Col1α1, Col3α1, fibronectin, and elastin show no difference between TCF21iCre-Scx^{TG} vs. TCF21iCre-Scx^{WT} control. Data are shown as mean ± SD, n=4.

1.4 Scleraxis upregulation in the fibroblasts does not trigger obvious structural, mechanical, or functional changes in small mesenteric resistance arteries.

1.4.1 Scleraxis upregulation in fibroblasts does not alter the structural properties of small resistance mesenteric arteries.

The geometric structure of cannulated mesenteric arteries was assessed using pressure myography technique. Mesenteric arteries were measured under inactive conditions (Ca^{2+}-free Krebs) at 60 mm Hg intraluminal pressure. No structural changes were identified in mesenteries of scleraxis over-expression mice vs. control mice in terms of CSA, media thickness and M/L ratio (Fig. 14). This result indicates that scleraxis upregulation in fibroblasts doesn't alter the geometrical parameters in mesenteric resistance arteries.

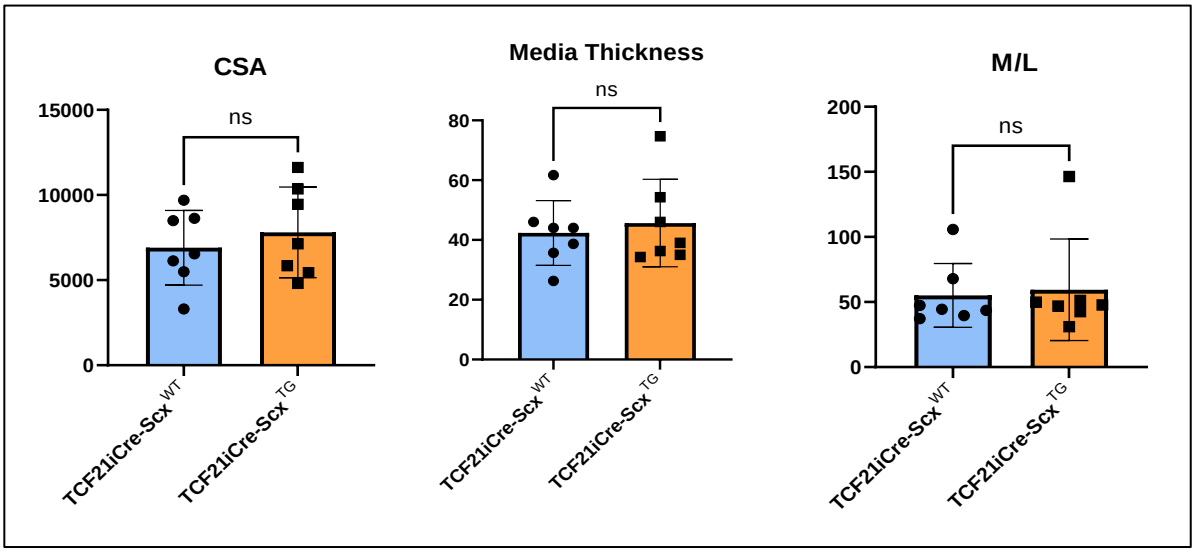

Figure 14. Structural parameters of small mesenteric resistance arteries from TCF21iCre-Scx^{TG} and TCF21iCre-Scx^{WT} mice.

No changes in media cross sectional area (CSA), wall thickness, and media to lumen ratio (M/L) ratio between the mesenteric arteries of TCF21iCre-Scx^{TG} vs. TCF21iCre-Scx^{WT} were observed. Data are shown as mean ± SD, n=7 .

1.4.2 Scleraxis upregulation in fibroblasts does not alter the mechanical properties and stiffness of small mesenteric resistance arteries.

Media stress and strain were calculated based on the lumen diameter and wall thickness parameters while increasing intraluminal pressure from 0 to 140 mm Hg. The resulting data was then plotted on a curve that illustrates vascular compliance, which is a measure of the ability of blood vessels to expand and contract in response to changes in pressure. Our findings show that there is no difference in the stress-strain curve in arteries from TCF21iCre-Scx^{TG} vs. TCF21iCre-Scx^{WT} (Fig. 15A). These curves were quantified through the k-value, which shows no differences between groups (Fig. 15B), suggesting that scleraxis over-expression in fibroblasts does not change vascular compliance in the small mesenteric arteries TCF21iCre-Scx^{TG}.

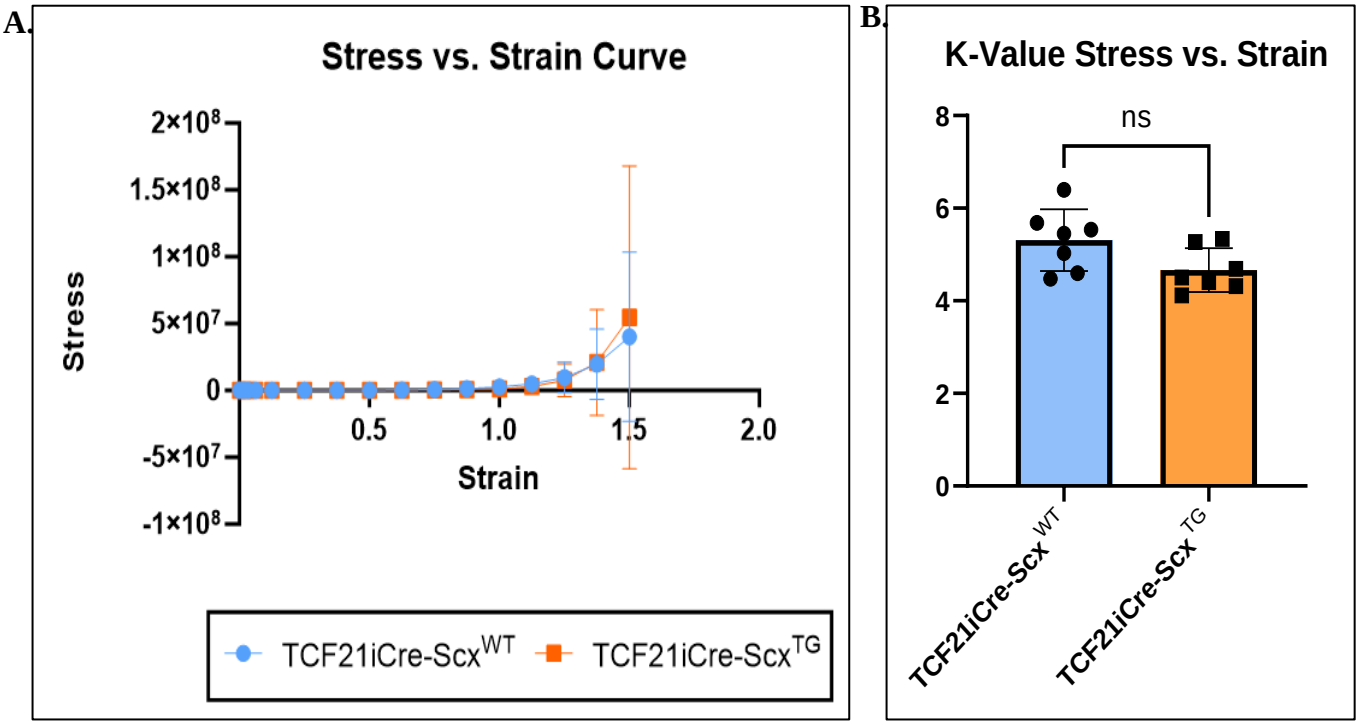

Figure 15. Wall stress-strain relationships for mesenteric arteries from TCF21iCre-Scx^{TG} mice.

(A) The stress-strain curve of TCF21iCre-Scx^{TG} shows no change compared to TCF21iCre-Scx^{WT} control mice. (B) The k-value data are non-significant. Data are shown as mean ± SD. n = 7.

The isobaric wall stress of TCF21iCre-Scx^{TG} mesenteric arteries is similar to controls, as represented by the stress–pressure curve and quantified by the slope of stress vs. pressure (Fig. 16A and16B).

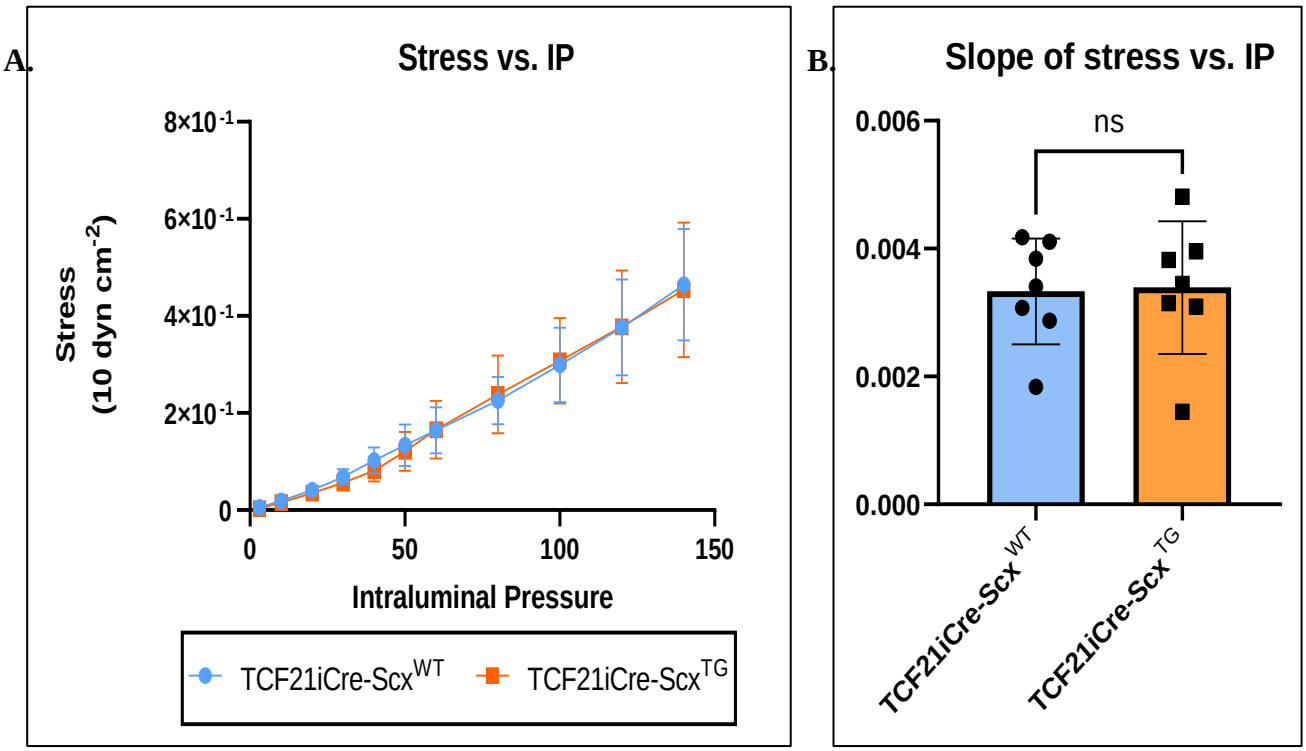

Figure 16. Isobaric stress plot of small mesenteric arteries in TCF21iCre-Scx^{TG} vs. TCF21iCre-Scx^{WT} mice.

(A) Stress–pressure curves in small mesenteric arteries are similar between TCF21iCre-Scx^{TG} compared to TCF21iCre-Scx^{WT} control. (B) Stress-pressure linear curves were quantified by comparing the slopes from TCF21iCre-Scx^{TG} vs. TCF21iCre-Scx^{WT} mice and showed no difference. Data are shown as mean ± SD. n = 7.

Elastic modulus is the arterial stiffness that is caused by arterial geometry and wall components and is calculated based on the exponential growth of the slope between stress and strain. The EM-intraluminal pressure (IP) curve thus represents the change in vascular stiffness due to changes in arterial wall components and geometry, while the EM-media stress curve identifies vascular stiffness alterations due to changes in vascular wall components only. Our findings, represented by the EM-pressure & EM-stress curves, show that scleraxis over-expression in fibroblasts does not alter mesenteric artery geometry or wall components (collagen and elastin), respectively (Fig. 17A, B; Fig. 18A, B). In general, our findings suggest that scleraxis upregulation in fibroblasts doesn't alter the geometry or wall components of mesenteric arteries, consistent with the lack of target gene expression changes in the aorta (Fig. 13).

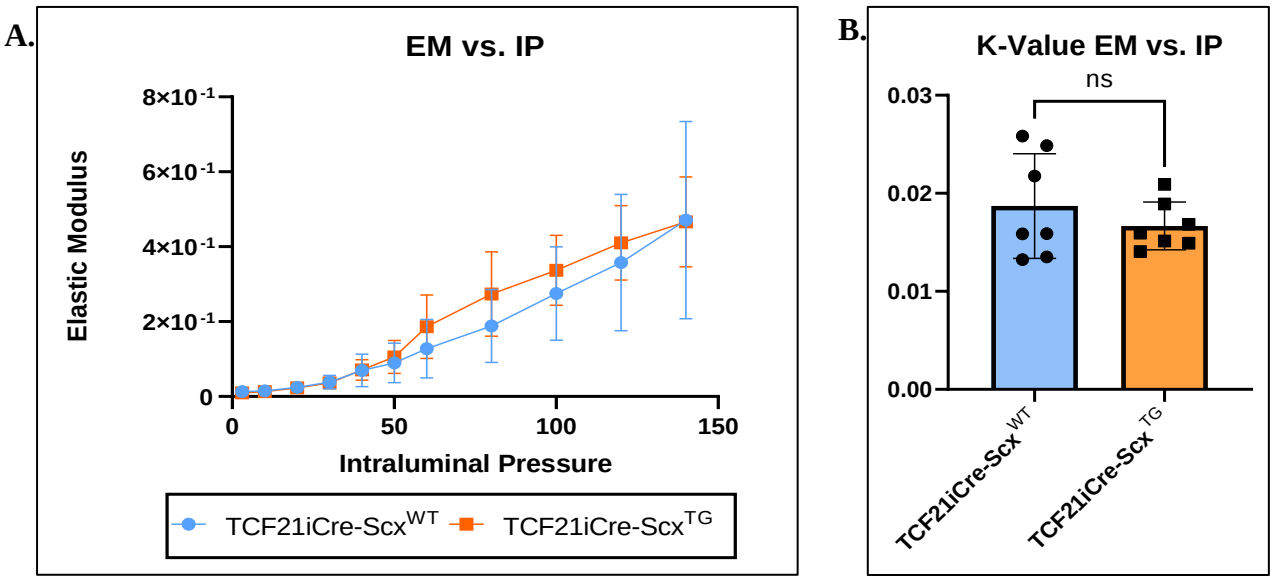

Figure 17. Isobaric elastic modulus of mesenteric arterioles from TCF21iCre-Scx^{TG} mice.

Elastic modulus determines arterial stiffness due to arterial geometry and wall component stiffness. (A) The elastic modulus–pressure curve shows no difference between TCF21iCre-Scx^{TG} and control mice. (B) Quantified k-values are not different between groups. Data are shown as mean ± SD. n = 7.

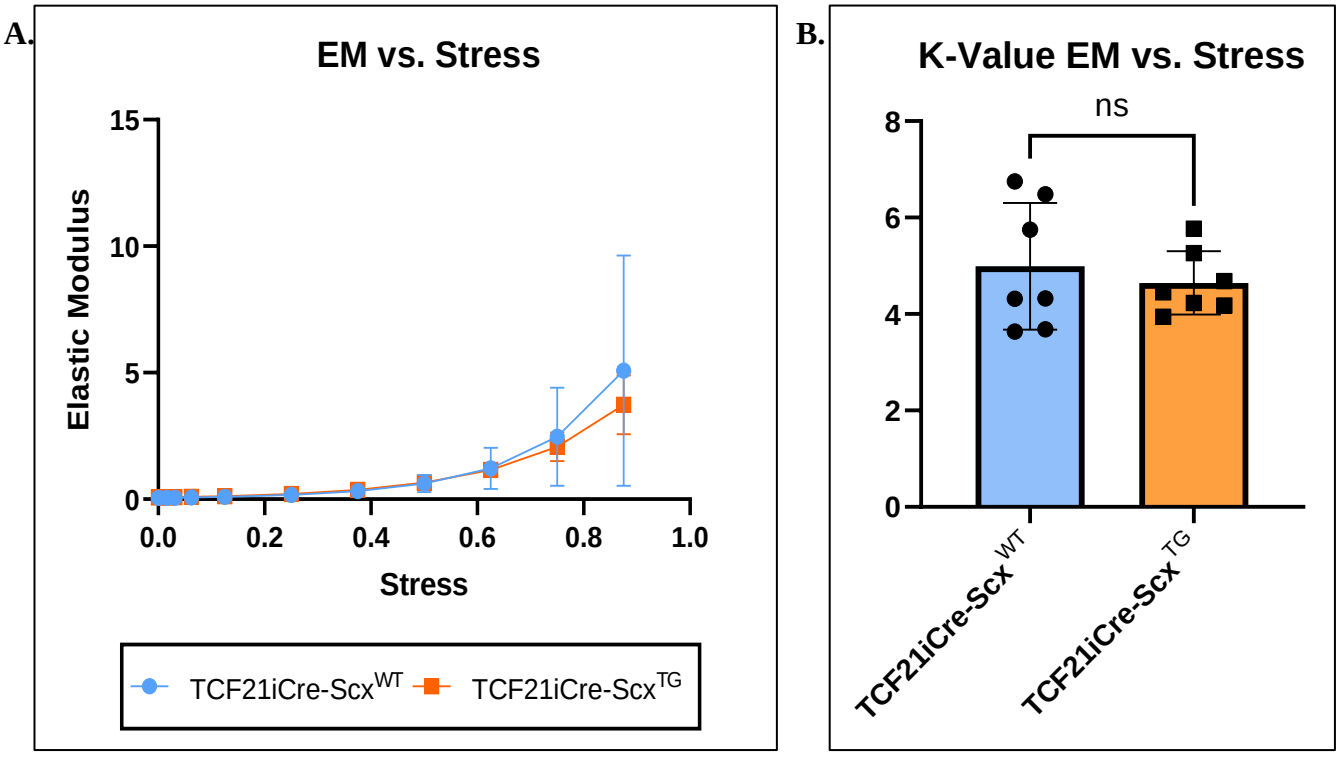

Figure 18. Stiffness of TCF21iCre-Scx^{TG} mesenteric arterioles due to changes in vascular wall components.

(A) The elastic modulus–stress curve is similar in TCF21iCre-Scx^{TG} vs control. (B) Quantified k-values are not different between groups. Data are shown as mean ± SD. n = 7.

1.4.3 Scleraxis upregulation in fibroblasts doesn't alter the cellular functions of mesenteric arteries.

Impaired cellular functional responses or altered vasorelaxation both can cause arterial stiffness. To evaluate the functional responses of the mesenteric arteries in TCF21iCre-Scx^{TG} mice, the 3rd order mesenteric artery was cannulated at a constant pressure of 60 mmHg and pre-constricted with 10^{-6} M norepinephrine. Our data show that there is a significant impairment in the vasodilation of TCF21iCre-Scx^{TG} mesenteries in response to increasing concentrations of acetylcholine ($P<0.001$) (Fig. 19A) compared to controls. On the other hand, there is no change in the vasodilation of TCF21iCre-Scx^{TG} mesenteries with the infusion of increasing concentrations of SNP (Fig. 19B). It is important to note the possibility that the altered relaxation response of TCF21iCre-Scx^{TG} mesenteries with increasing acetylcholine concentration may not be entirely due to the effect of scleraxis over-expression in this model, but rather may be due to the effect of tamoxifen gavage. This altered relaxation response is similar to the mesenteric relaxation response in WT mice treated with tamoxifen gavage (section 2.3.3).

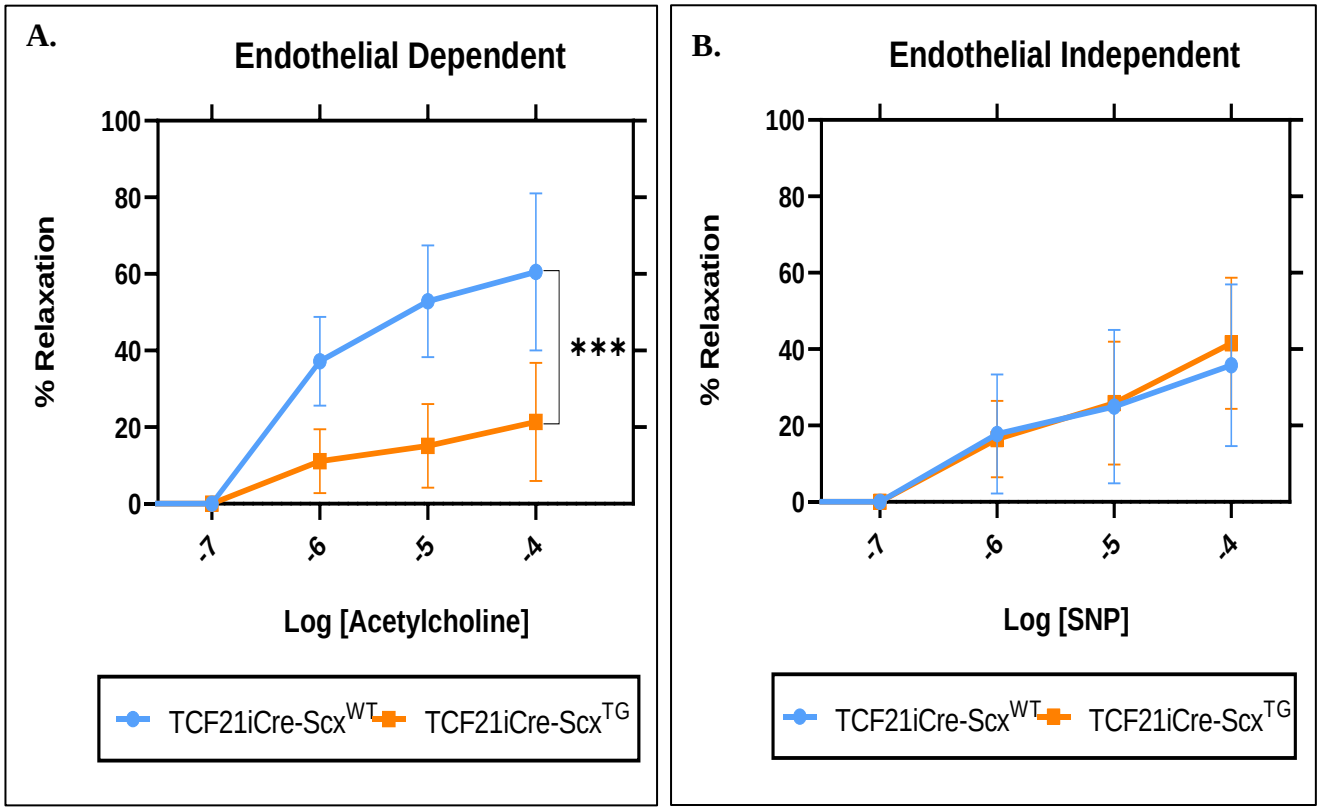

Figure 19. Assessment of mesenteric artery vasorelaxation function in TCF21iCre-Scx^{TG} mice.

(A) The relaxation in TCF21iCre-Scx^{TG} mesenteries in response to acetylcholine infusion is impaired compared to control mice (***P<0.001). Data are shown as mean ± SD, n=3. (B) Sodium nitroprusside infusion results in similar relaxation in TCF21iCre-Scx^{TG} vs. control mice. Data are shown as mean ± SD, n = 5-6.

2. Blood vessels in WT mice treated with CO vs TAM, compared to Scx^{KO} mice.

In our study, we included WT (non-transgenic) mice to control for the effect of tamoxifen alone. Additionally, we utilized Scx^{KO} mice in some experiments to gain a better understanding of the effects of scleraxis loss on vasculature function.

2.1 Blood pressure measurements in WT mice treated with CO vs. TAM.

The tail-cuff BP measurements at baseline and endpoint of WT mice treated with tamoxifen are comparable to the baseline and endpoint readings of WT mice treated with CO (Fig. 20). This indicates that tamoxifen gavage does not alter blood pressure in mice.

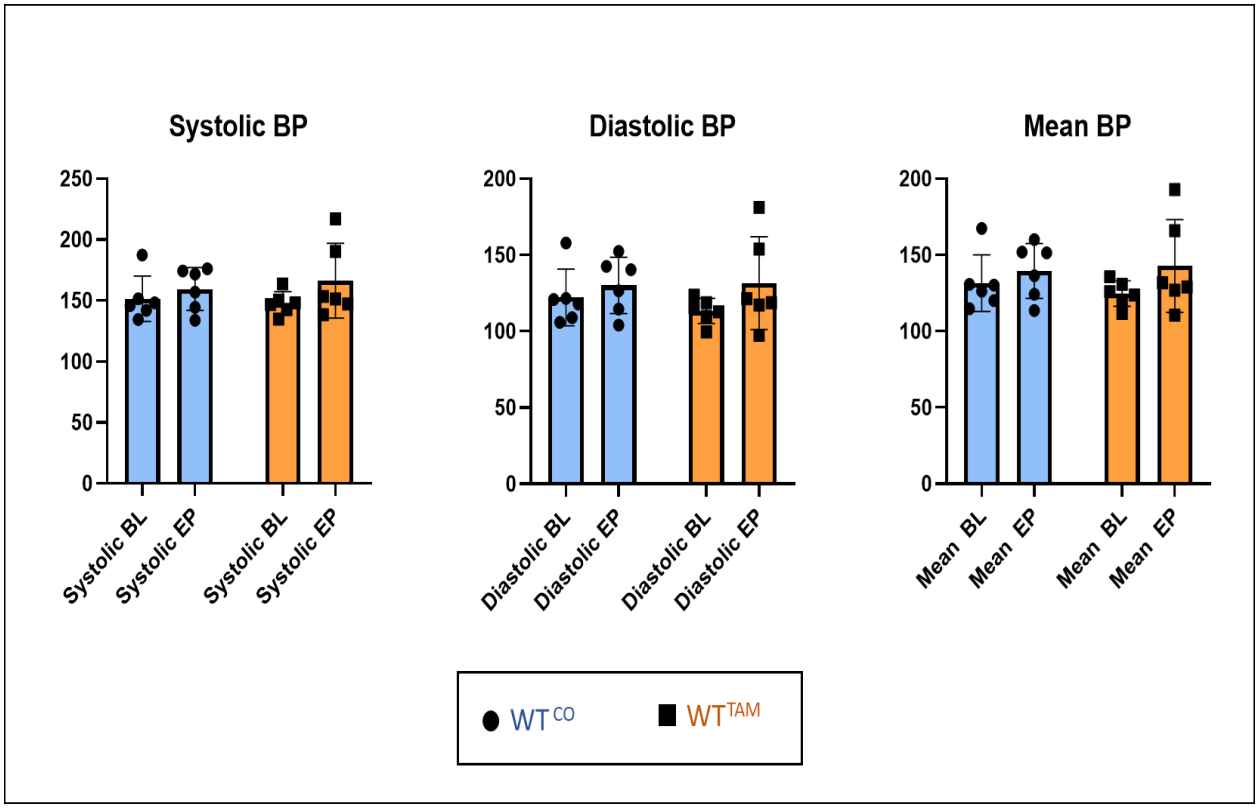

Figure 20. Blood pressure measurements for WT mice receiving CO or TAM.

Blood pressure was measured using tail-cuff plethysmography at baseline (age of 8 weeks) and endpoint before being sacrificed at age of 17-18 weeks. No significant alteration in blood pressure parameters was observed in WT^{TAM} mice in comparison to control mice WT^{CO}. Data are shown as mean ± SD, n=6.

2.2 Aortic structure comparison in WT mice vs. Scx^{KO} mice.

2.2.1 Assessment of aortic structure changes in response to tamoxifen or scleraxis knockout.

No changes were identified in WT^{CO} vs. WT^{TAM} aortic structures (Fig. 21), suggesting that tamoxifen gavage doesn't cause obvious changes in the aortic wall structure. On the other hand, genetic knockout of the scleraxis gene reveals an altered aortic structure when compared to Scx^{WT} aortas. Qualitatively, these observations of Scx^{KO} aortic vascular wall showed visibly less condensed elastin fibers when compared to the Scx^{WT} aorta (Fig. 22B). Additionally, the media in Scx^{KO} appears with localized gaps and more diffuse in PR staining compared to Scx^{WT} (Fig. 22C). In MT staining, the bluish color represents collagen fibers, while the pink color in the media represents the VSMC layers within the media. The localized gaps within the medial layer indicate possible alteration in VSMCs within the media of Scx^{KO} aortas (Fig. 22D). Collectively, these observations suggest that scleraxis may play a role in maintaining the integrity of the aortic wall structure. The absence of scleraxis appears to have a subtle impact on the media layer of aortas, particularly on the VSMC layer within the vessel wall.

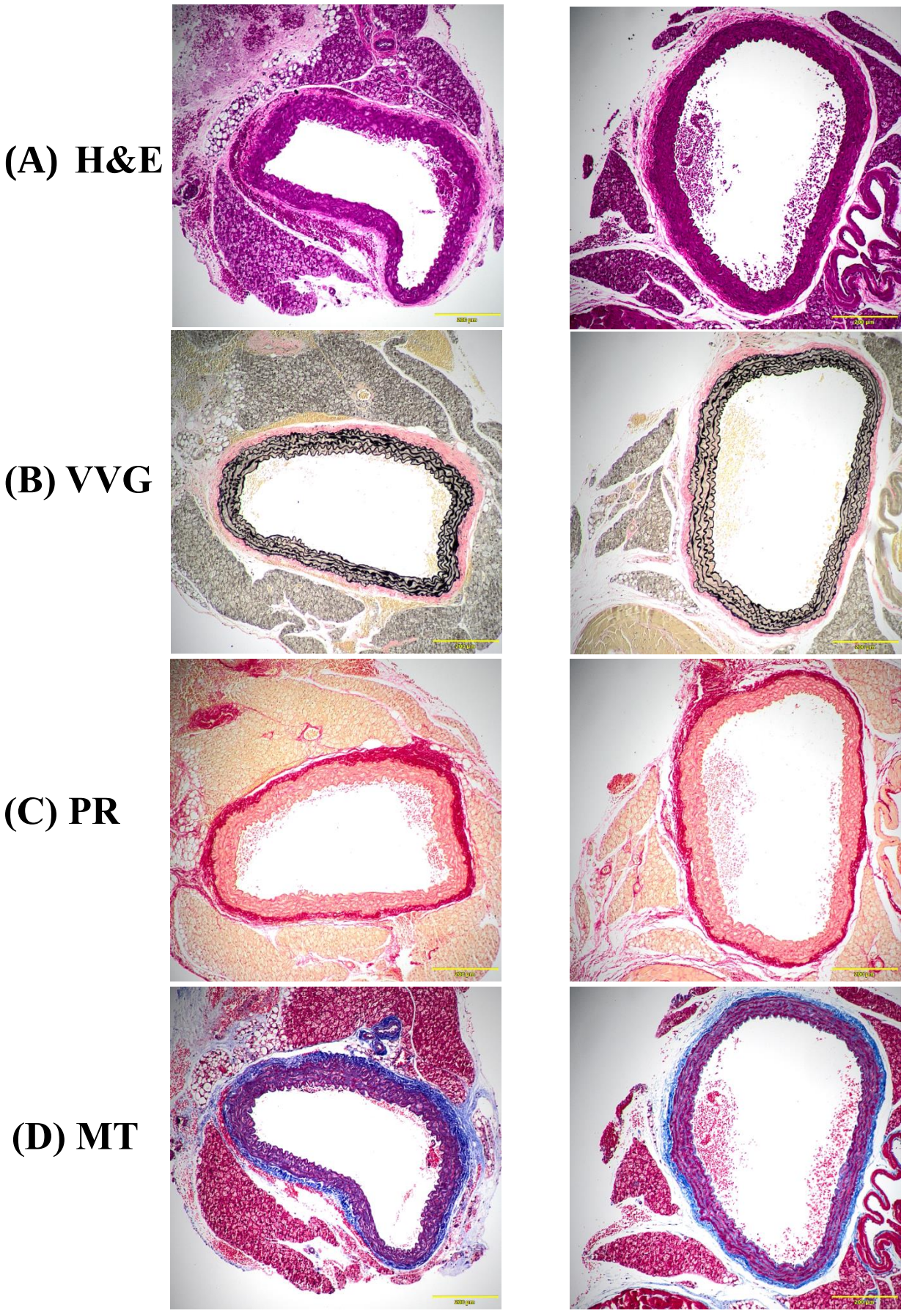
WT^CO
WT^TAM
(A) H&E
(B) VVG
(C) PR
(D) MT

Figure 21. Immunohistochemistry images of aortic sections from WT mice following CO or TAM gavage.

Immunohistochemical images of aortic sections from WT mice subjected to two different treatments: corn oil gavage (WT^{CO}) and tamoxifen gavage (WT^{TAM}) for 8 weeks. No visible structural changes were identified when comparing the aorta sections from WT^{TAM} mice to those from the control group, WT^{CO}. Multiple stains, including hematoxylin and eosin (H&E), Verhoeff-Van Gieson (VVG) for elastin, Picrosirius Red (PR) and Masson's trichrome (MT) for collagen, were utilized for structural analysis. No alterations were identified in aortic structure between the two experimental groups. Scale bar = 200 μm, representative of n= 2.

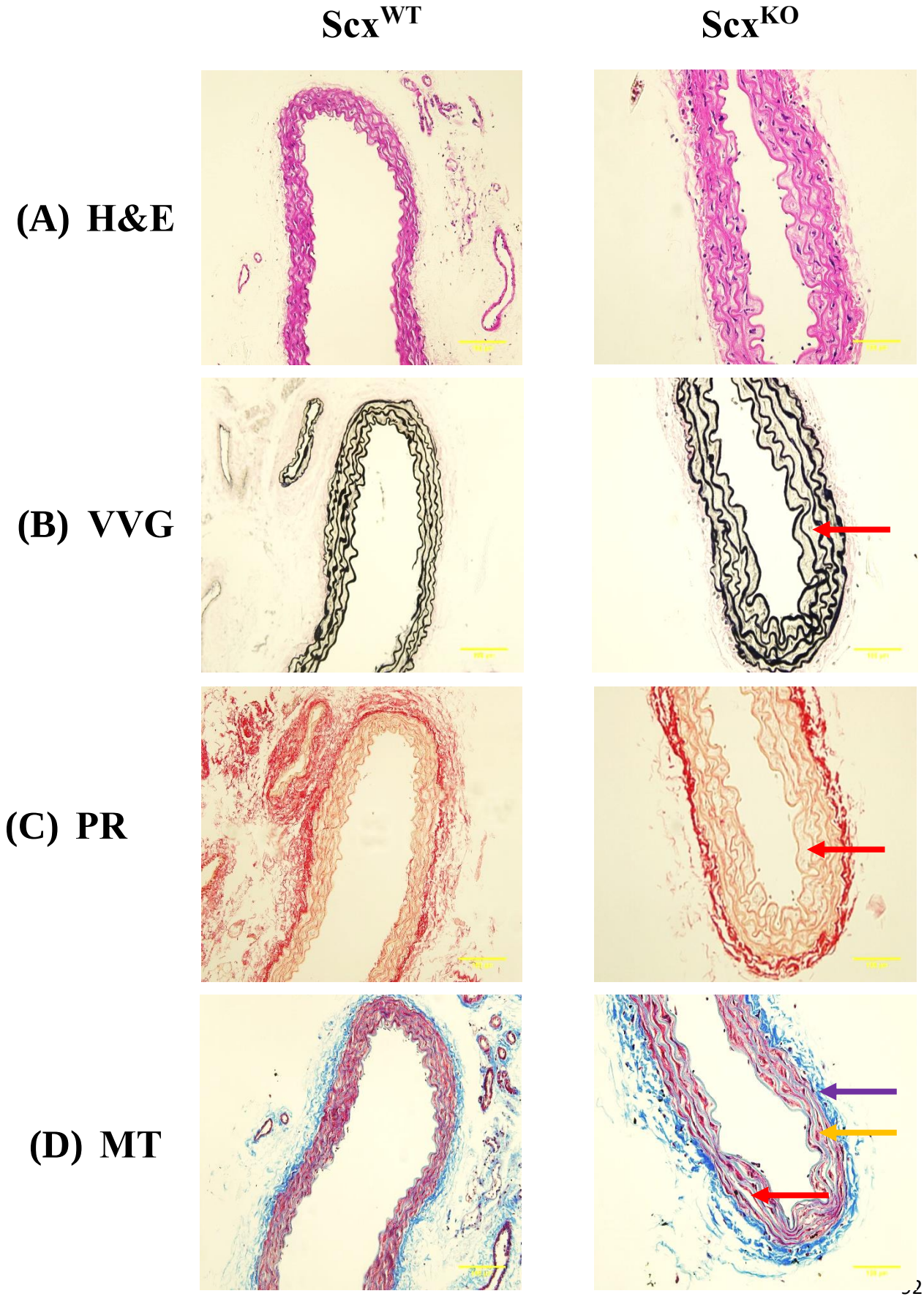
Scx^WT
Scx^KO
(A) H&E
(B) VVG
(C) PR
(D) MT

Figure 22. Comparison between histology sections of Scx^{WT} and Scx^{KO} mice aortas.

Representative immunohistochemical images comparing aortic sections from mice with a genetic knockout of the scleraxis gene (Scx^{KO}) vs. wild-type (Scx^{WT}) mice. Depletion of the scleraxis gene in the aortas of Scx^{KO} mice showed alterations in Scx^{KO} aortic structure compared to Scx^{WT}. These alterations are observed through using various stains. (A) hematoxylin and eosin (H&E) shows the overall aortic structure. (B) Verhoeff-Van Gieson (VVG) reveals spacing between the lamellae of elastin fibers in Scx^{KO} aortas when compared to the Scx^{WT} aortas (red arrow). (C) Picrosirius Red (PR) staining show that the media in the Scx^{KO} aortas exhibit localized gaps within the medial layers compared to the Scx^{WT}(red arrow). (D) Within the Masson's trichrome (MT) staining, the bluish color represents collagen fibers mainly in the adventitia (purple arrow), while the pink color represents the VSMC layers within the media (yellow arrow). (D) The gaps within the media in MT staining indicates possible alterations in VSMCs within the media of Scx^{KO} aortas (red arrow). Scale Bar= 100μm, n=3-5**.**

2.2.2 Aortic media in Scx^{KO} mice show lower cellularity compared to Scx^{WT} mice.

Immunofluorescence double staining was used to assess the impact of scleraxis knockout on VSMC cell number within the aortic medial layer compared to Scx^{WT} mice. Lower counts of DAPI-stained nuclei were observed in Scx^{KO} mice, indicating a potential reduction in cellularity in Scx^{KO} aortas compared to the Scx^{WT} control group (Fig. 23). However, statistical significance was not achieved, possibly due to the relatively small sample size (n=3). While additional investigations are necessary to validate these findings, they may suggest the potential impact of scleraxis absence on VSMC count in the media, potentially influencing the structure of the aorta in Scx^{KO} mice, as previously proposed (Fig. 22).

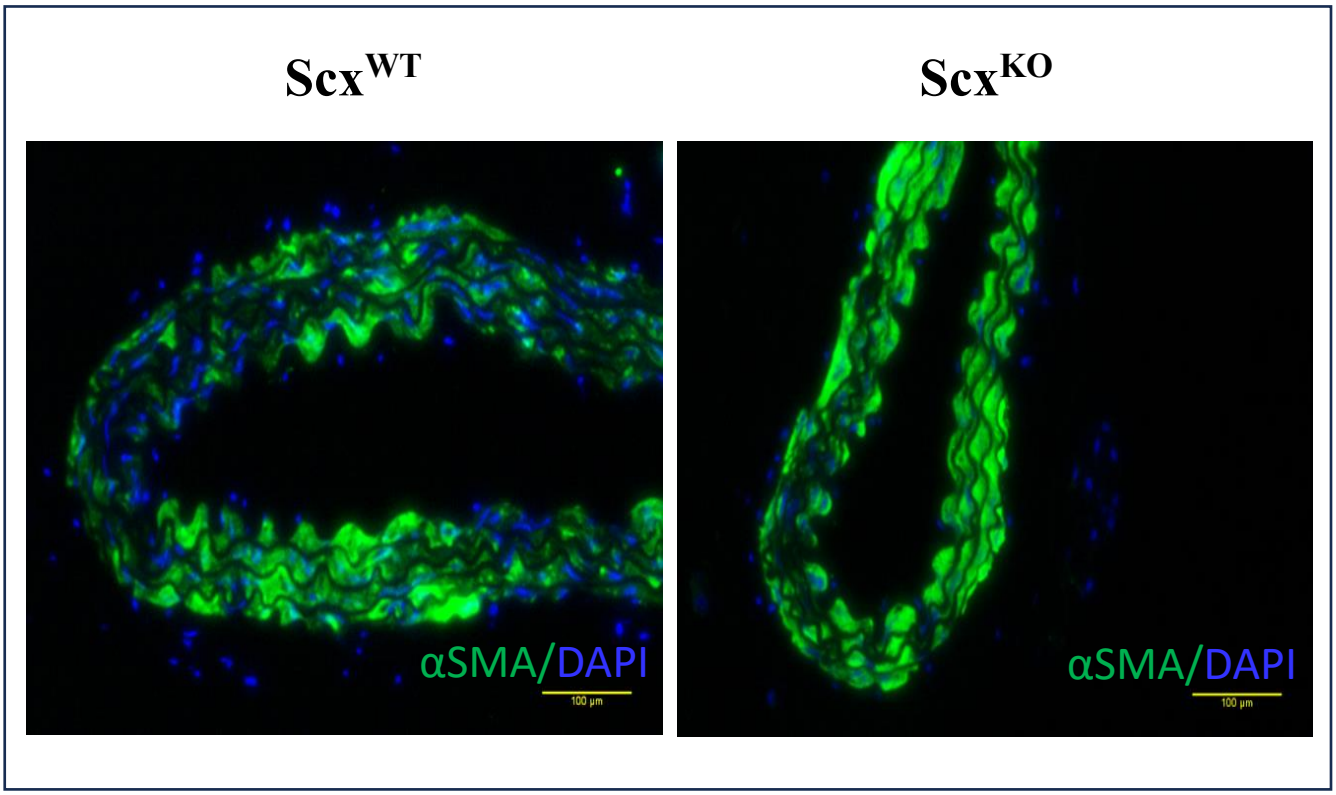

Figure 23. Nuclei depletion in Scx^{KO} aortas suggest lower cellularity in the media of aorta compared to Scx^{WT} control.

Representative immunofluorescence images of aortic tissue sections from Scx^{KO} mice and Scx^{WT} mice. The green color highlights alpha-smooth muscle actin (αSMA) indicating the demarcation of the media layer within the aorta, while the light-blue color within the aortic media represents nuclei stained with DAPI, identifying VSMCs within the aortic media. In the Scx^{KO} aortas, a notable reduction of DAPI-stained nuclei is observed when compared to Scx^{WT}. This visual evidence suggests a lower VSMC count within the media of Scx^{KO} aortas compared to Scx^{WT} controls. Scale bar= 100 µm, n = 3.

2.3 Structure and mechanical properties in small mesenteric arteries of WT^{CO}, $WT^{TAM,}$ and Scx^{KO} mice.

In this study, we aimed to identify whether corn oil or tamoxifen gavage could affect the function or mechanical properties of mesenteric arteries. We included Scx^{KO} mesenteries to explore whether the absence of scleraxis would alter the mechanical properties and structure of mesenteries in comparison to the WT groups.

2.3.1 Structure of mesenteric arteries in WT vs. Scx^{KO} mice.

Our findings show that there is no difference in cross sectional area (CSA), wall thickness, and media to lumen ratio (M/L) in mesenteric arteries of WT mice who were gavaged with tamoxifen compared to corn oil, suggesting that tamoxifen does not interfere with the overall structure of the mesenteric arteries (Fig. 24). When comparing the Scx^{KO} mesenteric arteries to the WT group, however, a significant reduction in CSA ($P<0.01$) and wall thickness ($P<0.05$) is observed, while there is no change in the M/L ratio (Fig. 24). The smaller size of Scx^{KO} mesenteric arteries may be related to the smaller overall size of Scx^{KO} mice. Previous studies from our lab showed that the weight of Scx^{KO} mice is significantly lower than that of WT mice. Specifically, our previous findings reported that body weight of WT mice was 20.2 ± 0.8 g, while Scx^{KO} mice weighed 12.2 ± 0.6; ($n = 9–12$; $P < 0.0001$) [142]

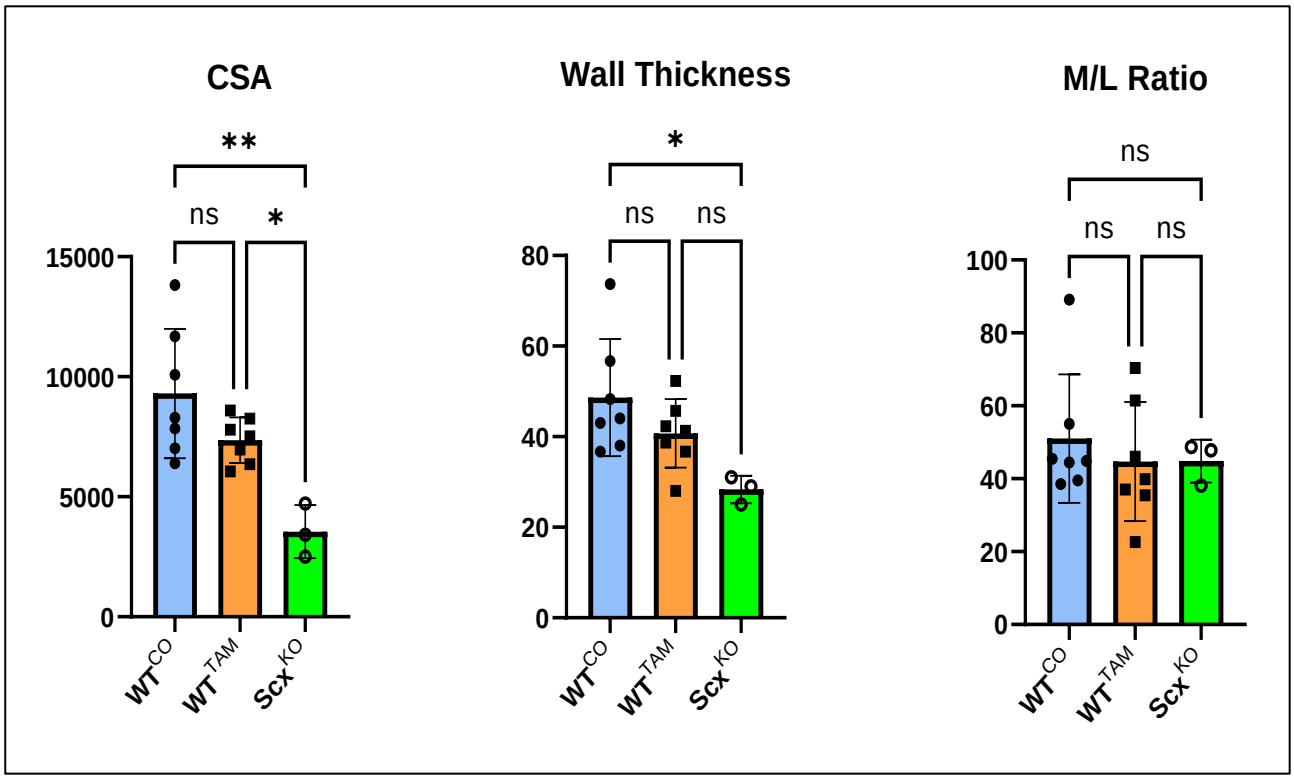

Figure 24. Structural parameters of mesenteric resistance arteries from WT^{CO}, WT^{TAM}, and Scx^{KO} mice.

No changes were observed in media cross sectional area (CSA), wall thickness, and media to lumen ratio (M/L) between mesenteric arteries of the two WT groups, WT^{CO} vs. WT^{TAM}. Meanwhile, there is a significant reduction in CSA of mesenteric arteries of Scx^{KO} compared to WT groups (**P<0.01 Scx^{KO} vs. WT^{CO}; *P<0.05 Scx^{KO} vs. WT^{TAM}). In addition, Scx^{KO} mesenteries have reduced wall thickness compared to the WT^{CO} group (*P<0.05), while the M/L ratio is similar in all groups. Data shown as mean ± SD, WT n=7 per group, Scx^{KO} n=3.

2.3.2 Mechanical properties of mesenteric arteries in WT vs. Scx^{KO} mice.

Stress-strain curves show no significant difference between WT^{CO} and WT^{TAM}, indicating that tamoxifen gavage does not affect mesenteric vascular mechanical properties (Fig. 25). However, Scx^{KO} mesenteric arteries exhibited lower stiffness and higher compliance compared to WT mesenteric arteries ($P < 0.01$), as shown by the rightward shift of the stress vs. strain curve and the reduction in k-value (Fig. 25). These results suggest that scleraxis plays a crucial role in maintaining mesenteric artery integrity and mechanics, as loss of scleraxis leads to reduced stiffness of mesenteric arteries and makes the mesenteric artery more compliant.

To identify the cause of reduced stiffness in mesenteric arteries, other parameters were determined i.e., EM v. IP, EM vs. stress, and stress vs. IP. No significant differences were observed between WT vs. Scx^{KO} parameters (Fig. 26). These findings suggest that the absence of scleraxis does not significantly alter vascular wall mechanical properties in Scx^{KO} mesenteries when compared to control.

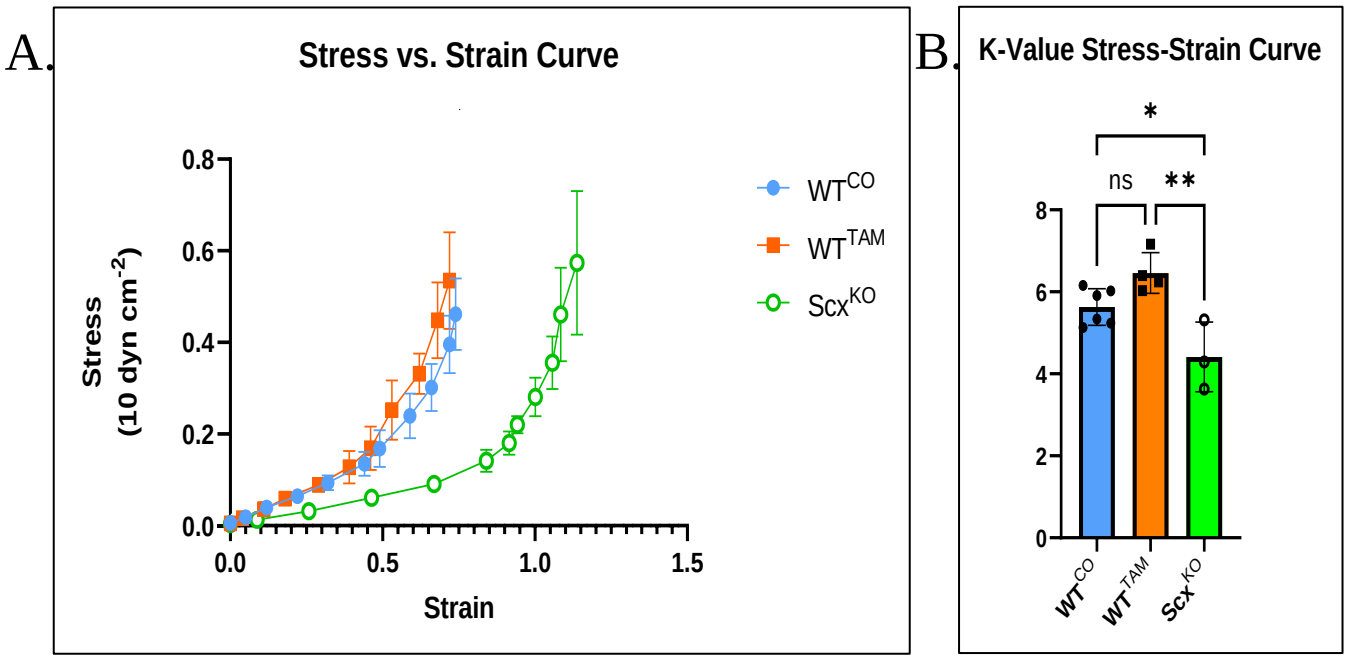

Figure 25. Wall stress-strain relationships for mesenteric arteries from WT vs. Scx^{KO} mice.

(A) Negligible change in the stress-strain curve is noted between mesenteries from wild-type mice receiving corn oil gavage (WT^{CO}) vs. wild-type mice receiving tamoxifen gavage (WT^{TAM}). However, the curve for scleraxis-knockout mice (Scx^{KO}) is shifted toward the right, indicating increased compliance. (B) The K-value represents the constant of rate change in the exponential growth equation used to fit the stress-strain curve data. The quantified k-value is insignificant between WT groups as anticipated, but the k-value is significantly reduced in Scx^{KO} vs. WT^{CO} (*P<0.05) and Scx^{KO} vs. WT^{TAM} (**P<0.01). The reduction of K-value in Scx^{KO} suggests that the blood vessel is more compliant and less stiff, allowing it to undergo greater deformation (strain) in response to a given amount of applied force (stress) along the stress-strain curve. Thus, the k-value is inversely related to the strain, meaning that the more dramatic the changes within the strain, the lower the K-value. Data are shown as mean ± SD, n = 3-5.

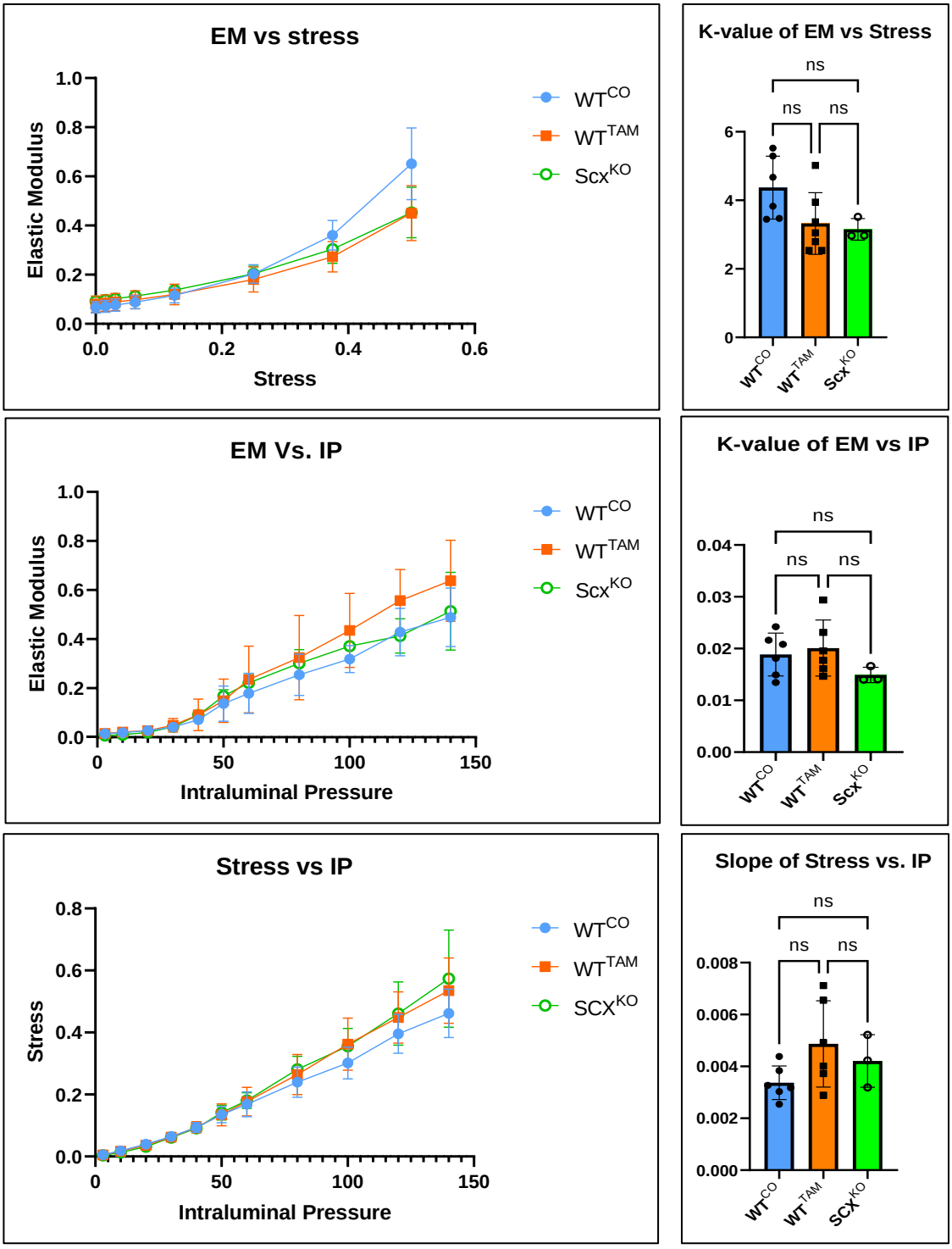

Figure 26. Mesenteric artery stiffness measurements in WT and Scx^{KO} mice.

No significant differences in the mesenteric artery stiffness parameters between WT and Scx^{KO} mice were noted. Data are shown as mean ± SD, n = 3-5.

2.3.3 Function of mesenteric arteries in WT^{CO} vs WT^{TAM}.

Functional measurements show that mesenteric artery relaxation is impaired in WT mice by tamoxifen gavage (Fig. 27A). These findings indicate that tamoxifen gavage alone significantly alters the function of endothelial cells in mesenteric arteries ($P<0.01$). This is similar to our previous data in TCF21iCre-Scx^{TG} mice (Fig. 19A). Meanwhile, the smooth muscle-dependent (endothelial-independent) relaxation response elicited using SNP is not altered in WT^{CO} vs. WT^{TAM} (Fig. 27B).

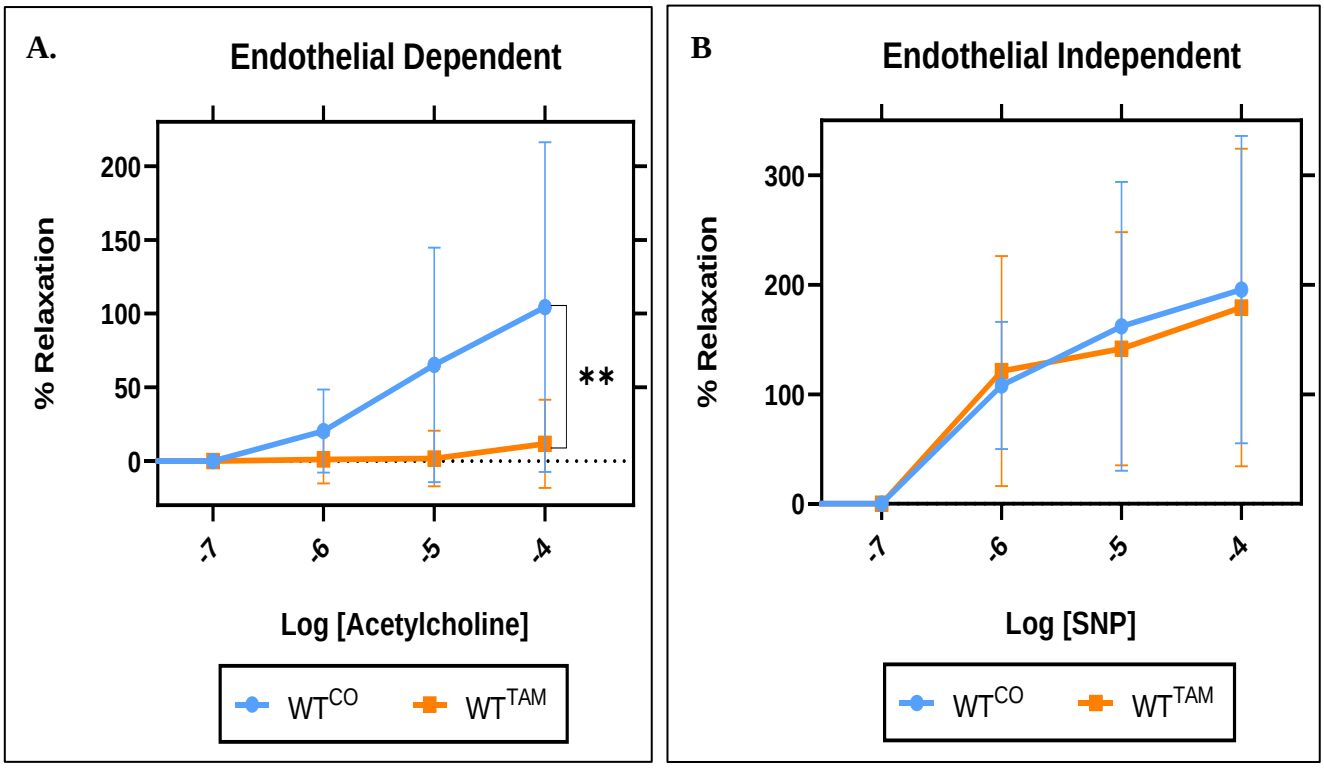

Figure 27. Vasomotor responses of mesenteric arteries from WT^{CO} vs. WT^{TAM} mice.

(A) The relaxation in WT^{TAM} mesenteries in response to acetylcholine infusion is impaired compared to WT^{CO} mice (**$P<0.01$). Data are shown as mean ± SD, n=5. (B) No significant differences were noted between mesenteric relaxation of WT mice treated with tamoxifen vs. corn oil upon sodium nitroprusside infusion. Data are shown as mean ± SD, n = 5-6.

3. Scleraxis upregulation in blood vessels of the VSMC-targeted scleraxis over-expression mouse model.

The largest layer in the arterial structure is the tunica media, and the main component in this layer is vascular smooth muscle cells, as they regulate vascular function and integrity. In this part of the study, we upregulated scleraxis expression in the smooth muscle cell layer in blood vessels to identify the role that scleraxis may play in these vessels. We only studied male mice in this model because the SMC specific Cre allele is inserted into the Y chromosome. Scleraxis was over-expressed by tamoxifen gavage as noted earlier, and animals were analyzed 8 weeks later.

3.1 Scleraxis upregulation is specifically limited to the smooth muscle cells in the Myh11Cre-Scx^{TG} mice.

To validate the specific upregulation of scleraxis in smooth muscle cells located in the aortic media of the Myh11Cre-Scx^{TG} mouse model, we conducted immunohistochemistry staining using a scleraxis antibody on aortic sections obtained from Myh11Cre-Scx^{TG} mice. DAB immunohistochemistry images clearly demonstrate positive brown precipitate staining for scleraxis within the media in both hematoxylin-stained (Fig. 28A) and non-hematoxylin-stained (Fig. 28B) images. A quantitative analysis was performed by counting the dark brown positive nuclei staining within four sections from each animal per unit area in both groups, for each of hematoxylin and non-haematoxylin sections to confirm the upregulation of scleraxis expression specifically within VSMCs located in the aortic media of Myh11Cre-Scx^{TG} mice. As previously mentioned, we conducted DAB immunohistochemistry staining both with and without hematoxylin to clearly visualize the scleraxis antibody staining within the nucleus in VSMCs. This approach avoids masking the scleraxis nuclear signal with the hematoxylin counterstain, ensuring

unbiased data. Both analyses revealed a significant increase in scleraxis-positive nuclei in Myh11Cre-Scx^{TG} aortas compared to Myh11Cre-Scx^{WT} (Fig. 28C, D).

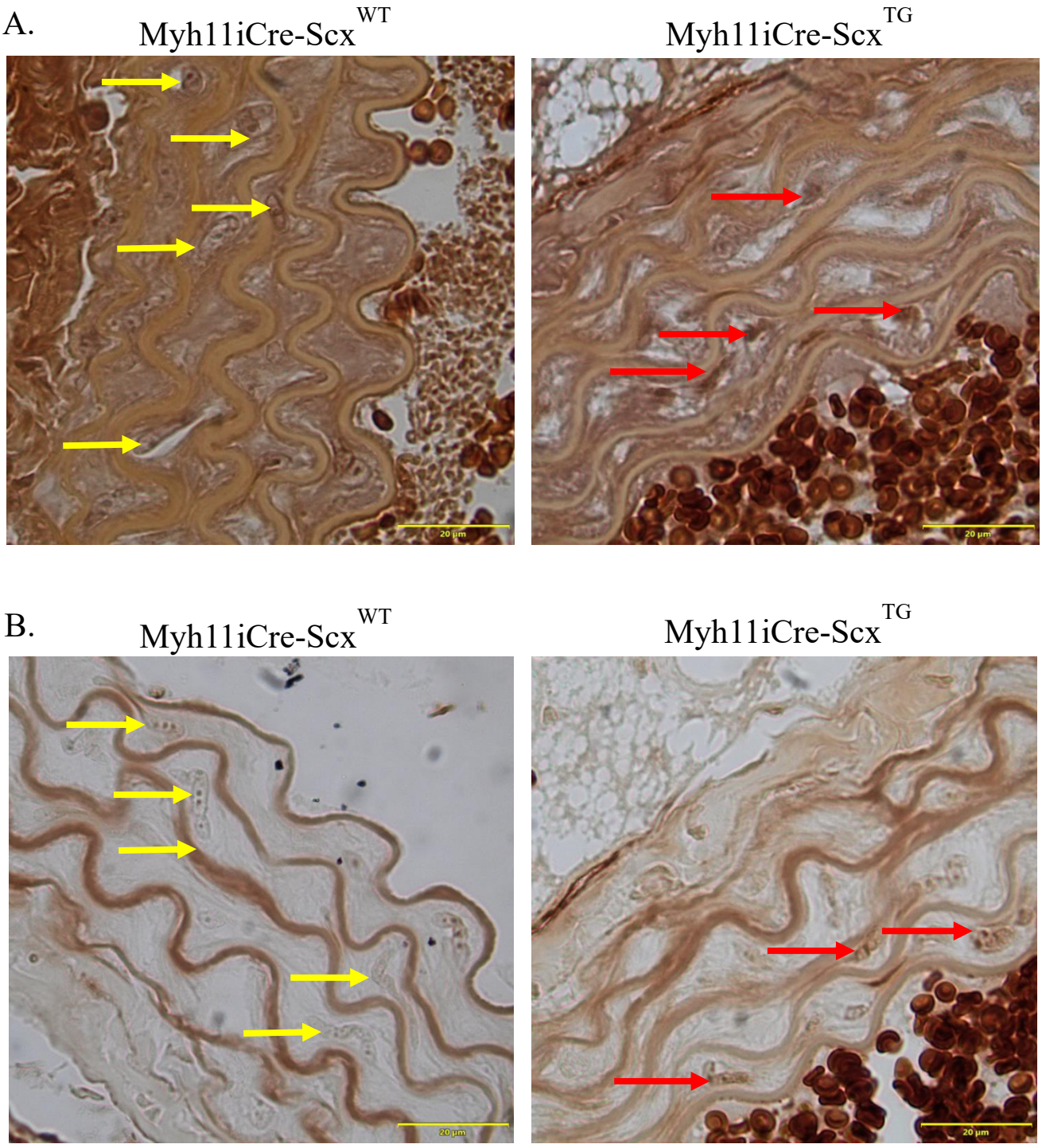

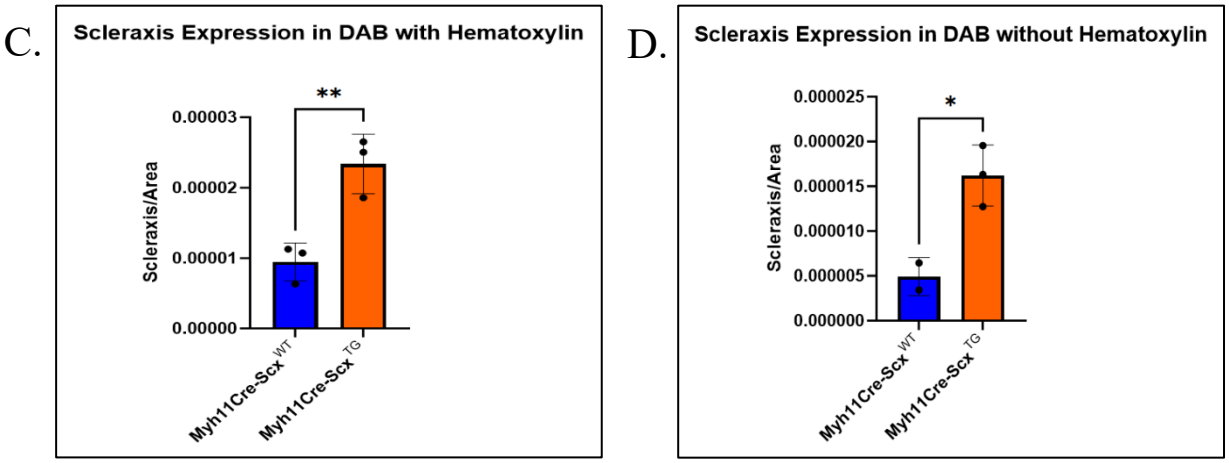

Figure 28. Scleraxis upregulation in VSMCs of aortas in Myh11Cre-Scx^{TG} mice.

DAB immunohistochemistry was performed on aortic sections from two groups: Myh11Cre-Scx^{TG}, where scleraxis overexpression in vascular smooth muscle cells (VSMCs) was induced by tamoxifen, and Myh11Cre-Scx^{WT}, which is the control group that received corn oil. DAB immunohistochemistry staining in these sections aimed to verify scleraxis upregulation within the VSMCs of the aortic media. (A) DAB immunohistochemistry-stained aortic sections, where nuclei were stained with hematoxylin as a counterstain. The darker brown nuclear precipitate observed in the media (marked by red arrows) indicates positive staining, indicating the increased expression of scleraxis expression in VSMCs within the aortic sections of Myh11Cre-Scx^{TG}. In contrast, the control nuclei from Myh11Cre-Scx^{WT} (yellow arrows) do not show scleraxis upregulation. (B) DAB images without the counterstain hematoxylin. Images from Myh11Cre-Scx^{TG} aortic sections (marked by red arrows), show a positive darker brown nuclear precipitate that is unmasked by hematoxylin staining, revealing the upregulation of scleraxis expression that is absent in control Myh11Cre-Scx^{WT} sections (yellow arrows). (D) Quantitative analysis demonstrates the significance of scleraxis-positive dark brown nuclei per square unit in hematoxylin-stained sections (*P<0.05) and non-hematoxylin sections (**P<0.01). Data are shown as mean ± SD. Scale bar =20 µm, n =3.

3.2 Scleraxis upregulation in smooth muscle cells does not alter blood pressure in Myh11Cre-Scx^{TG} mice.

Our data show no significant difference in any blood pressure parameters between baseline and endpoint following scleraxis upregulation in smooth muscle cells (Myh11Cre-Scx^{TG}) compared to controls (Myh11Cre-Scx^{WT}) (Fig. 29). This finding is demonstrated by similar changes in BP from baseline to endpoint in both groups. Our BP measurements indicate that scleraxis upregulation in the smooth muscle cells of the tunica media of the vessels is not sufficient to increase blood pressure in these mice.

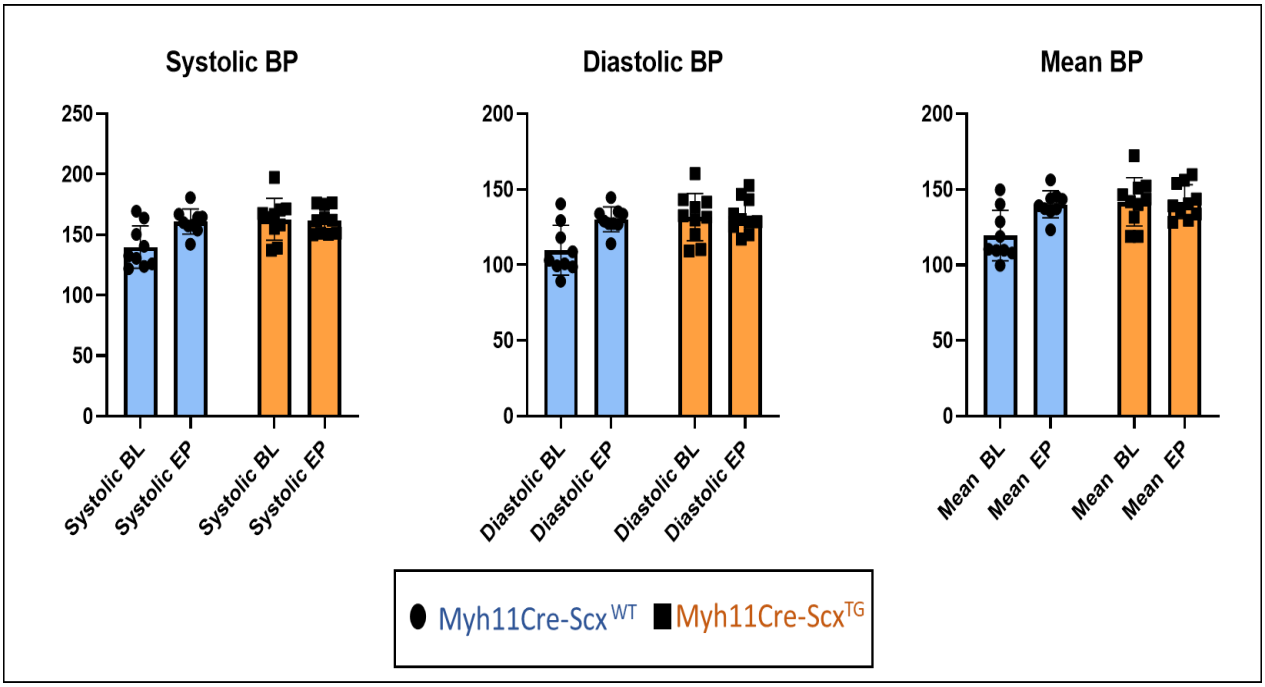

Figure 29. Blood pressure measurement for Myh11Cre-Scx^{WT} and Myh11Cre-Scx^{TG} mice. Blood pressure was measured using tail-cuff plethysmography at baseline at the age of 8 weeks and at endpoint before sacrificing at the age of 17-18 weeks. There are no changes in blood pressure parameters in Myh11Cre-Scx^{TG} mice compared to control mice Myh11Cre-Scx^{WT}. Data are shown as mean ± SD, n=9-10.

3.3 Scleraxis upregulation in smooth muscle cells does not alter aortic structure and molecular components.

3.3.1 Scleraxis upregulation in aortic VSMC does not alter structure in Myh11Cre-Scx^{TG} aortas.

Aortas from mice were harvested, sectioned, and stained with multiple staining techniques to assess the effect of scleraxis upregulation in VSMC on the aortic structure. These stains include hematoxylin and eosin (H&E) for overall assessment of aortic structure, Verhoeff-Van Gieson (VVG) staining to visualize elastin fibers, Picrosirius Red (PR), or Masson's trichrome (MT) for collagen visualisation.

No changes were observed in the aortic sections of Myh11Cre-Scx^{TG} aortas compared to control (Fig. 30 A-D). Our quantification of vessel structural parameters indicates no significant difference between Myh11Cre-Scx^{TG} aortas compared to control Myh11Cre-Scx^{WT} (Fig. 30E). This quantification assessed the quantity of collagen and elastin fibers, vascular wall thickness and CSA. Overall, this suggests that scleraxis upregulation in VSMC within tunica media doesn't substantially alter the structure of aortas in this model.

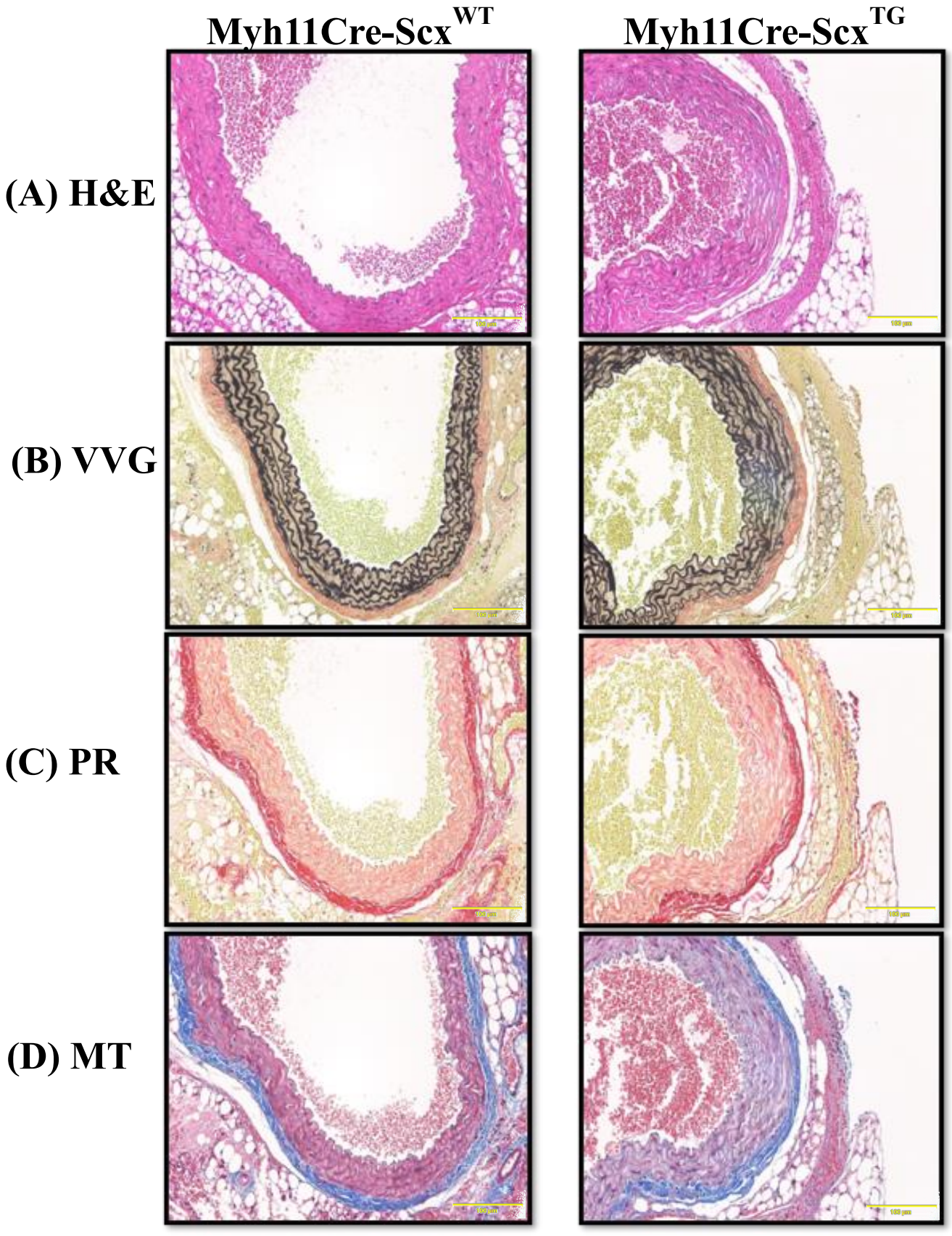
Myh11Cre-Scx^WT
Myh11Cre-Scx^TG
(A) H&E
(B) VVG
(C) PR
(D) MT

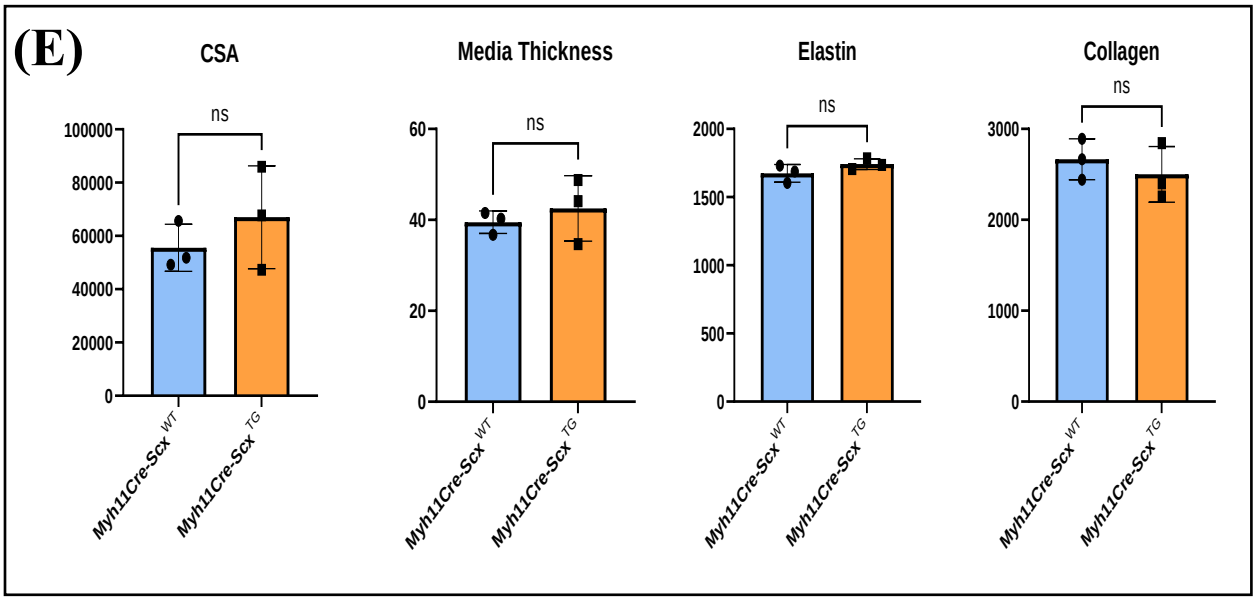

Figure 30. Representative images of histological sections to assess structural changes from Myh11Cre-Scx^{TG} mice.

Immunohistochemical images of aortic sections stained with (A) hematoxylin and eosin (H&E) for the overall assessment of aortic structure, where hematoxylin stains the cell nuclei dark purple, and eosin stains the overall structure with colors varying from purple to pink. (B) Verhoeff-Van Gieson (VVG) staining to visualize elastin content, which is represented by black fibers within the media (red arrow), (C) Picrosirius Red (PR) and (D) Masson's trichrome (MT) staining for collagen visualization. No obvious structural changes were identified following scleraxis over-expression in smooth muscle cells within the aorta sections from Myh11Cre-Scx^{TG} compared to aorta sections from control Myh11Cre-Scx^{WT}. Scale bar = 100 µm. (E) Histochemistry images are quantified by calculating cross-sectional area (CSA), wall thickness, collagen, and elastin content. The results show no significant differences between Myh11Cre-Scx^{WT} vs. Myh11Cre-Scx^{TG} aortas. Data are shown as mean ± SD, n = 3.

3.3.2 No changes in some molecular components in the aortas of the Myh11Cre-Scx^{TG} model.

Gene expression qPCR data show that transgenic VSMC-targeted scleraxis is significantly increased in Myh11Cre-Scx^{TG} aortas ($P<0.01$). However, this increase does not alter gene expression of specific ECM components within the aortic wall, such as Col3α1, Col1α1, fibronectin, and elastin in the aorta (Fig. 31). This data suggests that scleraxis upregulation in vascular smooth muscle cells does not increase vascular fibrosis in the aortas of Myh11Cre-Scx^{TG} mice. This finding agrees with histology images staining of extracellular matrix by PR or MT (Fig. 30C, D)

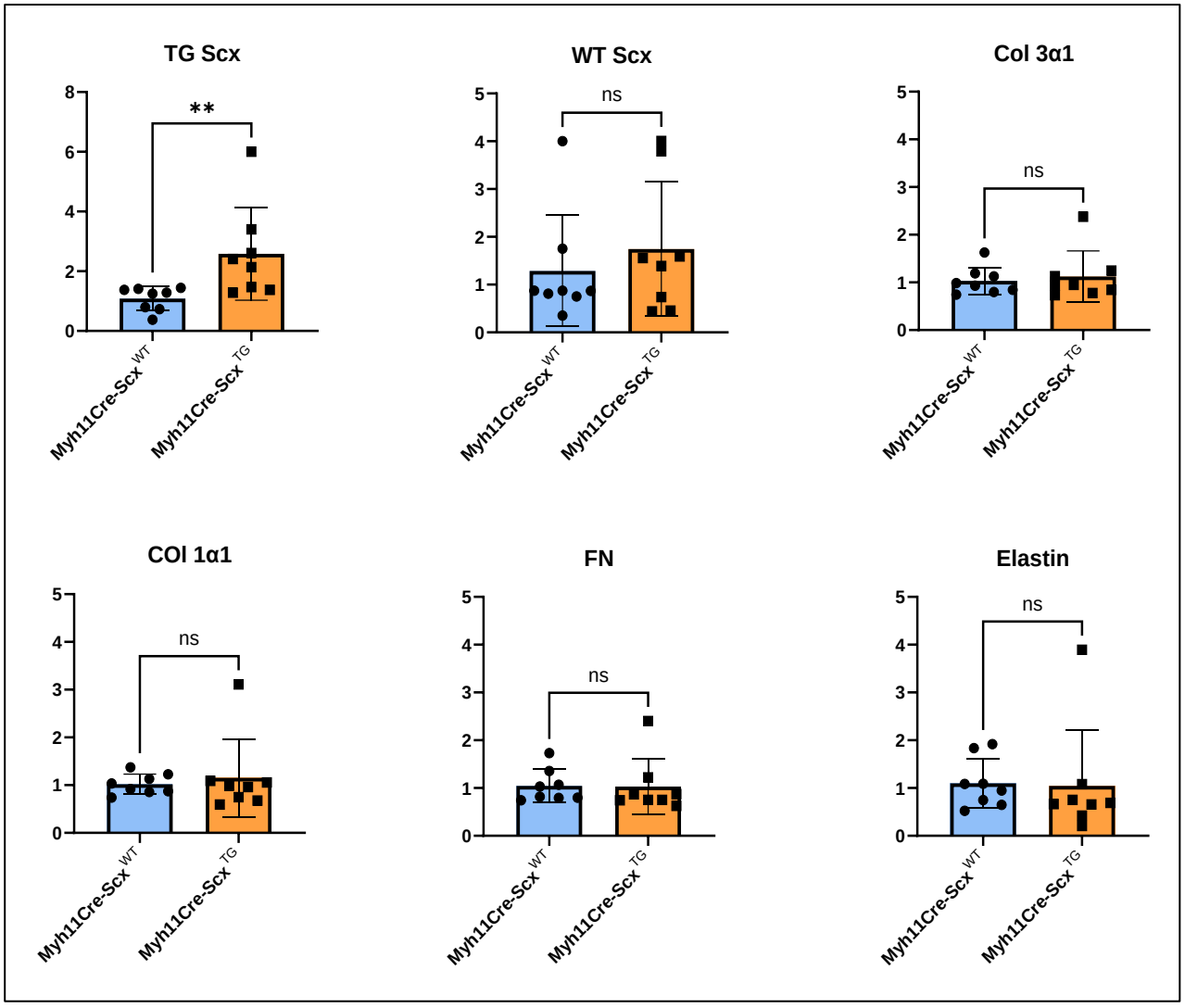

Figure 31. Gene expression from aortas of scleraxis over-expressed Myh11Cre-Scx^{TG} mice.

mRNA gene expression analysis shows no significant changes in ECM markers between Myh11Cre-Scx^{TG} and Myh11Cre-Scx^{WT} aortas, despite a significant increase in transgenic scleraxis gene expression (TG Scx) (**P<0.01). Wild type scleraxis (WT Scx) remains unaltered. Additionally, gene expression of specific ECM components within the aortic wall, such as collagen 3α1 (Col 3α1), collagen 1α1 (Col 1α1), fibronectin (FN), and elastin shows no significant alterations. Data are shown as mean ± SD, n = 8.

3.3.3 Scleraxis over-expression induces hyperplasia of aortic smooth muscle cells.

We performed immunofluorescence staining on the aortic sections of the mice for αSMA, and counter-stained for DAPI, to assess the impact of scleraxis upregulation on VSMC count in Myh11Cre-Scx^{TG} compared to control Myh11Cre-Scx^{WT}. We counted the number of DAPI-stained nuclei within the media, specifically within the demarcated area of the αSMA-positive vessel wall, for each group. Our quantification revealed that aortas overexpressing scleraxis have a significant increase in cellularity compared to control ($P<0.01$) (Fig. 32).

Based on the increase in cellularity in the aortic media of Myh11Cre-Scx^{TG} , we examined whether scleraxis overexpression would induce VSMC proliferation. Immunofluoresence data using the proliferation marker Ki67 show that Ki67-positive cells are significantly increaed in the aortic media of Myh11Cre-Scx^{TG} mice compared to control Myh11Cre-Scx^{WT} mice ($P<0.05$) (Fig. 33). These findings suggest that scleraxis upregulation induces VSMC proliferation and aorta cellularity.

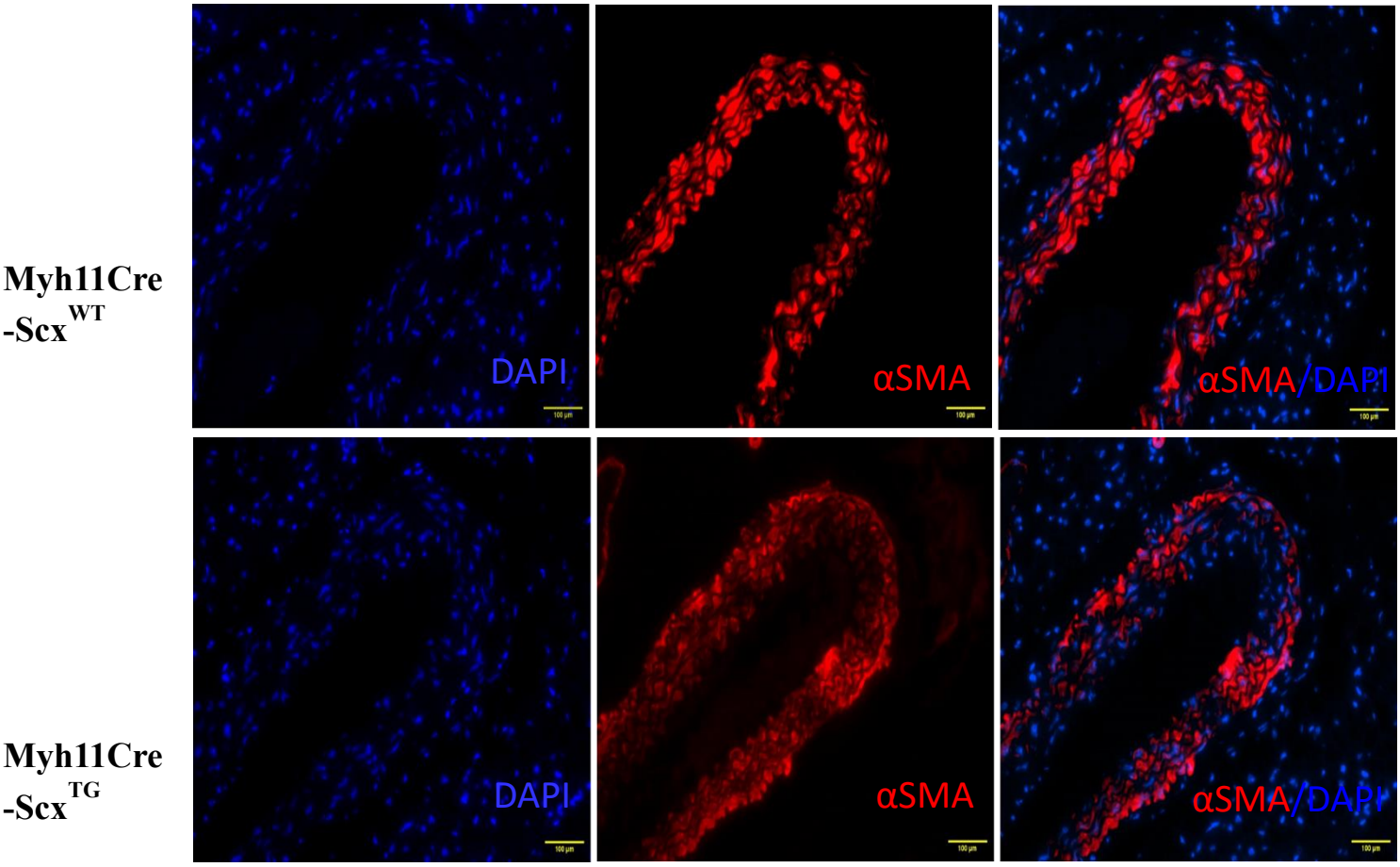

Figure 32. Scleraxis overexpression in the aorta induces medial hyperplasia.

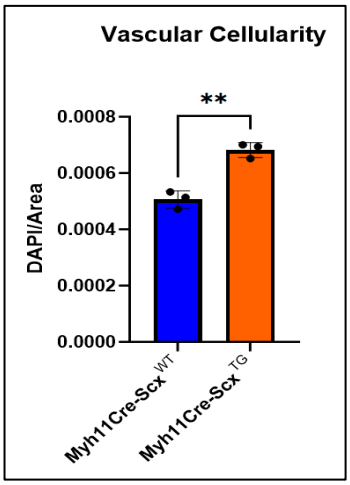

Representative immunofluorescence images of aortic sections from mice. The red color highlights alpha-smooth muscle actin (αSMA) indicating the demarcation of the media layer within the aorta, which was intensified to show the color contrast. The light-blue color within the aortic media represents nuclei-stained with DAPI, identifying the VSMCs within the aortic media. A significant increase of DAPI-stained nuclei per unit area is observed in scleraxis upregulated aortas of Myh11Cre-Scx^{TG} compared to control Myh11Cre-Scx^{WT} (**P<0.01). Scale bar =100 µm. Data are shown as mean ± SD, n = 3.

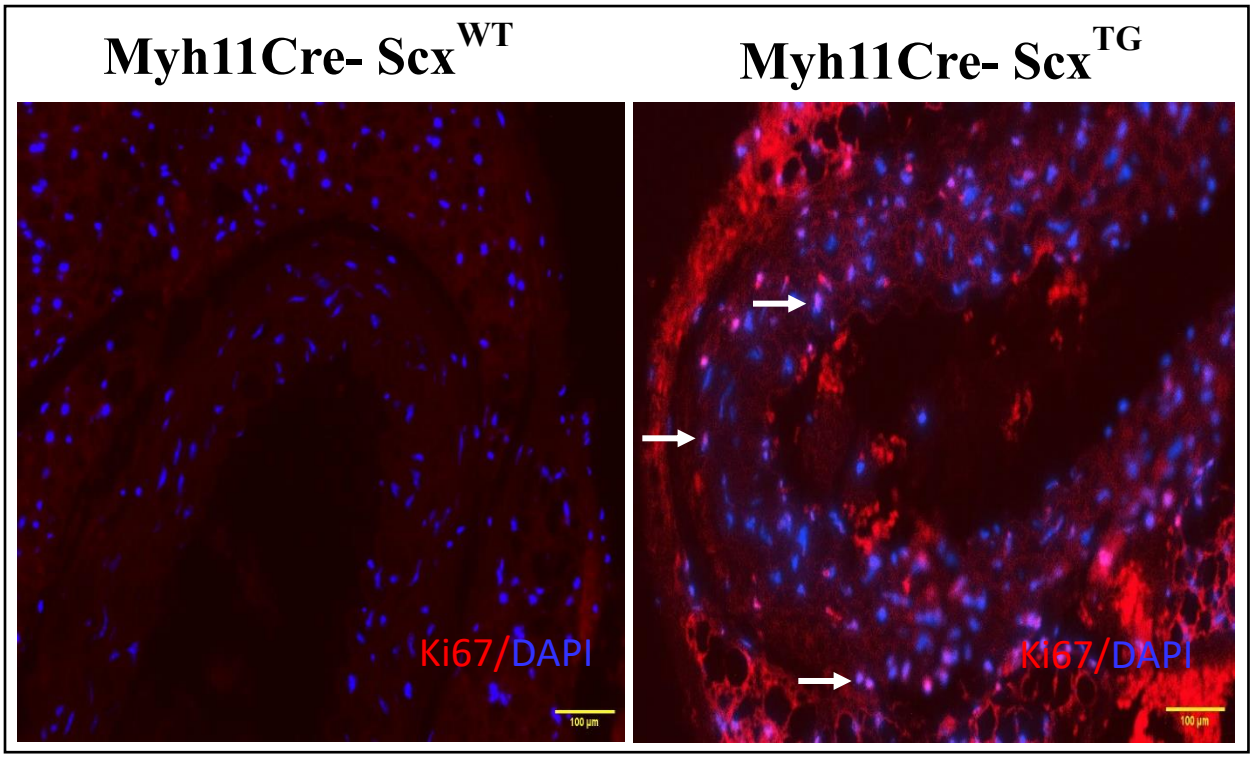

Figure 33. Scleraxis overexpression in Myh11Cre-Scx^{TG} aortas stimulate proliferation of VSMCs within aortic media.

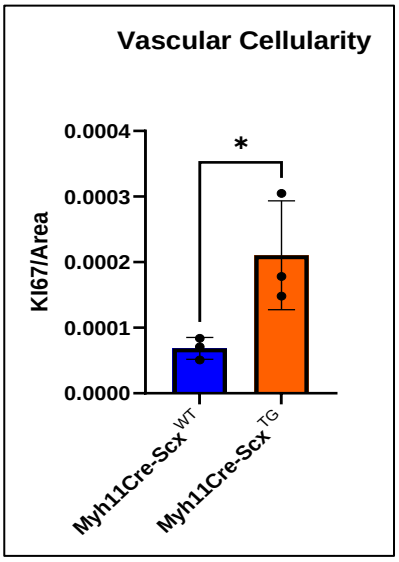

Representative immunofluorescence images of aortic sections from Myh11Cre-Scx^{WT} and Myh11Cre-Scx^{TG} mice. The bright red color highlights the proliferative marker Ki67, intensified to reveal a pink color that results from the overlap between red and blue. This increases the unspecific red background. While the blue color within the aortic media represents nuclei stained with DAPI. The pink color shows Ki67-positive nuclei within the aortic media (white arrows), suggesting VSMCs proliferation. A significant increase in the proliferative marker Ki67 (pink nuclei) is observed in the media of scleraxis-upregulated aortas of Myh11Cre-

Scx^{TG} compared to control Myh11Cre-Scx^{WT} (*P<0.05). Scale bar =100 µm. Data are shown as mean ± SD, n = 3.

3.4 Scleraxis over-expression in smooth muscle cells reduces resistance mesenteric artery compliance without influencing structure or function.

3.4.1 Scleraxis over-expression in VSMCs does not alter the geometrical properties of resistance mesenteric arteries.

Mesenteric arteries were cannulated for pressure myography, then their geometry was measured under inactive conditions (Ca^{2+}-free Krebs) at 60 mm Hg intraluminal pressure. From internal lumen diameter and wall thickness, we calculated CSA, M/L, and media thickness of mesentery resistance arteries. Our data demonstrate that there are no significant changes in vascular geometry between the mesenteries of Myh11Cre-Scx^{WT} vs. Myh11Cre-Scx^{TG} mice (Fig. 34).

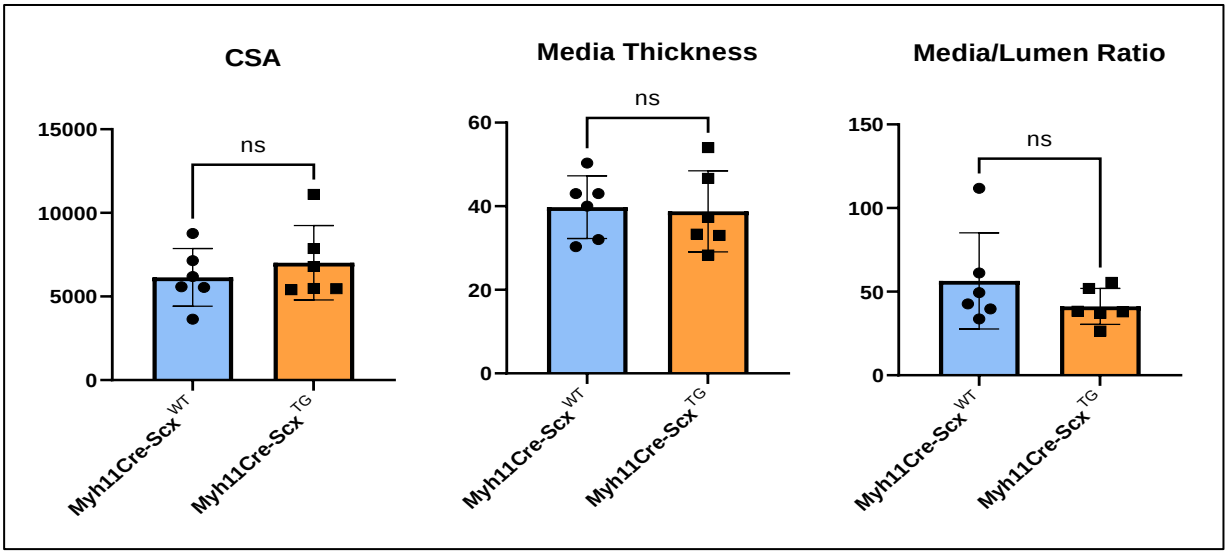

Figure 34. Structural parameters of small mesenteric resistance arteries from Myh11Cre-Scx^{WT} vs. Myh11Cre-Scx^{TG} mice.

Scleraxis upregulation in the smooth muscle cells in Myh11Cre-Scx^{TG} mice did not alter the geometry of mesenteric arteries compared to control Myh11Cre-Scx^{WT}. No changes were observed in media cross sectional area (CSA), media thickness, and media to lumen ratio (M/L) between the two groups. Data are shown as mean ± SD, n=6.

3.4.2 Scleraxis over-expression in VSMCs attenuates vascular compliance in mesenteric resistance arteries.

Pressure myography was used to evaluate the mechanical resistance of the mesenteric artery vessel wall under Ca^{2+} free conditions to remove myogenic tone. The artery was gradually pressurized from 3 to 140 mm Hg, and at each point, the wall thickness and internal lumen diameter were recorded. Stress and strain measurements were calculated and plotted to verify the mechanical compliance of the mesenteric arteries. Mesenteries over-expressing scleraxis showed an increase in vascular stiffness and reduced compliance compared to the control, as shown by a left-ward shift in the stress vs. strain curve (Fig. 35). This was quantified by measuring

significantly higher k-values ($P<0.01$) in Myh11Cre-Scx^{TG} vs. Myh11Cre-Scx^{WT} vessels (Fig. 35), indicating that over-expression of scleraxis in VSMCs of arteries makes them less compliant.

The elastic modulus (EM) is the arterial stiffness that is caused by arterial geometry and wall components, and is calculated based on the exponential growth of the slope between stress and strain. Our findings demonstrate that changes in the compliance of the mesenteric artery did not trigger changes in vascular wall components, as represented by the EM-stress curve (Fig. 36A) and quantified by the non-linear regression curve of the k-value of EM-stress. Also, no changes were noted in the vascular geometry or components in scleraxis over-expression mesenteric arteries, as represented by the stress-IP curve or EM-IP and quantified by the slope of the stress-IP and the k-value of EM-IP (Fig. 36 B, C, respectively). Interestingly, our data indicate that the over-expression of scleraxis in VSMCs within the tunica media layer of the blood vessels reduces arterial compliance. This reduction in compliance may not be related to vascular geometry or vascular wall components, including collagens and elastin, in agreement with the gene expression analysis in aortas (Fig. 31). Instead, it may be attributed to the impact of scleraxis upregulation on the proliferation of VSMC, which in turn promotes the stiffness of mesenteric arteries as indicated from the immunofluorescence analysis in aortas (Fig. 32, 33).

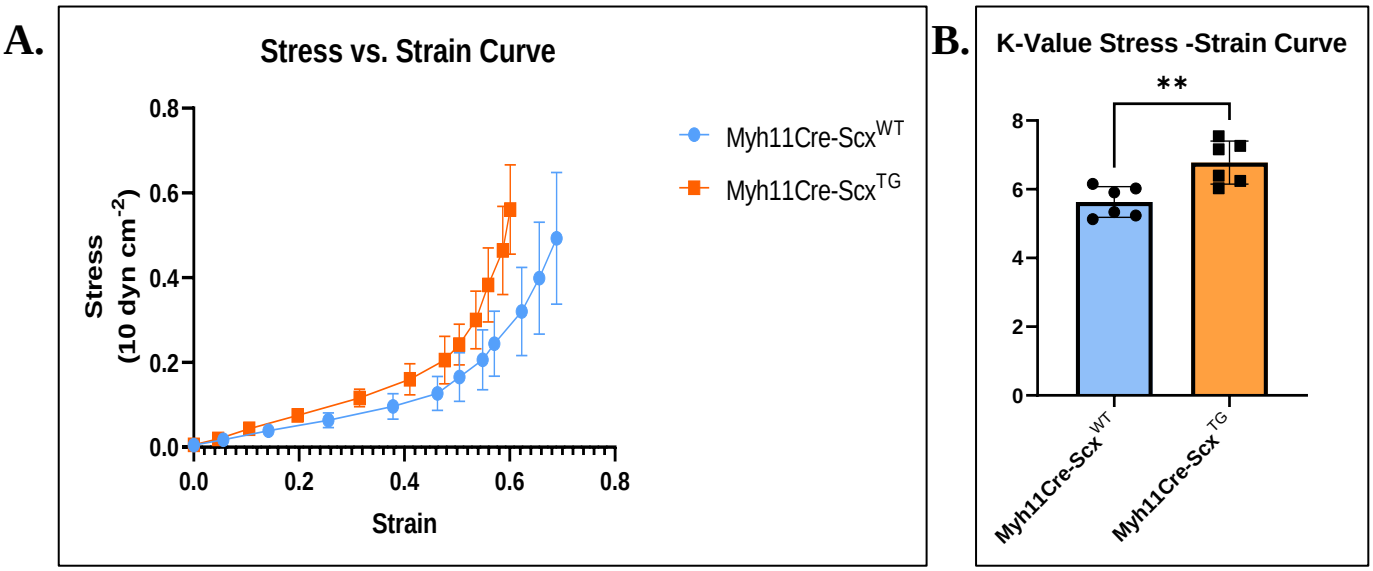

Figure 35. Wall stress-strain relationships for resistance mesenteric arteries from Myh11Cre-Scx^{TG} vs. Myh11Cre-Scx^{WT} mice.

(A) The stress-strain curve of mesenteric arteries was shifted to the left in Myh11Cre-Scx^{TG} mice compared to Myh11Cre-Scx^{WT} control mice, indicating a reduction in arterial compliance. (B) The stress-strain curve is quantified using the k-value, which is identified as the constant of rate change in the exponential growth formula that best fit the data of the stress-strain curve. The k-value exhibited a significant increase in mesenteric arteries with scleraxis overexpression Myh11Cre-Scx^{TG} (**P<0.01). This indicates that the scleraxis upregulation in these arteries has led to a significant increase in their stiffness, making them less compliant. Data are shown as mean ± SD, n =6.

A.

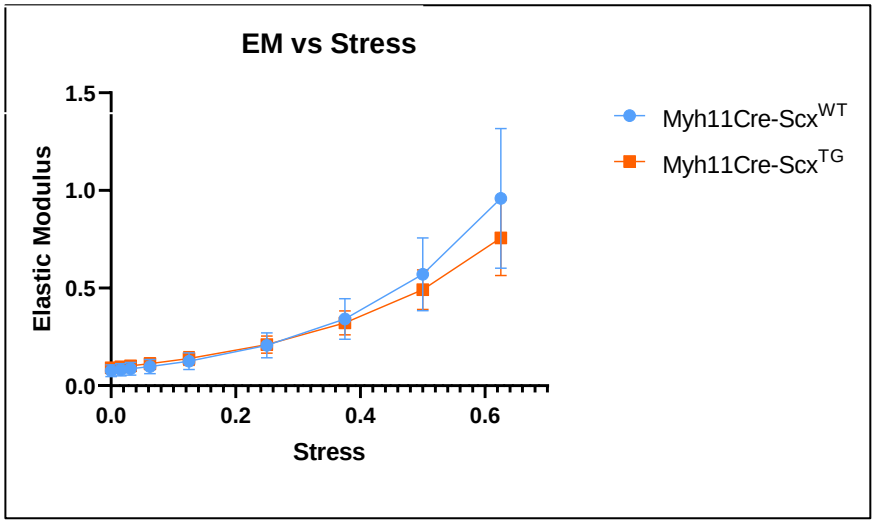
EM vs Stress
Elastic Modulus
1.5
1.0
0.5
0.0
0.0
0.2
0.4
0.6
Stress
Myh11Cre-Scx^WT
Myh11Cre-Scx^TG

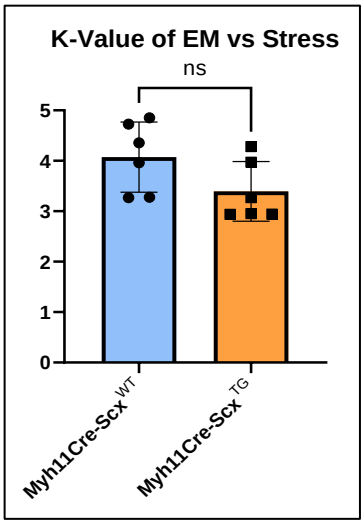
K-Value of EM vs Stress
ns
5
4
3
2
1
0
Myh11Cre-Scx WT
Myh11Cre-Scx TG

B.

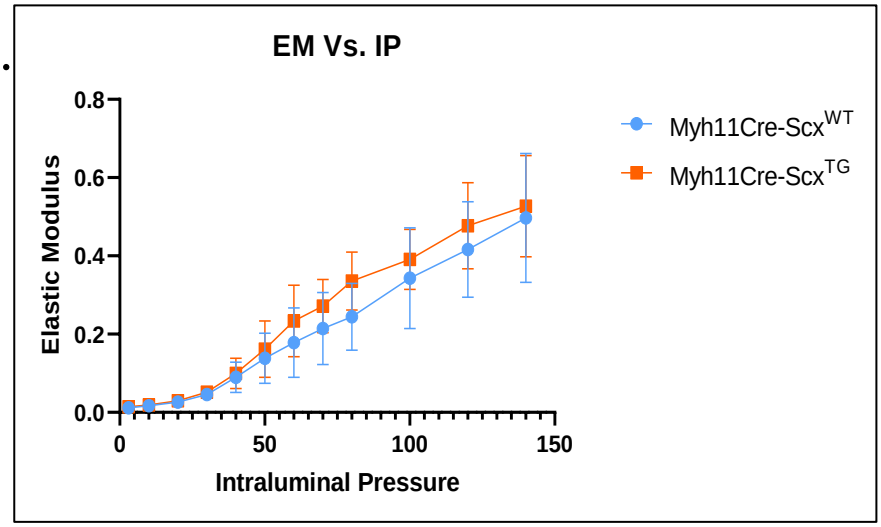
EM Vs. IP
Elastic Modulus
0.8
0.6
0.4
0.2
0.0
0
50
100
150
Intraluminal Pressure
Myh11Cre-Scx^WT
Myh11Cre-Scx^TG

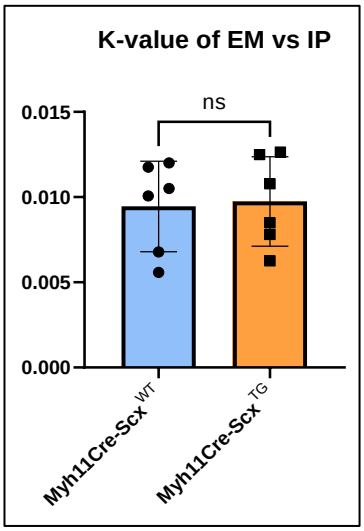
K-value of EM vs IP
ns
0.015
0.010
0.005
0.000
Myh11Cre-Scx WT
Myh11Cre-Scx TG

C.

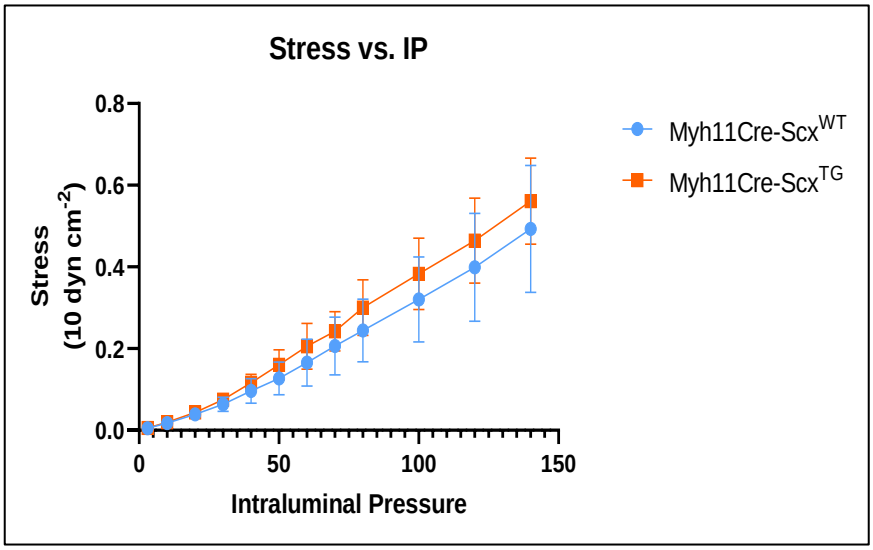
Stress vs. IP
Stress
(10 dyn cm-2)
0.8
0.6
0.4
0.2
0.0
0
50
100
150
Intraluminal Pressure
Myh11Cre-Scx^WT
Myh11Cre-Scx^TG

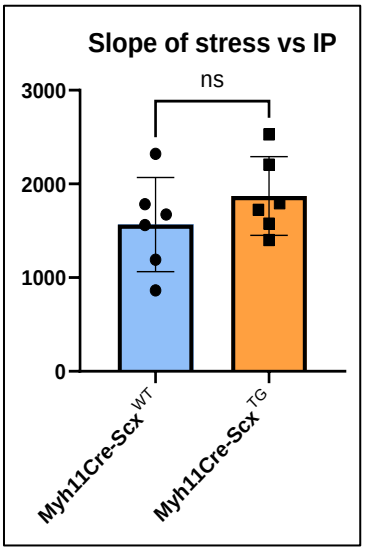
Slope of stress vs IP
ns
3000
2000
1000
0
Myh11Cre-Scx WT
Myh11Cre-Scx TG

Figure 36. Mesenteric artery stiffness parameters in Myh11Cre-Scx^{WT} vs. Myh11Cre-Scx^{TG} mice.

(A) The elastic modulus (EM) vs. media stress curve illustrates how the vessel's stiffness changes in response to different levels of stress, assessing the mechanical properties of mesenteric artery based on the vascular wall components including collagens, elastin fibers, and VSMC. Quantified data using the k-value of the EM vs. Stress curve show no significant changes in mesenteric wall components between Myh11Cre-Scx^{WT} vs. Myh11Cre-Scx^{TG} mice. (B) The EM-intraluminal pressure (IP) curve represents how the vessel's stiffness (elastic modulus) responds to changes in incremental pressure. Thus, a change in vascular stiffness can be due to changes in arterial wall components and on the geometrical alignment of the mesenteric artery, in response to incremental changes in pressure (IP) applied on the blood vessel. Quantified data using the k-value of the EM vs. IP curve show no significant alterations in mesenteric wall between Myh11Cre-Scx^{WT} vs. Myh11Cre-Scx^{TG} mice were noted. (C) Stress vs. IP curve identifies the ability of the blood vessel to adapt to force changes in response to the incremental pressure applied on its walls. No significant changes in vascular elasticity, or vascular wall components between Myh11Cre-Scx^{WT} vs. Myh11Cre-Scx^{TG} mice were noted. Data are shown as mean ± SD, n=6**.**

3.4.3 Scleraxis over-expression in VSMCs does not alter the cellular functions of mesenteric arteries.

To assess the functional responses of mesenteric arteries in Myh11Cre-Scx^{TG} mice, we cannulated the third-order mesenteric artery at a constant pressure of 60 mmHg and induced pre-constriction with 10^{-6} M norepinephrine. A higher percentage of relaxation on the Y-axis corresponds to greater vasodilation of the vessel, while a lower relaxation percentage indicates increased constriction, impaired functionality, and reduced responsiveness of the vessel to the vasodilatory effects of the administered drug. Our findings show that Myh11Cre-Scx^{TG} mesenteries exhibit an altered relaxation response to increased concentrations of acetylcholine, indicating an impaired endothelial-dependent response ($P<0.01$) (Fig. 37A). This impaired response is similar to our previous data from WT^{TAM} compared to WT^{CO} (Fig. 27A), where tamoxifen gavage rather than scleraxis gene over-expression alters endothelial function.

Although scleraxis is being over-expressed in VSMCs, this did not impair the vasodilatory function of smooth muscle cells in response to the gradual increase of SNP concentration (Fig. 37B). Thus, over-expression of scleraxis in VSMCs did not alter the function of smooth muscle cells in mesenteric arteries.

Our data suggest that scleraxis increases vascular stiffness likely by inducing smooth muscle cellular hyperplasia, as identified in the aortas in Myh11Cre-Scx^{TG} mice. These changes are unrelated to any alterations in vascular geometry or morphology of either the aortas or mesenteric arteries. Only the mechanical stiffness of the small resistance arteries is altered.

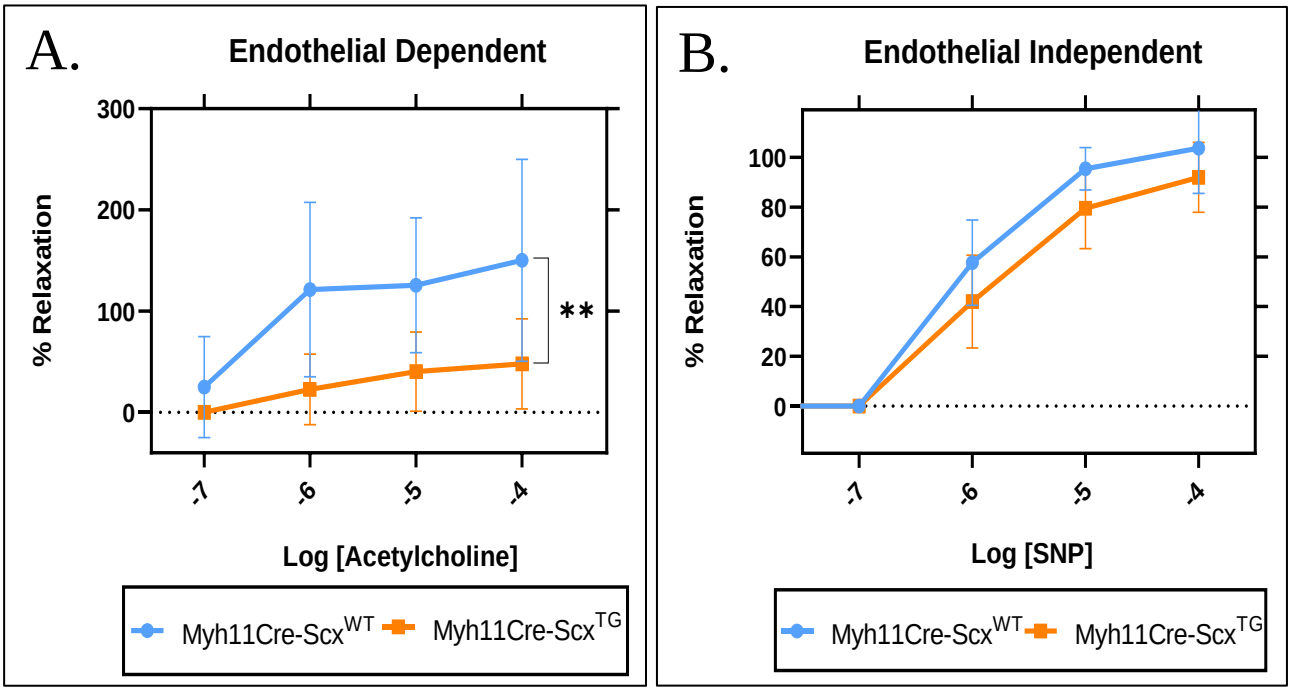

Figure 37 Vasomotor responses of mesenteric arteries from Myh11Cre-Scx^{TG} vs. Myh11Cre-Scx^{WT} mice.

(A) The relaxation in Myh11Cre-Scx^{TG} mesenteries in response to acetylcholine infusion is impaired compared to Myh11Cre-Scx^{WT} mice (**P<0.01). Data are shown as mean ± SD, n=4-5. (B) No significant difference between mesenteric relaxation of Myh11Cre-Scx^{TG} vs. Myh11Cre-Scx^{WT} mesenteric arteries upon sodium nitroprusside infusion. Data are shown as mean ± SD, n= 4.

4. Scleraxis over-expression in VSMCs in arteries of the AngII-induced hypertensive mouse model.

We showed that VSMCs are the major component affected by scleraxis over-expression, and contribute to reducing arterial compliance, particularly in mesenteric resistance arteries. Since mesenteric arteries are the main arteries contributing to blood pressure regulation, we therefore wanted to challenge our VSMC scleraxis over-expression model by raising the blood pressure through the use of mini-osmotic pumps that infuse AngII, to investigate whether scleraxis and AngII synergistically affect the stiffness of these arteries. Myh11Cre-Scx^{TG} or Myh11Cre-Scx^{WT} mice were randomized to receive mini-pumps releasing AngII (1 mg/kg/day) or saline and examined four weeks after pump implantation (Fig. 8B).

4.1 AngII infusion elevates blood pressure regardless of scleraxis overexpression but does not affect peak velocity in all groups.

Telemetry measurements were used in mice with implanted pumps to verify the expected release of AngII and to confirm the proper functioning of the pumps. Telemetry allows for continuous monitoring of changes that might occur throughout the day or night. Telemetry method provides more accurate and reliable readings compared with traditional tail cuff measurements, which can be influenced by the stress experienced by the mice when restrained. The telemetry measurement data obtained from AngII-infused mice shows an increase in blood pressure starting from the midpoint to the endpoint of the study (Fig. 38). This increase is significant in the endpoint measurements of systolic and mean blood pressure in both AngII/Scx^{WT} and AngII/Scx^{TG} mice (Fig. 38). This suggests that scleraxis upregulation does not

play a significant role in blood pressure regulation, and that the increase in blood pressure measurements is primarily attributed to the effects of AngII infusion.

However, the increase in blood pressure in AngII- infused Myh11Cre-Scx^{TG} mice did not alter the pulse-wave velocity (PWV) measurements (Fig. 39). This data indicates that neither the combination of AngII infusion and scleraxis overexpression in VSMCs in the AngII/Scx^{TG} group, nor AngII infusion alone in the AngII/Scx^{WT} group, had any significant impact on the measurement of PWV. PWV measures how quickly pressure waves generated by the heartbeat travel along the arterial system and is used to assess arterial stiffness. In this context, the function of the femoral artery remained unchanged, and there is no noticeable increase in large artery stiffness.

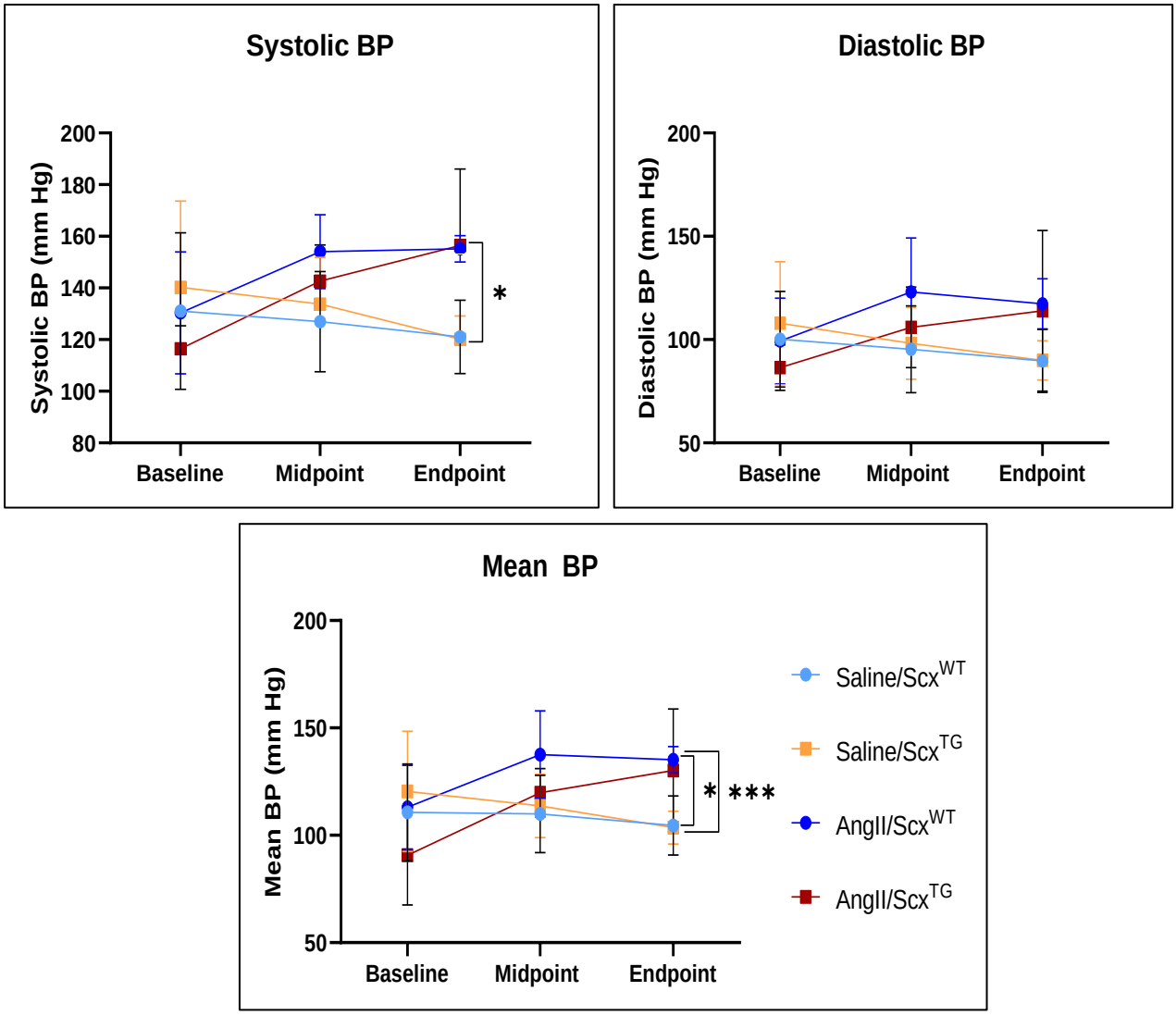

Figure 38. Telemetry blood pressure measurements were taken in all Myh11Cre-mice with implanted pumps.

Measurements were taken at baseline before pump induction, at the midpoint one week after tamoxifen induction and at the endpoint just before mouse sacrifice. The mean baseline measurement are the average blood pressure measurements at baseline that provide a reference point for understanding the initial state of blood pressure, while the mean endpoint reflects the state of blood pressure after the intervention and at the end of study. The timing between the

baseline and endpoint measurements is important to assess the changes in blood pressure over the duration of study. Systolic and mean blood pressure measurements are significantly increased in AngII-induced mice. In systolic BP at the endpoint, *P<0.05 Saline/Scx^{WT} vs AngII/Scx^{WT} and AngII/Scx^{TG}, *P<0.05 Saline/Scx^{TG} vs. AngII/Scx^{WT} and AngII/Scx^{TG}. In mean BP at endpoint, *P<0.05 Saline/Scx^{WT} vs AngII/Scx^{WT}, ***P<0.001 Saline/Scx^{TG} vs. AngII/Scx^{WT}. Data are shown as mean ± SD, n=4-5.

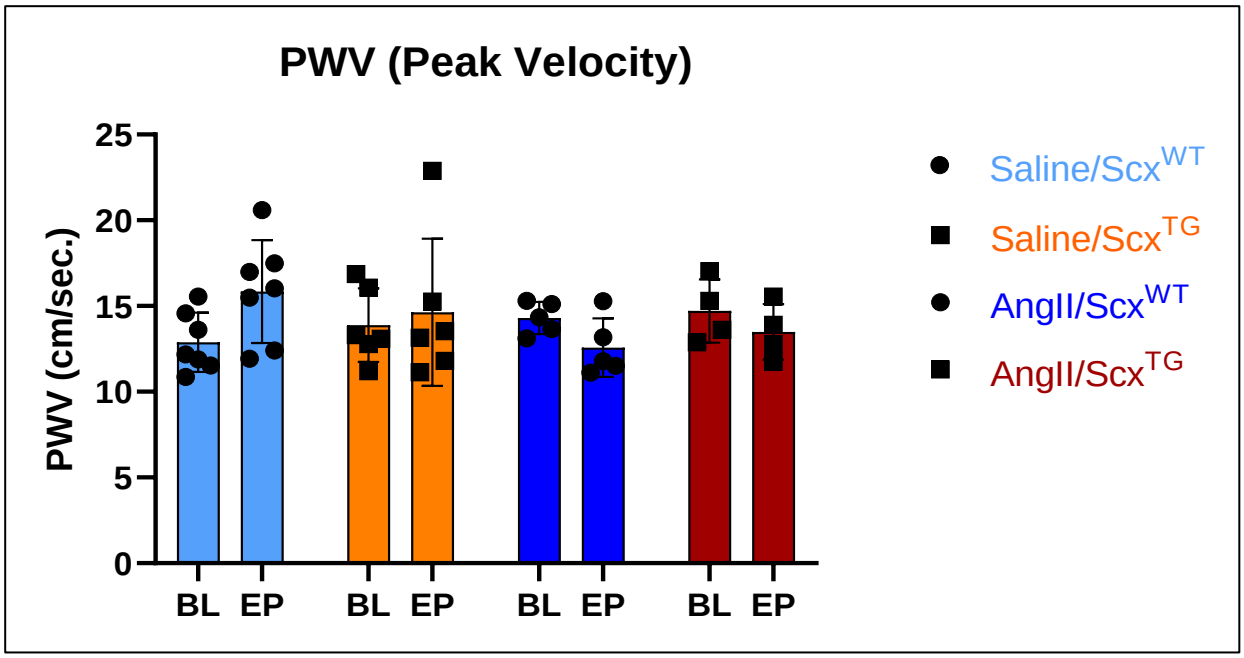

Figure 39. Pulse Wave Velocity - Peak Velocity Measurements on Myh11Cre – mice with implanted pumps measured from the femoral artery.

Measurements were taken in all groups at the baseline (BL), and at the endpoint (EP) just before sacrifice. The animal groups are as follows: Saline/Scx^{WT}, received saline infusion without scleraxis overexpression. Saline/Scx^{TG}, received saline infusion with transgenic scleraxis upregulation. AngII/Scx^{WT}, received Angiotensin II infusion without scleraxis overexpression. AngII/Scx^{TG}, received Angiotensin II infusion with transgenic scleraxis upregulation. No significant difference is observed between groups. Data are shown as mean ± SD, n=4-7.

4.2 AngII+Scleraxis over-expression induces vascular remodeling in large elastic arteries.

4.2.1 AngII+Scleraxis over-expression induces structural changes in the aortic wall of AngII/Scx^{TG} mice.

Aortas from mice were harvested, sectioned, and stained with multiple techniques to assess the effect of AngII infusion in combination with scleraxis upregulation in VSMC on the aortic structure. These stains include hematoxylin and eosin (H&E) for overall assessment of aortic structure, Verhoeff-Van Gieson (VVG) staining to visualize elastin fibers and Picrosirius Red (PR), or Masson's trichrome (MT) for collagen visualisation.

Our findings from the histochemistry experiments indicate that there are some observable changes in the aortic media in AngII infusion aortas and when the scleraxis gene is over-expressed along with AngII infusion. Although the changes from these histological images were not quantified, we noted alterations in the arrangement of elastic fibrils, characterized by elastin discontinuity in the VVG staining images in saline/Scx^{TG} and AngII/Scx^{TG} (Fig. 40). The over-expression of scleraxis shows some changes in the fibrillar arrangement and elastin discontinuity in Saline/Scx^{TG} (Fig. 41B). AngII infusion alone shows medial expansion represented as voids in the trans-lamellar layers of the AngII/Scx^{WT} aortic wall (Fig. 41C, D). However, when both AngII infusion and scleraxis over-expression are present together in AngII/Scx^{TG} aortas, our data visibly show a decrease in voids expansion within the media in the vessel wall, and a noticeable elastin disruption (Fig. 41, B-D). These observations may suggest potential functional consequences such as changes in wall composition that alters the vascular compliance and the elasticity of AngII/Scx^{TG} aortic arteries.

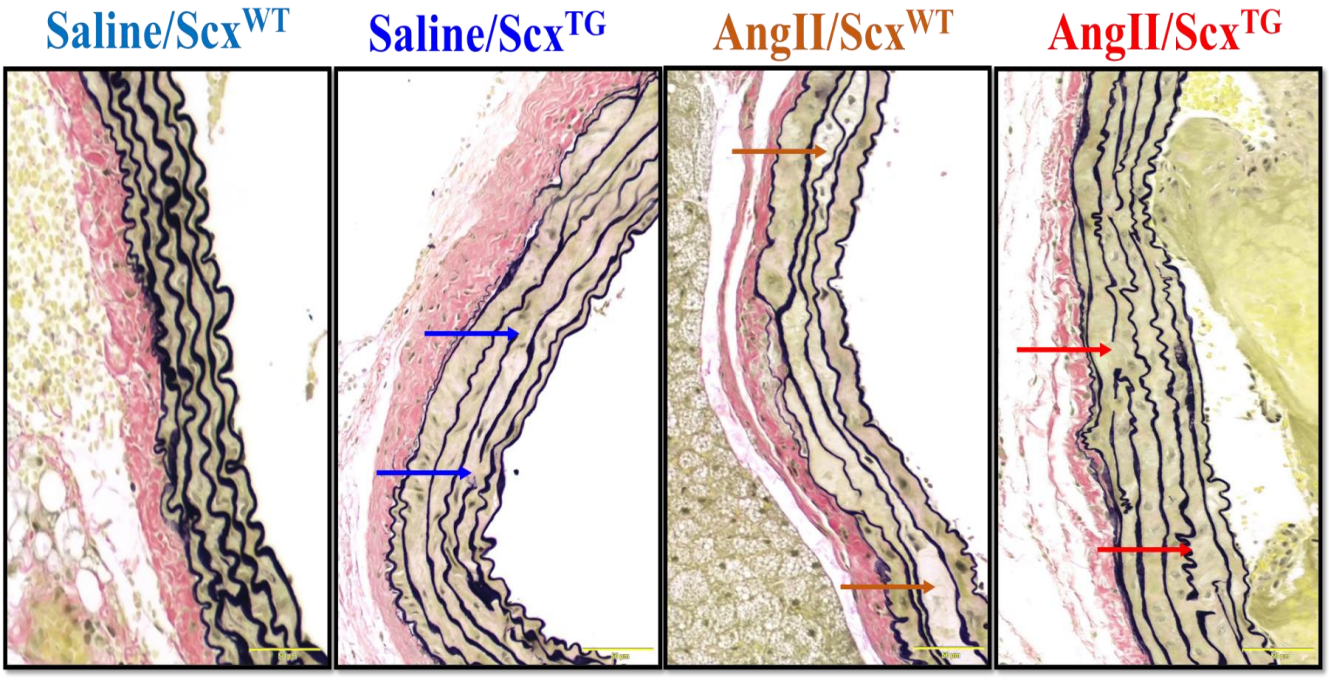

Figure 40. Representative close-up images of Van-Verhoef Gieson Staining for aortic sections from Myh11Cre-mice with implanted pumps.

These images show signs of remodelling in the aortic arterial wall, including elastin discontinuity in saline/Scx^{TG} aortas (blue arrows). In AngII/Scx^{WT} aortas, there is a medial expansion represented as "voids" within the media (orange arrows). AngII/Scx^{TG} aortas exhibit elastin disruption prominent (red arrows). Scale bar = 50 µm. n=3-4

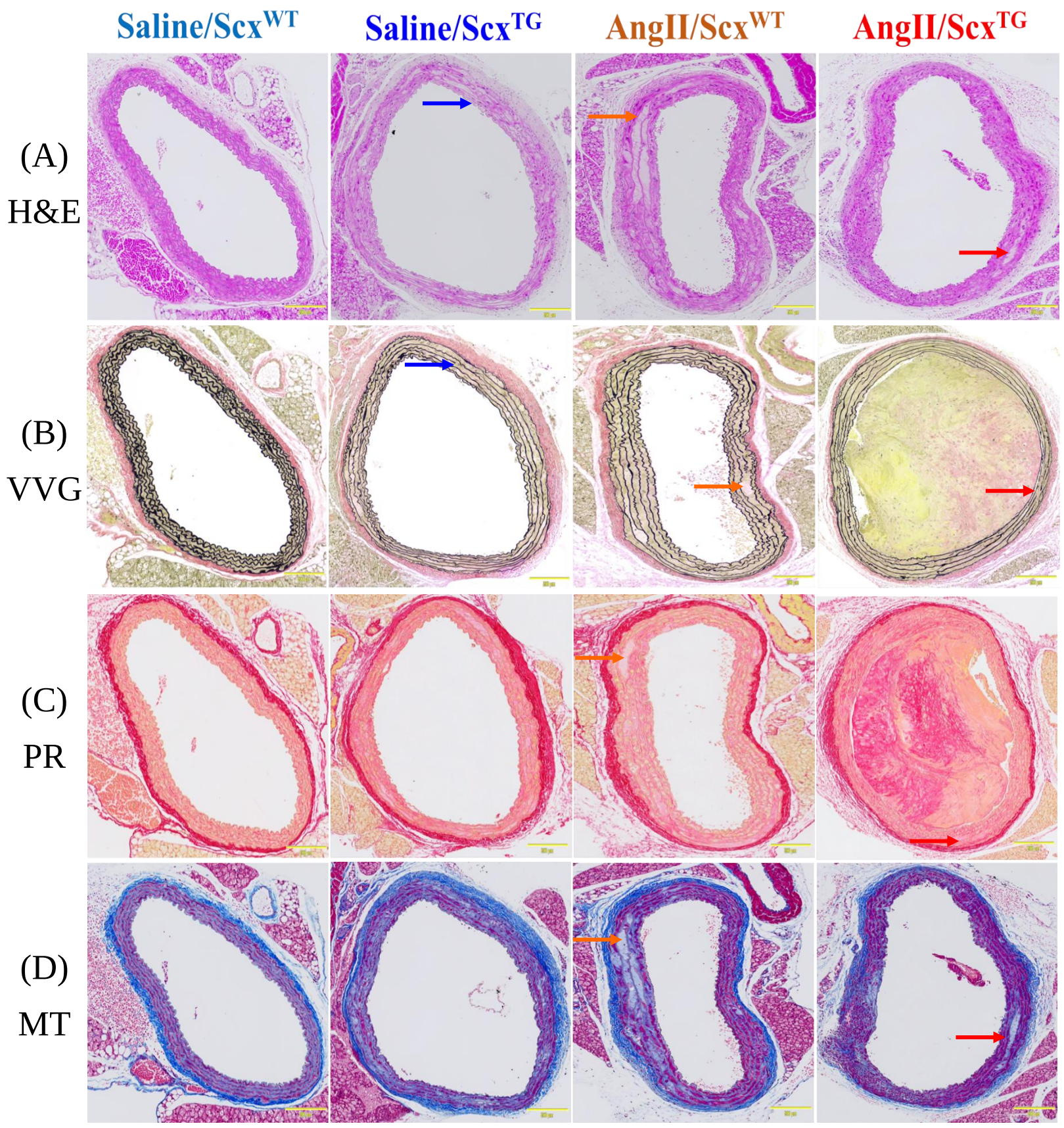
Saline/Scx^WT
Saline/Scx^TG
AngII/Scx^WT
AngII/Scx^TG
(A)
H&E
(B)
VVG
(C)
PR
(D)
MT

Figure 41. Histology sections with immunohistostaining to assess structural changes from Myh11Cre-mice aortas with implanted pumps.

Representative immunohistochemical images of aortic sections stained with (A) hematoxylin and eosin (H&E) for the overall assessment of aortic structure. The images show changes of fibrillar arrangement in scleraxis upregulated aortas in saline/Scx^{TG} (dark-blue arrow), and a trans lamellar voids expanding within the media of AngII infusion aortas in AngII/Scx^{WT} (orange arrow). Conversely, aortas from AngII/Scx^{TG} mice where scleraxis upregulation is combined with AngII infusion exhibit a lower level of voids when compared to AngII/Scx^{WT} aortas (red arrow). The control aorta from Saline/Scx^{WT} mice where saline is infused with wild type scleraxis expression and serves as a reference point of comparison. (B) Verhoeff-Van Gieson (VVG) staining is used to visualize elastin content, which is represented by black fibers within the media. Over-expression of scleraxis alone in saline/Scx^{TG} aortas and in AngII/Scx^{TG} visually shows elastin discontinuity (dark-blue arrow, red arrow) respectively. AngII/Scx^{WT} shows an increase in expanded voids (orange arrow). (C) Picrosirius Red (PR) and (D) Masson's trichrome (MT) staining are employed for collagen visualization, with a clear visualisation of expanded voids in AngII/Scx^{WT} (orange arrow) showing a notable increase in the aortic media when compared to AngII/Scx^{TG} (red arow). Scale bar = 200 μm, n = 3-4.

4.2.2 AngII+scleraxis over-expression significantly attenuates ECM gene expression in the aorta.

Our gene expression data show that aortas from AngII+scleraxis over-expression mice have reduced mRNA expression of the main ECM components, including fibronectin (P<0.001), Col 1α1(P<0.01), Col 3α1(P<0.05) and elastin (P<0.01) within the aortic wall compared to AngII/Scx^{WT} (Fig. 42).

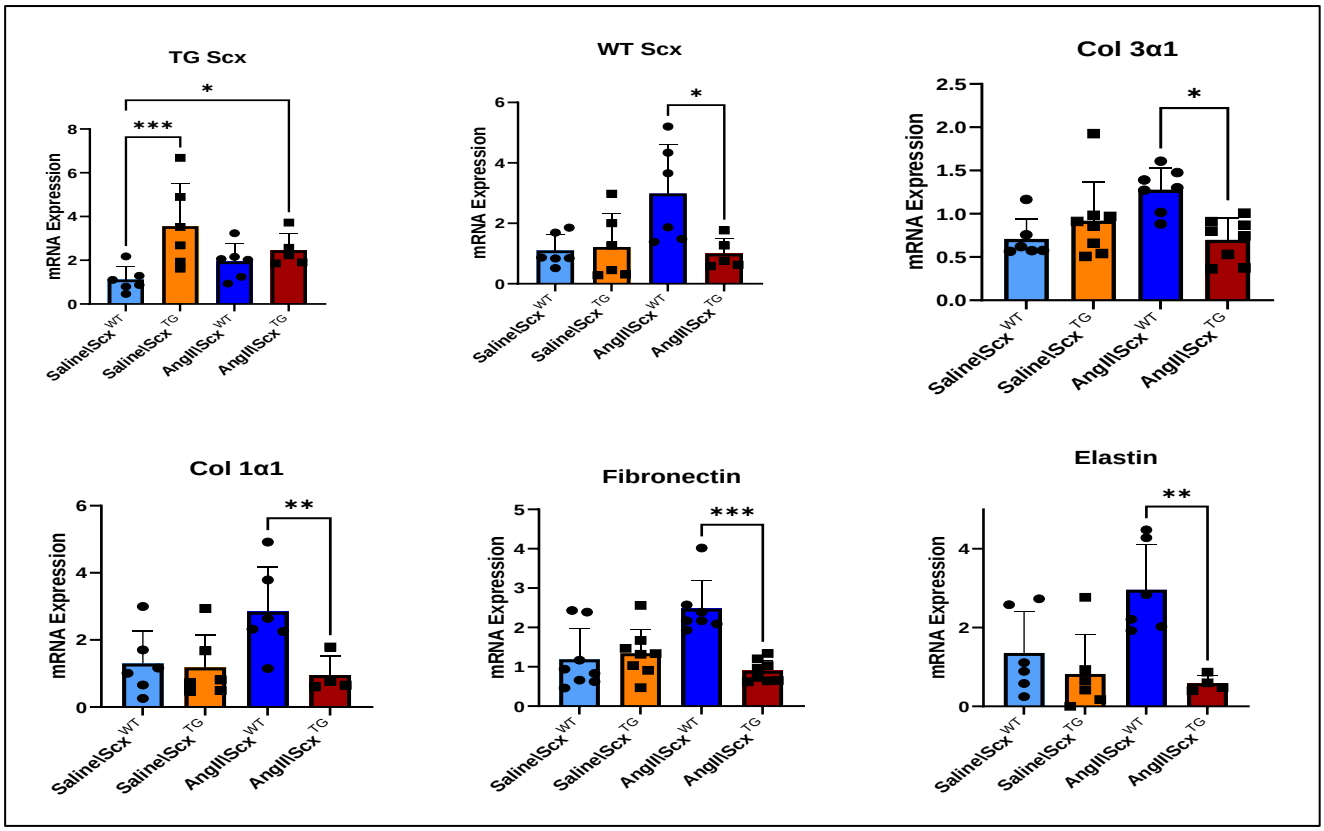

Figure 42. mRNA gene expression in the aortas of Myh11Cre-mice with implanted pumps.

Transgenic scleraxis (TG Scx) is significantly increased in Saline/Scx^{TG} vs. control ***P<0.001, and in AngII/Scx^{TG} vs. control *P<0.05. ECM gene expression is reduced in AngII/Scx^{TG} vs. AngII/Scx^{WT} for collagen 3α1 (Col 3α1) (*P<0.05), Collagen 1α1 (Col 1α1) (**P<0.01), fibronectin (FN) (***P<0.001, and elastin (**P<0.01). Data are shown as mean ± SD, n=7-8.

4.3 AngII+scleraxis over-expression significantly increases small mesenteric artery stiffness as a result of structural modifications.

4.3.1 AngII+scleraxis over-expression alters some geometrical properties of resistance mesenteric arteries.

At normal physiological intraluminal pressure of 60 mmHg, our data shows that there are no changes in media CSA and media wall thicknesses between all groups (Fig. 43). Intriguingly, significant changes in M/L were shown between AngII/Scx^{TG} mice in comparison with the Saline/Scx^{WT} control group ($P<0.05$) (Fig. 43). This finding indicates that the internal lumen diameter is significantly reduced in AngII+scleraxis over-expression mesenteric arteries, suggesting eutrophic inward remodeling of the mesenteric resistance vessels in the AngII/Scx^{TG} group.

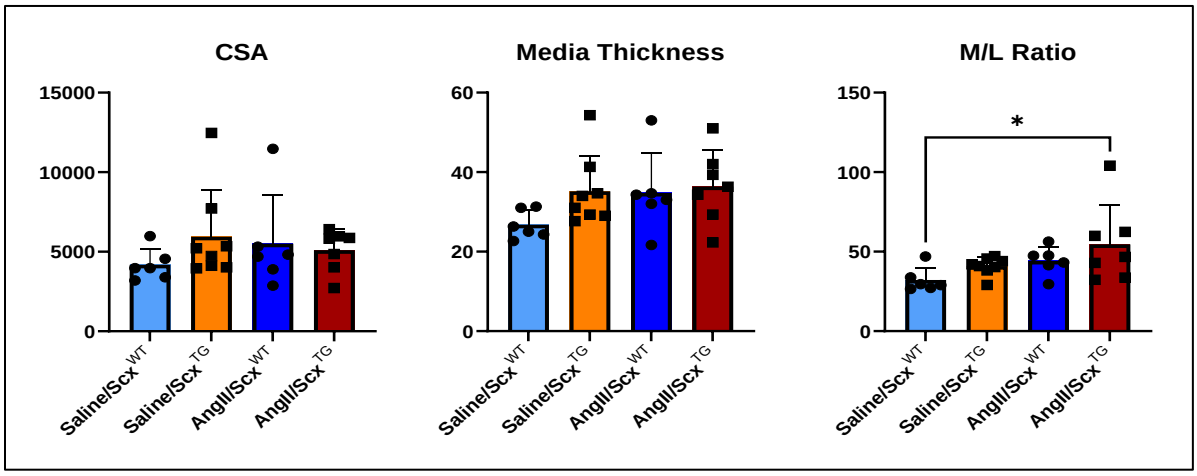

Figure 43. Media CSA, wall thickness and M/L ratio of mesenteric resistance arteries from Myh11Cre-mice with implanted pumps.

No changes in mesenteric media cross sectional area (CSA) and wall thickness are observed between groups. However, a significant difference is noted in the media to lumen ratio (M/L) between the mesenteries of the scleraxis overexpression combined with AngII infusion in AngII/Scx^{TG} compared to control Saline/Scx^{WT} group *$P<0.05$. Data are shown as mean ± SD, n=6-8.

4.3.2 AngII+scleraxis over-expression significantly attenuates vascular compliance in mesenteric resistance arteries.

Mechanical studies performed on mesenteric arteries show that AngII infusion along with scleraxis over-expression in the mesenteries results in the highest arterial stiffness and exhibits a significant reduction in vascular compliance in AngII/Scx^{TG} mesenteries when compared to other groups, including AngII/Scx^{WT} as shown by leftward shifting of the stress vs. strain curve (Fig. 44). This is quantified by the k-value between the curves of stress-strain of all groups.

The reduction in vascular compliance can be due to changes in vascular wall components from both AngII-infusion and scleraxis overexpression in AngII/Scx^{TG} as verified by the measurement of the slope between EM vs. change in stress ($P<0.01$) (Fig. 45). Other parameters such as EM vs. IP or stress vs. IP, which are related to changes in the geometrical alignment of blood vessels, show no significant differences (Fig. 45). These findings suggest notable shifts in how the blood vessel wall reacts to higher levels of stress, potentially reflecting alterations in vascular structure, as illustrated in Figure 43. However, there aren't significant changes observed in how the blood vessels respond to slight increases in force applied through small increments in intraluminal pressure.

In summary, our data indicate that AngII infusion alone can stimulate vascular remodeling in resistance blood vessels, and the effect of AngII infusion is more potent when combined with scleraxis over-expression, i.e. the combination of AngII and scleraxis over-expression results in stiffer vessels than either factor alone. Thus, AngII/Scx^{TG} mesenteric arteries have an augmented vascular remodeling represented geometrically by the reduction of internal lumen diameter and mechanically by changes in wall components as identified in the curve changes between EM vs. stress.

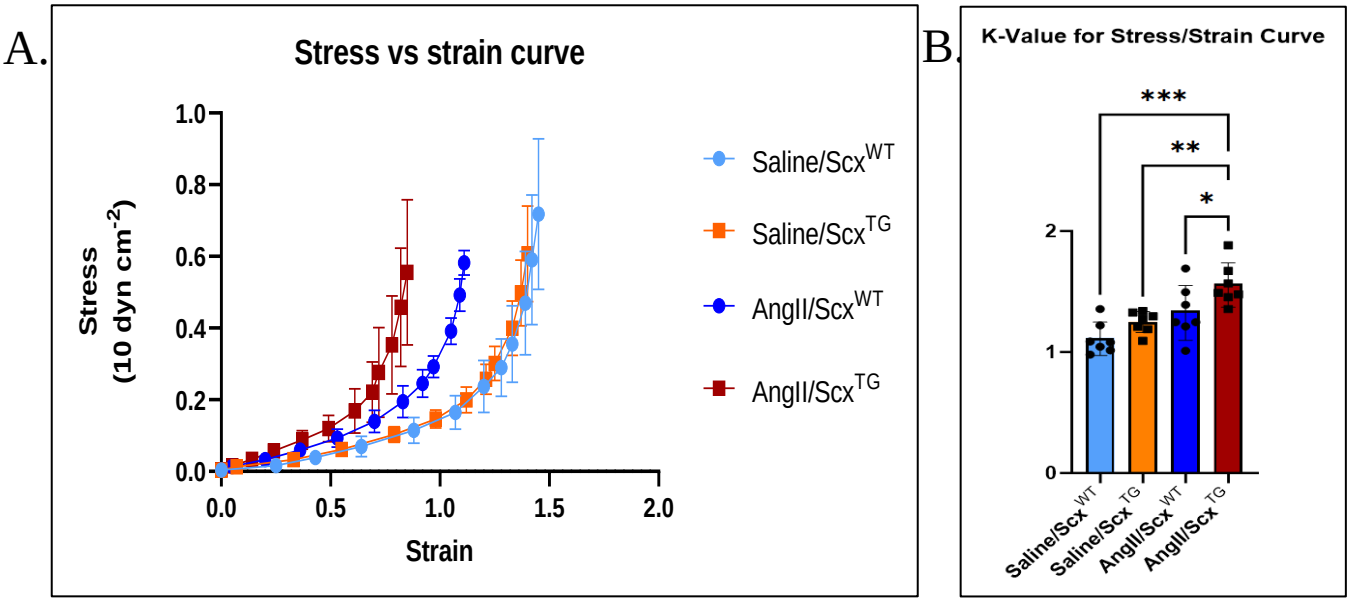

Figure 44. Wall stress-strain relationships for resistance mesenteric arteries of Myh11Cre- mice with implanted pumps and their effect on vascular compliance.

(A) The stress-strain curve of AngII-infused arteries was shifted to the left and was further shifted in combination with scleraxis over-expression (B) The k-value shows significance in AngII+scleraxis over-expression arteries when compared to controls. ***P<0.001 saline/Scx^{WT} vs AngII/Scx^{TG}, **P<0.01 saline/Scx^{TG} vs AngII/Scx^{TG}, *P<0.05 AngII/Scx^{WT} vs. AngII/Scx^{TG}. Data are shown as mean ± SD, n = 6-7.

A.

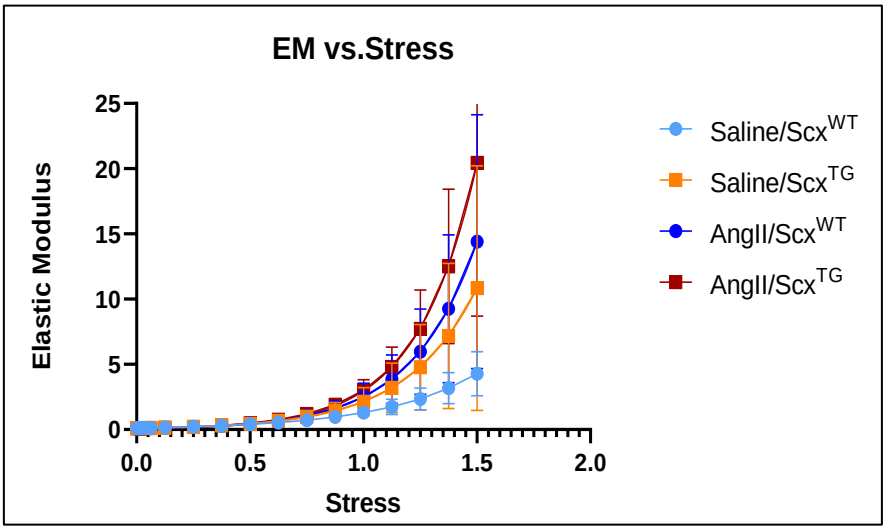
EM vs.Stress
Elastic Modulus
25
20
15
10
5
0
0.0
0.5
1.0
1.5
2.0
Stress
Saline/Scx^WT
Saline/Scx^TG
AngII/Scx^WT
AngII/Scx^TG

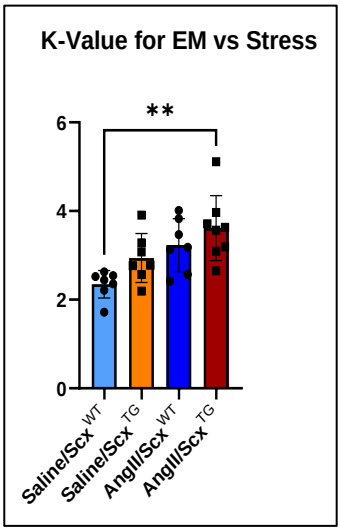
K-Value for EM vs Stress
**
6
4
2
0
Saline/Scx WT
Saline/Scx TG
AngII/Scx WT
AngII/Scx TG

B.

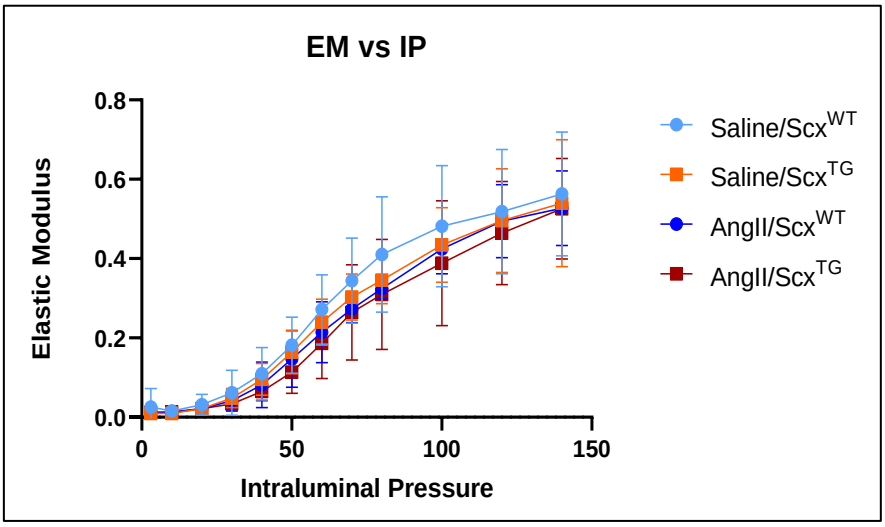
EM vs IP
Elastic Modulus
0.8
0.6
0.4
0.2
0.0
0
50
100
150
Intraluminal Pressure
Saline/Scx^WT
Saline/Scx^TG
AngII/Scx^WT
AngII/Scx^TG

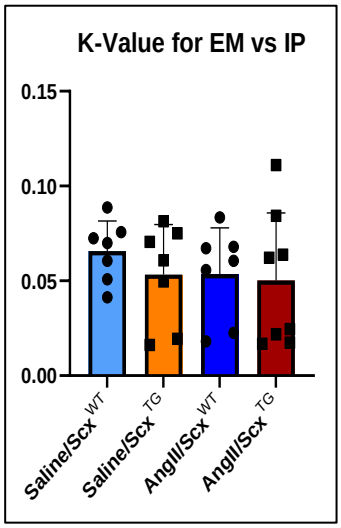
K-Value for EM vs IP
0.15
0.10
0.05
0.00
Saline/Scx WT
Saline/Scx TG
AngII/Scx WT
AngII/Scx TG

C.

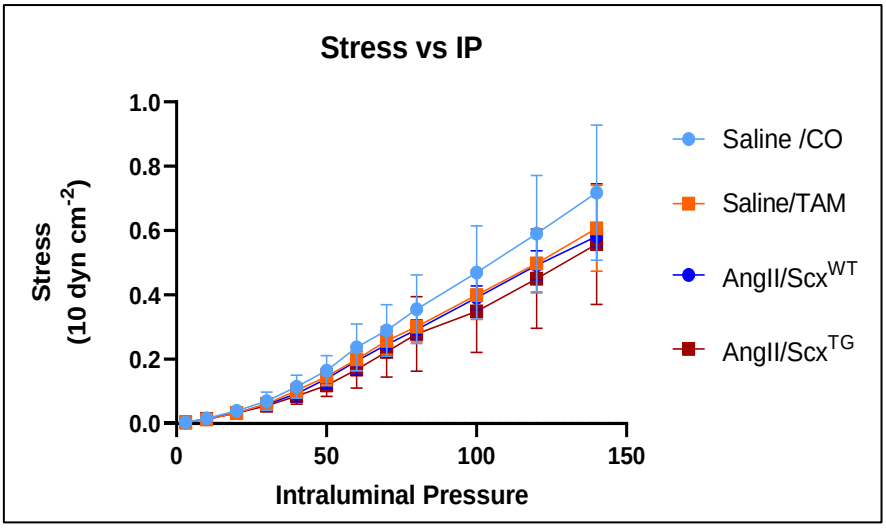
Stress vs IP
Stress
(10 dyn cm^-2)
1.0
0.8
0.6
0.4
0.2
0.0
0
50
100
150
Intraluminal Pressure
Saline /CO
Saline/TAM
AngII/Scx^WT
AngII/Scx^TG

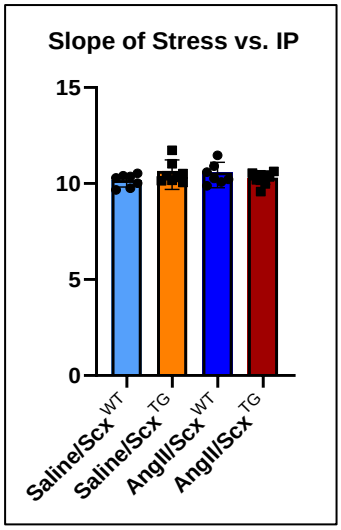
Slope of Stress vs. IP
15
10
5
0
Saline/Scx WT
Saline/Scx TG
AngII/Scx WT
AngII/Scx TG

Figure 45. Mesenteric artery stiffness parameters from Myh11Cre-mice with implanted pumps.

(A) The elastic modulus (EM) vs. media stress curve illustrates how the vessel's stiffness changes in response to different levels of stress, assessing the mechanical properties of mesenteric artery based on the vascular wall components including collagens, elastin fibers, and VSMC. Significant changes in vascular wall components represented by the k-value of EM to stress curve, **P<0.01 Ang/Scx^{TG} vs. Saline/Scx^{WT} were noted. (B) The EM-intraluminal pressure (IP) curve represents how the vessel's stiffness (elastic modulus) responds to changes in incremental pressure. Thus, a change in vascular stiffness can be due to changes in arterial wall components and on the geometrical alignment of the mesenteric artery, in response to incremental changes in pressure (IP) applied on the blood vessel. Quantified data using the k-value of the EM vs. IP curve show no significant alterations in mesenteric wall between all groups were noted. (C) Stress vs. IP curve identifies the ability of the blood vessel to adapt to force changes in response to the incremental pressure applied on its walls. No significant changes were identified in vascular elasticity or geometrical alignment, which are quantified by changes in the slope or K-value between all groups. Data are shown as mean ± SD, n=6-7.

4.3.3 AngII+scleraxis over-expression impairs the relaxation of the VSMCs in small mesenteric resistance arteries.

AngII induction independent of scleraxis over-expression impairs the endothelial cell-dependent relaxation response in mesenteric arteries (Fig. 46A). However, VSMC function is significantly impaired in AngII + scleraxis over-expression arteries (Fig. 46B).

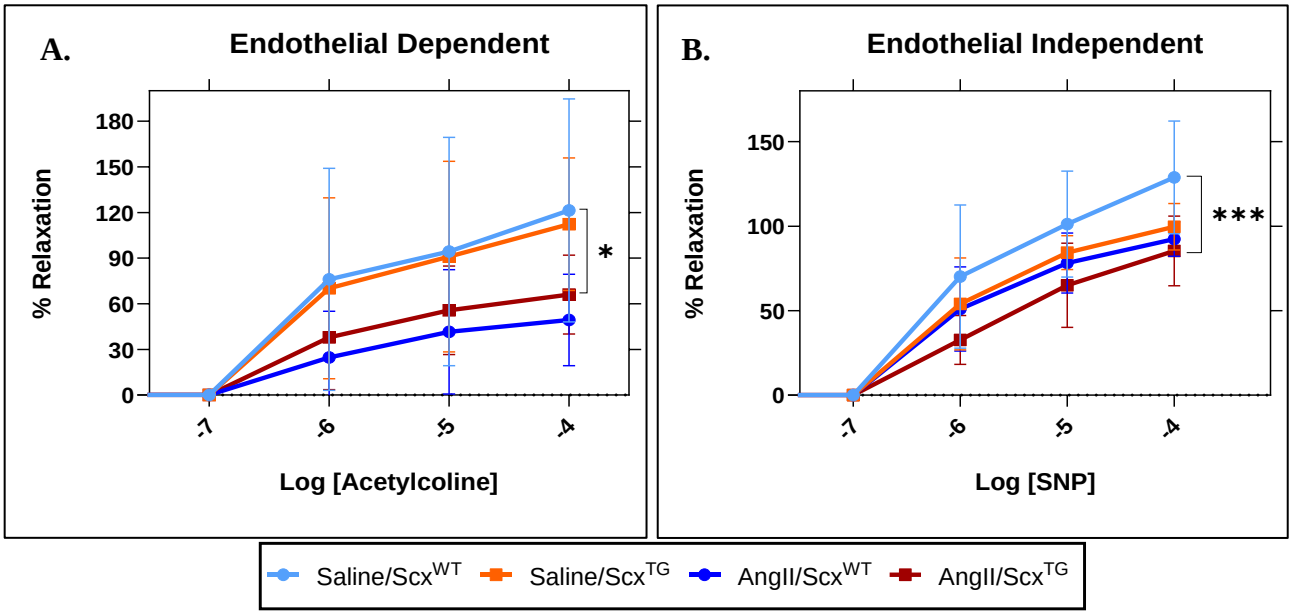

Figure 46. Vasomotor responses of mesenteric resistance arteries from Myh11Cre-mice with implanted pumps.

(A) The vasodilatory response of endothelial cells is reduced in all mice groups with AngII infusion pumps upon gradual infusion of acetylcholine (*P<0.05, Saline/Scx^{WT} vs. AngII/Scx^{TG}). Data are shown as mean ± SD**,** n=4-6. (B) The smooth muscle relaxation function is impaired upon gradual infusion of SNP in AngII-treated mesenteries and is severely reduced in AngII+scleraxis over-expression mesenteries (*** P<0.001, Saline/Scx^{WT} vs AngII/Scx^{TG}). Data are shown as mean ± SD**,** n=5.

5 Scleraxis over-expression in Human Aortic Smooth Muscle Cells (HAOSMCs) *in vitro*

HAOSMCs were used to extend and validate our animal model studies where scleraxis is being over-expressed in smooth muscle cells. We wanted to clarify or explain some data from the animal studies alone. For example, in the first study where scleraxis was upregulated upon induction of tamoxifen in Myh11Cre-Scx^{TG} mice and these mice were sacrificed 8-weeks later. Scleraxis over-expression in the vascular smooth muscle cells of Myh11Cre-Scx^{TG} -mice changed the mechanical compliance of mesenteric resistance arteries (Fig. 35) without showing any significant changes in other parameters of stiffness including EM vs. IP or EM vs. stress (Fig. 36). In addition, aortic DAPI staining indicated increased cellularity in scleraxis-over-expressed aortic sections (Fig. 32). In AngII+scleraxis over-expression aortas, surprisingly, there was a reduced level of ECM gene expression when compared when AngII infusion aortas alone (Fig. 42). However, the mesenteric arteries of AngII-Scx^{TG} show a significant increase in stiffness that is related to increased wall components which can include ECM or cells (Fig. 44,45). This intriguing data needed further investigation to explore the role of scleraxis over-expression and in combination with AngII treatment *in vitro* in HAOSMC.

5.1 Effect of scleraxis over-expression in HAOSMCs on cell proliferation

5.1.1 Scleraxis over-expression induces smooth muscle cell proliferation.

To investigate the role of scleraxis overexpression on HAOSMC proliferation, HAOSMCs were infected with adenovirus expressing scleraxis or a control adenovirus or left untreated. HAOSMC proliferation rate was measured by optical density after 24, 48, and 72 hours. Our data show that the number of HAOSMCs is increased with scleraxis over-expression and reaches significance after 72 hours of infection ($P<0.0001$) (Fig. 47).

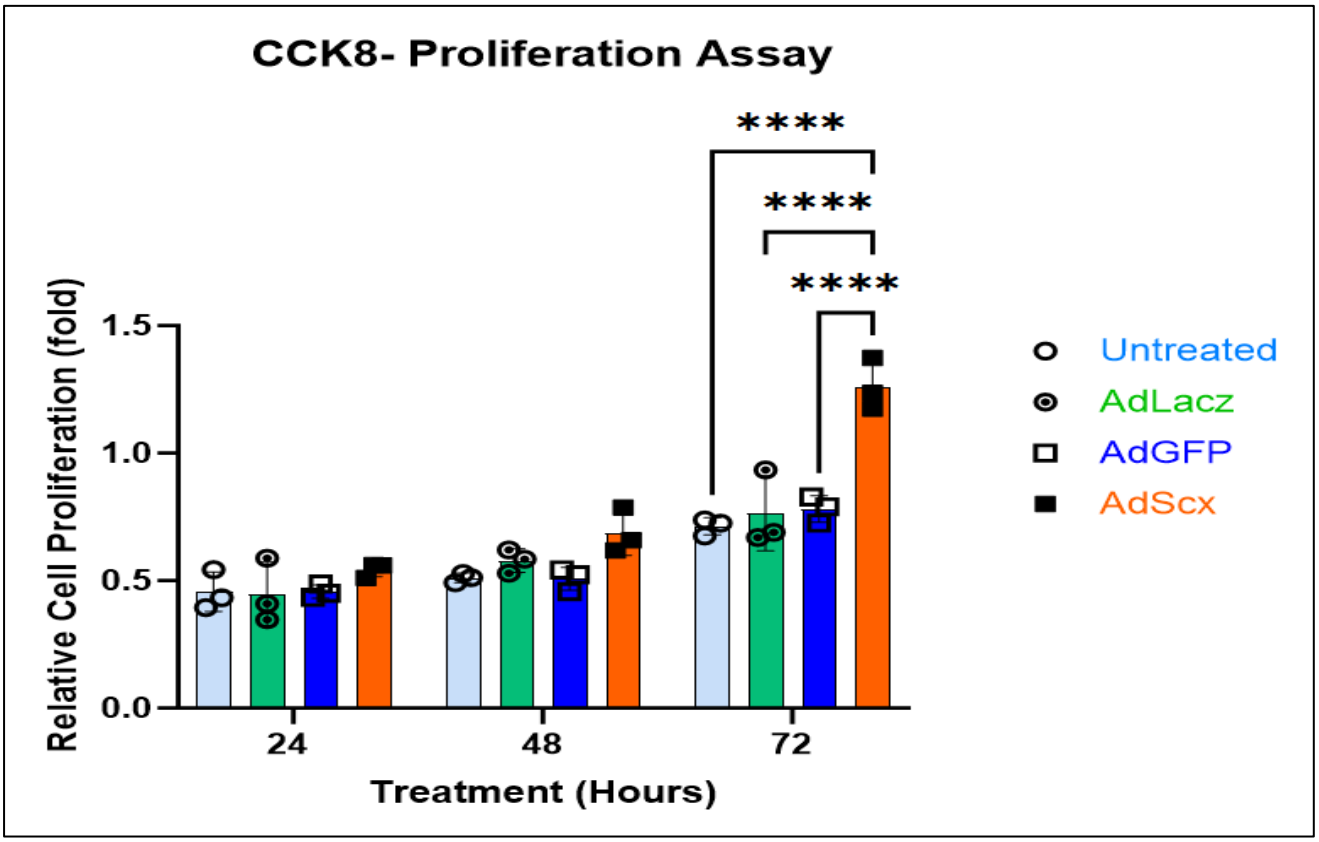

Figure 47. Measuring HAOSMC proliferation in response to scleraxis over-expression.

HAOSMCs were infected with either AdScx to over-express scleraxis (orange bars) or control viruses including AdGFP (dark blue bars) and AdLacz (green bars) or were left untreated (light blue bars). Cell proliferation was measured in each of these groups over the course of 24, 48, and 72 hours. Scleraxis over-expression in HAOSMC significantly increases cell proliferation after 72 hours when compared with controls (untreated, AdGFP, AdLacz) ****P<0.0001. Data are shown as mean ± SD, n=3.

To confirm the previous findings where the scleraxis upregulation would induce HAOSMC proliferation, we measured the protein level of proliferative markers in scleraxis over-expressing HAOSMCs and found that Ki67 is significantly increased as a result (Fig. 48). PCNA shows a trend to increased expression following scleraxis over-expression, although this effect did not reach significance compared to control viruses (AdGFP, AdLacz) and uninfected cells.

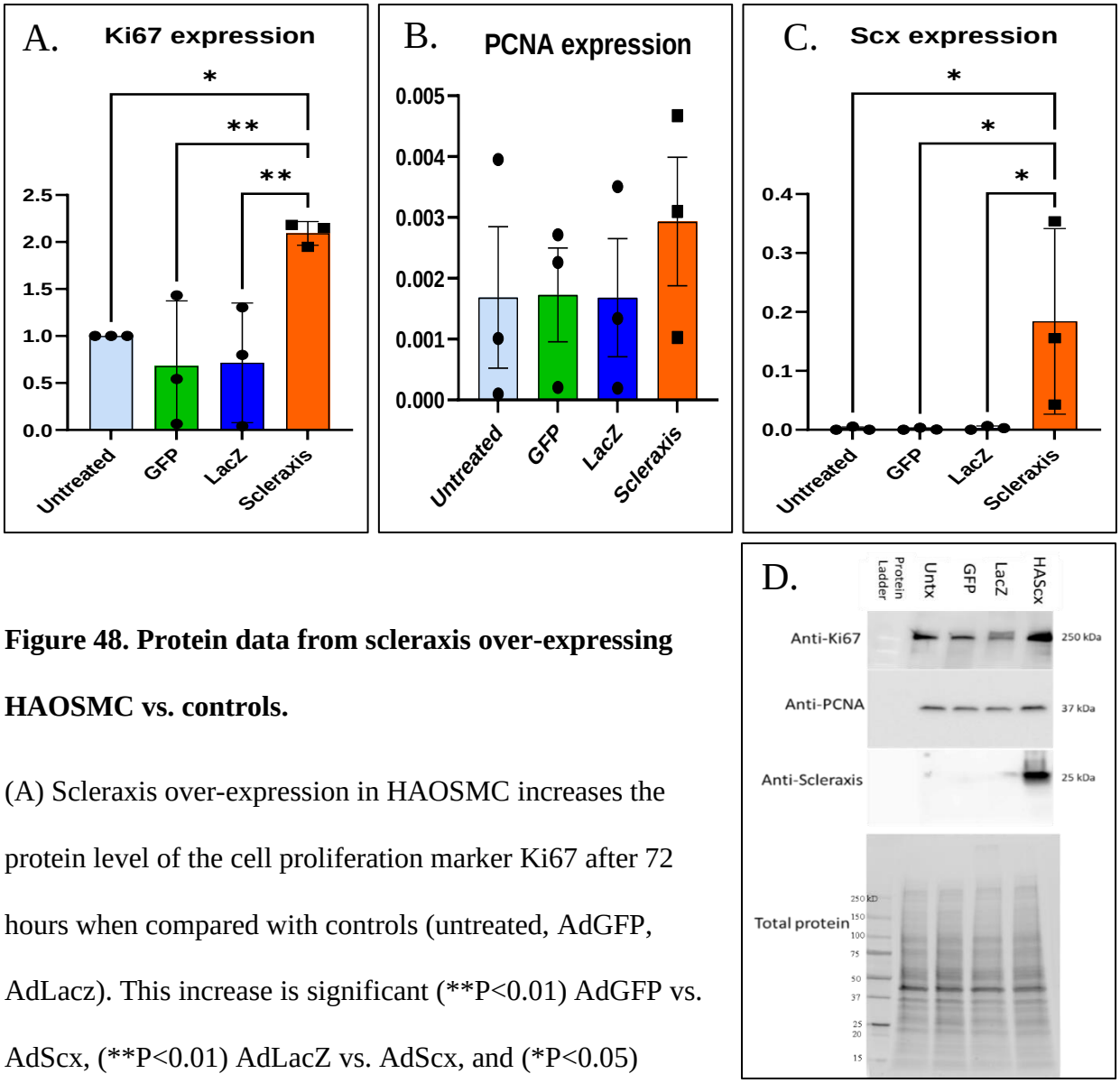

Figure 48. Protein data from scleraxis over-expressing HAOSMC vs. controls.

(A) Scleraxis over-expression in HAOSMC increases the protein level of the cell proliferation marker Ki67 after 72 hours when compared with controls (untreated, AdGFP, AdLacz). This increase is significant (**P<0.01) AdGFP vs. AdScx, (**P<0.01) AdLacZ vs. AdScx, and (*P<0.05) Untreated vs. AdScx. (C) Scleraxis protein over-expression was verified, showing that AdScx-infected HAOSMC induce significantly higher scleraxis protein levels than controls. (*P<0.05) (untreated, AdGFP, AdLacZ vs. AdScx). (B) Although PCNA shows a similar trend, when quantified, this increase was not significant when compared to controls. (D) The protein blot showing protein expression as verified by antibodies of anti-Ki67, anti-PCNA and anti-scleraxis and the blot of total protein as a loading control. Data are shown as mean ± SD, n=3.

This figure was generated with the assistance of Teri Moffatt – WB run & quantification.

5.1.2 Scleraxis over-expression induces the smooth muscle cell proliferative phenotype.

Our findings suggest that scleraxis may promote the conversion of smooth muscle cells from the contractile to the proliferative phenotype. To verify this possibility, we assessed the mRNA expression of VSMC contractile markers including calponin, SMMHC and SM22α. Calponin and SM22α regulate smooth muscle cell contraction through actin interactions. Calponin binds to actin filaments, inhibiting actomyosin ATPase and actin movement. When phosphorylated, calponin's binding to actin weakens, allowing myosin-actin interaction and contraction. SM22α, similar to calponin, modulates VSMC contraction but independently of the Ca^{2+}/MLCK phosphorylation pathway. SMMHC, a primary contractile protein, promotes VSMC contraction by ATP hydrolysis, generating mechanical force. Each of these contractile proteins are markers for VSMCs in the contractile state.

Our findings show that scleraxis upregulation in HAOSMCs significantly reduces the mRNA expression of both calponin ($P<0.05$) and SMMHC ($P<0.01$) , but this does not occur for SM22α (Fig. 49). This data indicates that scleraxis may play a role in facilitating the transition of VSMCs from a contractile to a proliferative phenotype, ultimately promoting VSMC proliferation and growth.

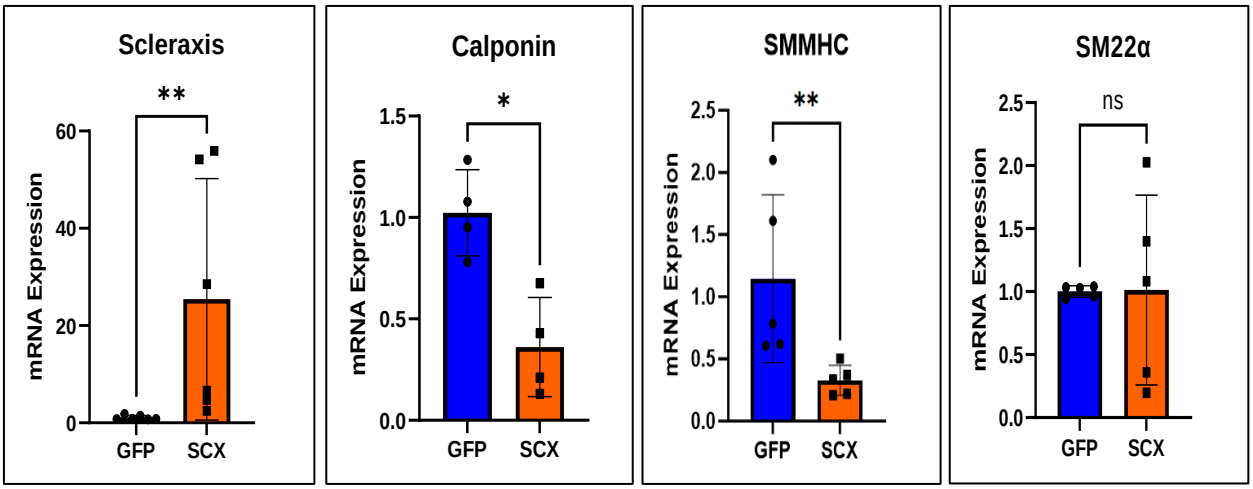

Figure 49. Contractile marker gene expression in HAOSMCs through qPCR following scleraxis over-expression.

The first panel from the left shows a significant increase of scleraxis over-expression in HAOSMCs in comparison to control, AdScx vs. AdGFP (**P<0.01). Scleraxis over-expression significantly reduced the expression of some contractile markers after 72 hours, including calponin (*P<0.05) and Smooth Muscle- Myosin Heavy Chain (SMMHC) (**P<0.01). No significant change in transgelin (SM22α) gene expression was observed between the two groups. Data are shown as mean ± SD, N=4-5.

5.2 Role of scleraxis over-expression in HAOSMC combined with AngII treatment.

5.2.1 The over-expression of scleraxis changes the effect of AngII on the plastic properties of smooth muscle cells.

Different studies have suggested that AngII can induce VSMC proliferation and hypertrophy. In our study, we investigated if over-expression of scleraxis would synergistically interact with AngII treatment to alter the phenotype of HAOSMC. Specifically, we aimed to measure the proliferation rate in all treated groups of HAOSMCs using flow cytometry (Fig. 50). To assess the proliferation rate, we used the proliferation marker 5-Ethynyl-2'-deoxyuridine (EdU) which incorporates into the newly synthesized DNA during active DNA synthesis at the S-phase of cell division. EdU is conjugated to a fluorescent dye, Alexa Fluor 647, to allow for the detection of EdU by flow cytometry. In flow cytometry, the HAOSMC suspension from each group through a laser beam and emits fluorescence signals based on the presence or absence of the EdU. The flow cytometer records these signals and generates data on the number of cells that have incorporated EdU, indicating the proliferation status of cell populations. The resulting histogram represents each cell as a dot, and divides cell cycle phases by coloured groups.

The cell distribution histogram demonstrates a clear separation of cells in S phase (DNA synthesis, including EdU incorporation) and cells in either G_2/M or G_0/G_1 (Fig. 50). Our findings indicate that scleraxis treatment alone induces the highest number of EdU+ cells in the DNA synthesis phase, suggesting that scleraxis upregulation induces HAOSMC proliferation (Fig. 50B), which was quantified ($P<0.01$) (Fig. 50E). Meanwhile AngII treatment induced HAOSMC proliferation but to a lesser extent compared to when scleraxis is upregulated alone (Fig. 50C).

Intriguingly, HAOSMCs treated with both scleraxis and AngII (Scx+AngII) displayed a reduced rate of proliferating cells marked by less EdU positivity compared to cells with either AngII or scleraxis alone (Fig. 50D). Specifically, Scx+AngII-treated cells exhibited a significantly lower proliferation rate in comparison with scleraxis over-expression alone ($P<0.05$) (Fig. 50E).

A.

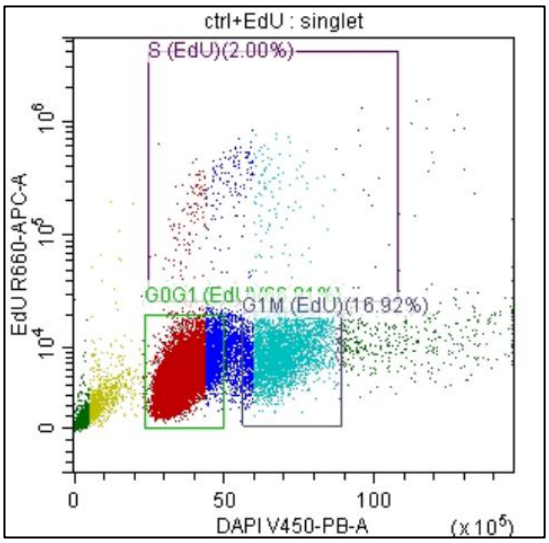

B.

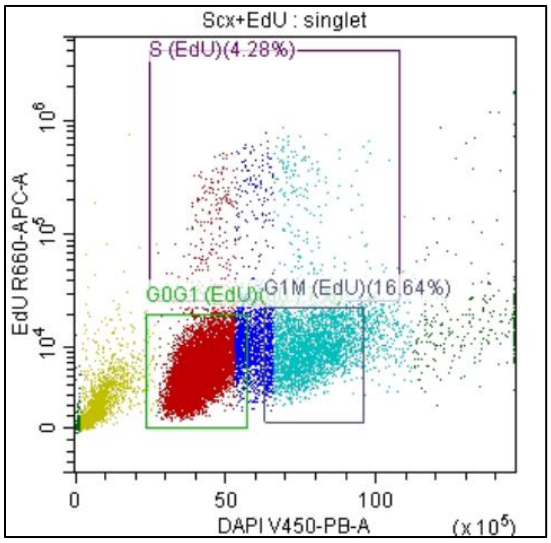

C.

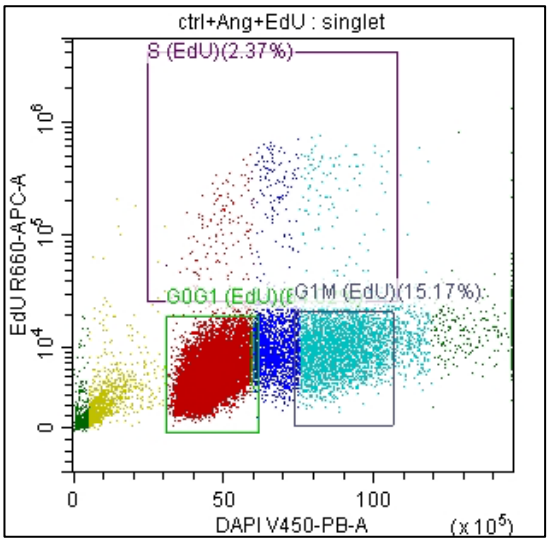

D.

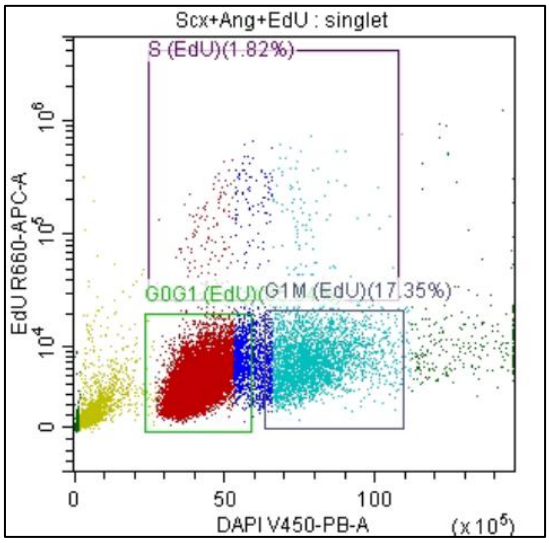

Figure 50. Flow cytometry analysis to assess the proliferation rate of HAOSMCs treated with scleraxis and/or AngII treatment.

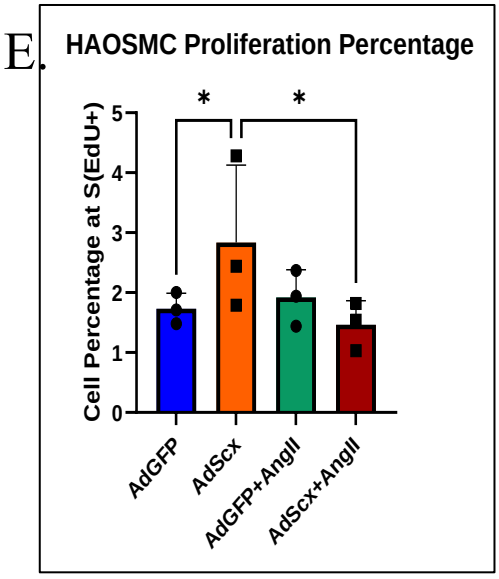

The samples were co-stained with DAPI to indicate cell cycle and EdU for active cell proliferation. The EdU positive cells are indicated in the purple rectangular region. The coloured dots represent the distribution of cells based on their DNA content, categorizing the cells into different phases of the cell cycle including G_0/G_1 (the beginning of cell cycle and cell growth) and G_2/M (cell growth maintained, preparing for cell division/ mitosis) and S (DNA synthesis). Each color on the graph corresponds to a distinct cell population within a specific phase of the cell cycle. For example, yellow signifies cells at subG0 phase, the red signifies cells in G0/G1 phase, the light blue signifies cells at G1M phase, and the purple signifies the percentage of cells in S phase. The dot plots (A-D) provide a direct measurement of the proportion of positive cells in the S-cycle, which reflects the proliferative capacity of HAOSMCs. (A) a representative histogram dot plot showing the percentages of control HAOSMC cell at different phases of cell division and proliferation. (B) a histogram shows the percentage of cell distribution in the scleraxis overexpression HAOSMC group, showing the highest percentage of cells in S-phase, indicating the highest proliferation rate. (C) a histogram for cell distribution representing AngII-treated HAOSMC. (D) a histogram showing cell distribution of AngII-treated HAOSMCs in combination with scleraxis overexpression. (E) Quantification of proliferative VSMC flow cytometry data from S (EdU+) from all groups. Scleraxis over-expression alone induces an increased proliferation rate,

while AngII reverses this effect (*P<0.05) AdGFP vs. AdScx, (*P<0.05) AdScx vs. AdScx+AngII, Data are shown as mean ± SD, n=3.

5.2.2 Scx+AngII treated cells exhibit an increase in contractile marker gene expression.

To investigate the effect of scleraxis over-expression along with AngII treatment on HAOSMC gene expression, we measured key mRNA levels for each group of cells. We found that after 72 hours of treatment, the contractile markers calponin and SMMHC are reduced in the scleraxis over-expressing cells and in the AngII-treated cells. Conversely, Scx+AngII treated cells reversed this effect (P<0.01), to levels similar to the control (Fig. 51). SM22α was decreased only by AngII, but the combination of Scx+AngII also increased SM22α expression.

Overall, scleraxis overexpression alone reduces contractile markers and induces the proliferation of HAOSMCs. However, Scx+AngII induces a contractile phenotype of VSMC, through increasing contractile marker gene expression.

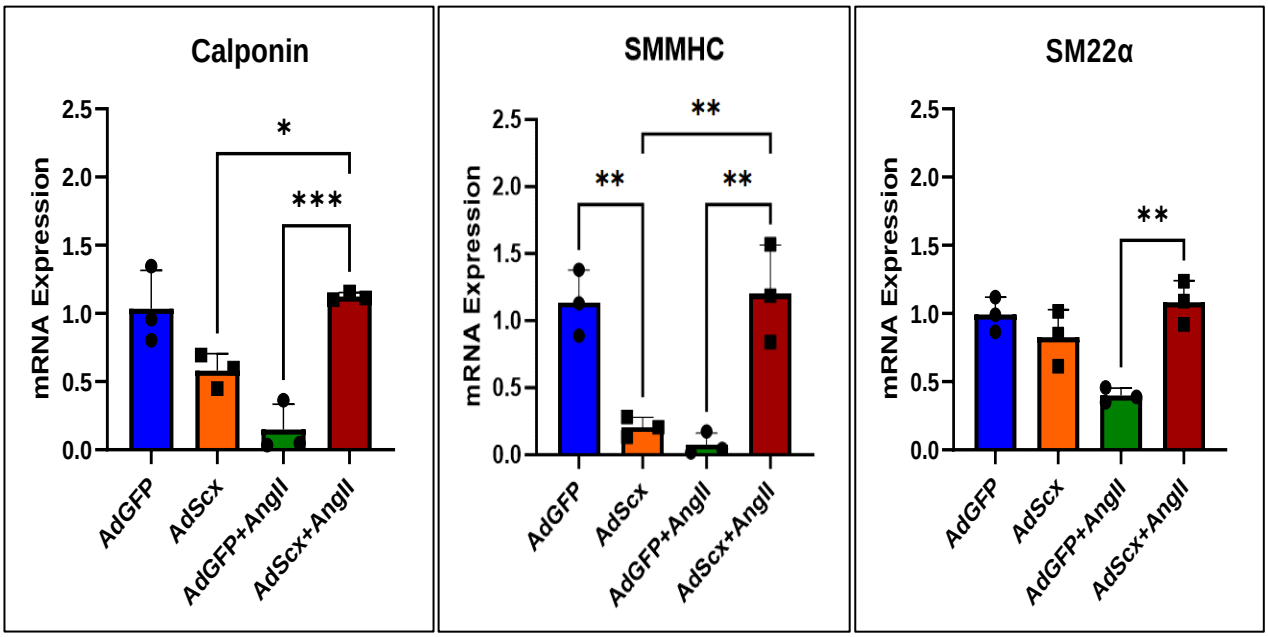

Figure 51. Contractile marker gene expression in HAOSMC.

HAOSMCs were infected with either AdScx or AdGFP as a control. After 24 hours, the cells were treated with either AngII (100 nM) or saline and then were harvested 48 hours later for qPCR analysis. The data shows a significant reduction in the expression of contractile markers including calponin, smooth muscle myosin heavy chain (SMMHC) in both the scleraxis over-expression (AdScx) and AngII treatment groups. This loss is reversed in AdScx+AngII cells to levels similar to control. *P<0.05, **P<0.01, ***P<0.001. Data is shown as mean ± SD, n=3.

CHAPTER 4: DISCUSSION

Arterial stiffness is a medical condition that can have significant impacts on overall health and well-being. This condition is strongly associated with a variety of cardiovascular diseases, including hypertension and atherosclerosis, which when exacerbated lead to worse outcomes such as heart attack or stroke.

Arterial stiffness is characterized by the loss of elasticity in blood vessels, which can disrupt the normal function of blood pressure regulation and arterial homeostasis. This loss of elasticity makes it harder for the blood vessels to expand and contract in response to changes in blood pressure, ultimately leading to altered blood flow. Arterial stiffness can be caused by dysregulation in vascular wall components or impairment in cellular function.

The physical characteristics of the vessel wall, including stiffness, are influenced by both ECM protein elements such as collagen and elastin as well as by the cellular composition including endothelial cells and, in particular, VSMCs. Increased proliferation of VSMCs or increased ECM components can interfere with arterial function, contributing to vascular stiffness and altering blood pressure regulation at the organ level.

Marfan syndrome patients have an associated increase in aortic and mesenteric artery stiffness [182, 183]. Mesenteric artery stiffness, identified from a mouse model of Marfan syndrome, showed an increased shift in stress-strain curve and an impaired endothelial and VSMC relaxation response [183]. In aortic aneurysm, there is a notable shift in the phenotype of VSMCs from the contractile to the proliferative state, accompanied by a reduction in the expression of contractile markers such as calponin and SMMHC, ultimately contributing to increased VSMC proliferation [184]. RNA-seq analysis of full-thickness aortic biopsies from patients with Marfan syndrome revealed that scleraxis is highly expressed [158].

A single-cell RNA sequencing study has confirmed that scleraxis is expressed in aortic and airway smooth muscle cell tissues [155]. However, the role of scleraxis in the vasculature remains unknown. Therefore, in our study, we investigated the role of scleraxis in arterial stiffness, with the hypothesis that increased scleraxis expression would increase vascular stiffness by upregulating ECM protein expression. This was because we noticed that ECM expression is regulated by scleraxis in the heart. We utilized two different mouse models to characterize the effects of scleraxis over-expression in different layers of the arterial wall, specifically by over-expressing scleraxis in the fibroblasts of the tunica adventitia in TCF21iCre-Scx^{TG} or in the vascular smooth muscle cells of the tunica media in Myh11Cre-Scx^{TG}.

To our surprise, scleraxis overexpression in arterial fibroblasts did not increase vascular stiffness in small mesenteric arteries, nor it did change the structure of the aortas in TCF21iCre-Scx^{TG} mice, thus scleraxis upregulation did not induce ECM gene expression as presumed. In contrast, scleraxis overexpression in VSMC`s increased vascular stiffness in mesenteric arteries and by increasing VSMC count in the aorta without any noticeable changes to the ECM protein expression in the aortas.

In our study, we investigated the potential for a change of vascular stiffness and impaired elasticity in the arteries of scleraxis over-expression mice. To achieve this goal, we employed various measurements including molecular and histological characteristics in large arteries, as well as geometrical, functional, and mechanical responses in small resistance arteries. Small resistance mesenteric arteries are the main arteries contributing to the total peripheral resistance and are highly reactive to blood pressure fluctuations, responding with either vasoconstriction or vasodilation to maintain homeostasis. Any alteration in the mesenteric artery`s functional or structural components may trigger or exacerbate different diseases, such as hypertension.

Finding 1: Scleraxis induces vascular stiffness.

Findings from Myh11Cre-Scx^{TG} mesenteric arteries indicate a noticeable reduction in mesenteric compliance, which implies impaired expansion ability of mesenteric arteries due to changes in the intraluminal pressure, as indicated by the leftward shift in the stress-strain curve in Myh11Cre-Scx^{TG} mesenteric arteries (Fig. 35). No significant changes in the geometry of Myh11Cre-Scx^{TG} mesenteric arteries compared to control were noticed (Fig. 34), nor were any alterations observed in the specific mechanical parameters of EM vs. Stress, Stress vs. IP, and EM vs. Stress (Fig. 36), indicating that there were no observable changes in the vascular wall components and geometry of these vessels.

The increase in Myh11Cre-Scx^{TG} mesenteric artery stiffness may be attributed to the impact of scleraxis upregulation, which alters the characteristics of VSMCs towards a proliferative phenotype. One possible explanation is that scleraxis upregulation modifies VSMC characteristics by promoting VSMC proliferation, leading to increased stiffness and reduced compliance of the mesenteric arteries. Since mesenteric arteries rely on VSMCs to maintain vascular resistance and respond to changes in intraluminal pressure, an increase in VSMC density within the vascular wall may lead to reduced compliance, thus making the vessels stiffer. However, no geometrical changes were observed in the CSA, media thickness, or M/L ratio between the mesenteric arteries of Myh11Cre-Scx^{TG} compared to control (Fig. 34). This lack of change may be due to an increase in the concentric alignment of VSMCs within the vessel wall that does not significantly alter the overall geometry of Myh11Cre-Scx^{TG} mesenteries.

Similar findings have been reported in the aortic media of patients with Marfan syndrome who have associated aortic aneurysms. RNA-seq analysis of full-thickness aortic biopsies from these individuals revealed that scleraxis is highly expressed [158]. In cases of aortic aneurysm,

there is a notable shift in the phenotype of VSMCs from the contractile to the proliferative state, accompanied by a reduction in the expression of contractile markers such as calponin and SMMHC [184]. These findings, coupled with our present data, suggest that scleraxis may play a significant role in the pathophysiology of aortic tissues in patients with Marfan syndrome with aortic aneurysms, by altering VSMC proliferation. Additionally, aortic and small resistance artery stiffness is increased in Marfan syndrome patients [182, 183], which is consistent with our findings indicating that scleraxis upregulation induces vascular stiffness in mesenteric arteries.

Scleraxis deficiency in Scx^{KO} mesenteric arteries significantly reduced CSA and media thickness, while the M/L ratio remained unchanged (Fig. 24). The decrease in the overall size observed in Scx^{KO} mesenteric arteries could be due to the smaller overall size of Scx^{KO} mice. Previous studies conducted in our lab demonstrated that the weight of Scx^{KO} pups is significantly lower compared to Scx^{WT} pups. Specifically, our prior findings reported that body weight of Scx^{WT} pups averaged 20.2 ± 0.8 g, while Scx^{KO} pups weighed 12.2 ± 0.6; ($n = 9–12$; $P < 0.0001$) [142] . Additionally, the changes observed in CSA and wall thickness may be potentially attributed to alterations in the VSMC count in these mesenteric arteries, similar to our findings in Scx^{KO} aortas (Fig. 23). The reduction in VSMC count might also explain our observations of increased mechanical compliance and greater distensibility in Scx^{KO} mesenteries compared to Scx^{WT} mesenteries (Fig. 25). As VSMCs play a crucial role in maintaining the mechanical properties of blood vessels, they contribute to the vessel's tone and stiffness. When there is a reduction in the number of VSMCs, as seen in Scx^{KO} mesenteric arteries, it can lead to decreased vessel wall rigidity and increased distensibility. In conclusion, the Scx^{KO} model highlights the importance of physiological scleraxis gene expression in both small and large arteries. The deficiency of scleraxis significantly alters the structure and stiffness of these arteries.

Finding 2: Scleraxis upregulation induces VSMC proliferation.

Scleraxis upregulation in the aortas of Myh11Cre-Scx^{TG} mice, resulted in a significant increase in the VSMC count and evidence of a rise in the proliferation marker Ki67 compared to control Myh11Cre-Scx^{WT} (Fig. 32, 33). This data indicates that scleraxis upregulation induces VSMC proliferation in the aortas of Myh11Cre-Scx^{TG} mice.

Despite an increase in overall cellularity within the scleraxis over-expressing aortas of Myh11Cre-Scx^{TG} mice, no geometrical changes were observed in the CSA, media thickness, or M/L ratio between Myh11Cre-Scx^{TG} compared to control Myh11Cre-Scx^{WT} mice (Fig. 30E). This lack of change may be due to an increase in the concentric alignment of cells within the vessel wall that does not significantly alter the geometry of Myh11Cre-Scx^{TG} aortas.

In contrast, our findings demonstrate that the absence of scleraxis in Scx^{KO} mice significantly alters the structure of the aortic wall (Fig. 22). This is visibly represented by more localized gaps in the media between elastin fibers within the aortic wall of Scx^{KO} mice when compared to wild type controls. This localized gap pattern in the aortic media correlates with the changes in VSMC density as evidenced by fluorescent staining of the Scx^{KO} aortas, where a significant reduction in the number of VSMCs compared to WT aortas was observed (Fig. 23). Taken together, these findings suggest that scleraxis deficiency alters the structure of the aortic wall, particularly within the media, resulting in a reduced VSMC count. This reduction in VSMCs may be associated with scleraxis' role in regulating VSMC proliferation, implying that scleraxis deficiency could negatively impact VSMC number within the media.

A previous study suggested that VSMC apoptosis in the aortic media could lead to medial degradation, potentially resulting in localized medial gaps and the presence of multiple localized elastic lamina breaks [185]. These findings of VSMC loss in aortic media align with our

observations in Scx^{KO} aortas, suggesting that scleraxis deficiency may reduce or inhibit VSMC turnover, proliferation, and growth within the arterial wall. Interestingly, data from our lab suggests that scleraxis loss may induce apoptosis of cardiac myofibroblasts [181]. Thus, scleraxis may play a role as an anti-apoptotic factor.

Our *in vitro* data using HAOSMCs revealed that scleraxis over-expression induces smooth muscle cell proliferation as shown by an increase in proliferation detected with the CCK-8 kit (Fig. 47). Additionally, protein data from scleraxis over-expressing HAOSMCs showed a significant increase in the cell proliferation marker Ki67, with a trend of increased PCNA, although this did not reach statistical significance (Fig. 48). Ki67 is a specific marker for cell proliferation and ribosomal RNA transcription that is highly expressed during the mitosis stage of the cell cycle. Therefore, the Ki67 increase due to scleraxis overexpression in HAOSMCs supports a role for scleraxis in promoting HAOSMC proliferation. Additional findings show that scleraxis upregulation significantly induced HAOSMC proliferation, as evidenced by an increased number of EdU+ cells in the DNA synthesis phase in HAOSMCs where scleraxis is overexpressed as shown from the flow cytometry data (Fig. 50B, E).

Typically, an increase in VSMC proliferation is associated with a reduction in contractile markers, which aligns with our observations following the upregulation of scleraxis in HAOSMCs. Our findings show that scleraxis upregulation in HAOSMCs promotes a reduction in the expression of VSMC contractile gene markers (calponin, SMMHC) (Fig. 49). In addition, SMMHC gene expression is significantly reduced in scleraxis upregulated HAOSMCs compared to control (Fig. 51). Each of these contractile genes is an important marker that modulates smooth muscle phenotype. Both calponin and SM22α modulate actin cytoskeleton contraction and ATPase activity, while SMMHC modulates the force of contraction of the smooth muscle

cells. These markers were reduced in scleraxis-over-expressing HAOSMCs, thus indicating changes in their phenotype.

In conclusion, scleraxis over-expression in smooth muscle cells triggers a proliferative phenotype. This suggests the possibility that scleraxis may play a role in vascular diseases characterized by VSMC proliferation including atherosclerosis, Marfan syndrome and re-stenosis.

Finding 3: Scleraxis' effects are altered in the presence of AngII.

AngII is known to contribute to stiffness in blood vessels. It can induce aortic stiffness in hypercholesteremic mice [186]. In addition, AngII can stimulate aortic wall remodeling via triggering VSMC hypertrophy (phenotypic switching) and ECM protein deposition, thereby altering the biomechanical properties of the arteries and inducing arterial stiffness [187].

In our study, we investigated the impact of scleraxis over-expression in a mouse model with induced hypertension using mini pumps that released AngII. We confirmed the proper functioning of the AngII infusion pumps by measuring a significant increase in systolic and mean arterial blood pressure measurements in mice subjected to AngII infusion for four weeks (Fig. 39).

Finding 3.1: Combination of scleraxis and AngII reduces AngII-induced ECM accumulation.

Immunohistochemistry images of the AngII/Scx^{WT} aortas revealed voids in the aortic media, while AngII/Scx^{TG} aortas showed an increase in elastin fiber discontinuity (Fig. 40) and a notable reduction in the appearance of voids within the aortic media (Fig. 41). Additionally, AngII/Scx^{TG} aortas showed reduced collagen, elastin and fibronectin mRNA gene expression

when compared to AngII/Scx^{WT} (Fig. 42). This suggests that AngII infusion induces ECM expression, while the combination of AngII and scleraxis reduces ECM accumulation.

Infusion of AngII alone for a duration of 4 weeks at 1mg/kg/day triggered the development of aortic aneurysm and transmural ruptures within the aortic media in hypercholesterolemic mouse models such as ApoE-/- and LDLR-/- mice [188]. Additionally, AngII infusion led to an increase in media thickness and the accumulation of ECM components [189]. The transmural ruptures are indicative of medial degeneration and are characterized by the presence of interlamellar mucoid extracellular matrix accumulation (I-MEMA) without altering the interlamellar units in the aortic media, a feature that can be also observed in the histological sections of patients with thoracic aortic aneurysms [190].

Our histological analysis of AngII-infusion aortas in AngII/Scx^{WT} mice revealed a pattern of vascular remodelling resembling I-MEMA within the aortic media which we described as void expansion within the media. Initially, we anticipated that the impact of AngII-induced vascular remodelling represented by ECM accumulation would be either similar or exacerbated when combined with scleraxis upregulation in AngII/Scx^{TG} aortas. However, our findings suggest that the combination of scleraxis and AngII attenuates AngII-induced vascular ECM accumulation, in particular the I-MEMA medial expansion that is visible in AngII/Scx^{WT} aortas, which appears to be smaller in AngII/Scx^{TG} aortas. One possible explanation is that the interaction between AngII and scleraxis upregulation leads to specific alterations in gene expression of ECM and VSMCs that counteract some of the vascular remodeling effects typically induced by AngII alone. These interactions may result in a more balanced response within the arterial wall, preventing ECM accumulation and structural changes.

Finding 3.2: Combination of scleraxis and AngII induces the HAOSMC contractile phenotype.

Our *in vitro* findings in HAOSMCs indicated that the combination of AngII and Scx upregulation alters VSMC characteristics by promoting a contractile phenotype. This is supported by our data from qPCR analysis, which demonstrated a significant increase in mRNA expression of contractile marker genes including calponin, SMMHC, and SM22α in AngII+Scx treated cells (Fig. 51). Furthermore, the combination of scleraxis and AngII treatment in HAOSMCs led to reduced proliferation rate when compared to scleraxis treatment alone as evidenced by flow cytometry (Fig. 50D, E). Collectively, these results suggest that scleraxis upregulation in combination with AngII treatment influences the characteristics of VSMCs, driving them toward a contractile phenotype. This transition may be an adaptive response to enhance the internal stiffness in these cells.

A previous study reported that increased vascular stiffness in aging, as measured by Atomic Force Microscopy (AFM), is associated with increased intrinsic stiffness in VSMCs [191]. Another study, which also used AFM to measure the internal cellular stiffness, demonstrated that an increase in VSMC size and an increase in contractile protein expression can contribute to greater internal cellular stiffness [35]. These observations are consistent with the concept that the contractile phenotype of VSMCs induces internal stiffness within VSMCs. Therefore, the leftward shift of the stress and strain curve, and the reduced compliance in AngII/Scx^{TG} mesenteric arteries may be attributed to the transition of VSMCs toward the contractile phenotype (Fig. 44), which further contributes to the increase in vascular stiffness.

Some studies have demonstrated that an increased expression of contractile genes can elevate VSMC stiffness in the aorta of SHR. Additionally, these studies suggested that applying

inhibitors that downregulate these contractile markers results in reduced VSMC stiffness [35]. Therefore, it is possible that the synergistic effect of scleraxis and AngII may subject HAOSMCs to greater stress, prompting the cells to adapt by inducing the expression of contractile marker genes. These markers play a crucial role in increasing stiffness and maintaining a contractile phenotype in VSMCs, potentially aiding in their response to the stressors imposed by scleraxis and AngII.

Other studies have provided additional insights into the correlation between contractile proteins and VSMC stiffness. Cytoskeletal proteins, such as actin and intermediate filaments, play a crucial role in mechanotransduction in VSMCs. These proteins allow VSMCs to sense and respond to mechanical stimuli by regulating VSMC contractile function. Contractile proteins like calponin and SM22α interact with the cytoskeletal proteins in response to mechanical forces, contributing to the regulation of smooth muscle contractility and mechanotransduction as an adaptive response to stimuli [192].

Finding 3.3: Combination of scleraxis and AngII exacerbates vascular stiffness.

Despite evidence of reduced ECM deposition in the aortas of AngII/Scx^{TG} mice, the scleraxis upregulation in combination with AngII infusion synergistically shifted the stress-strain curve to the left, thus inducing exacerbated arterial stiffness in mesenteric arteries (Fig. 44). This increase in stiffness significantly impacts the mechanical properties that affect vascular wall elasticity when subjected to an applied force and represented by an increase in EM vs. Stress parameters of AngII/Scx^{TG} arteries (Fig. 45). These alterations are influenced by the vascular wall components such as ECM or VSMCs. Additionally, the increase in vascular stiffness in AngII/Scx^{TG} mesenteric arteries could be attributed to the transition of VSMCs toward the contractile phenotype (Fig. 44). The shift in VSMC phenotype to contractile phenotype is

suggested to enhanced internal VSMC stiffness, as supported by the study in which VSMC internal stiffness was measured by AFM, showing an increase in contractile protein expression [35].

The significant increase in the M/L ratio in AngII/Scx^{TG} compared to control Saline/Scx^{WT} group (Fig. 43), suggests a form of inward eutrophic remodeling encroaching the lumen area. This could be potentially associated with a reorganization of VSMC in the vascular wall around the reduced lumen. Similar remodeling patterns can be observed in peripheral resistance arteries from patients with mild essential hypertension [116]. This study revealed that the increased M/L ratio observed in hypertensive patients is not associated with VSMC hyperplasia or hypertrophy, but it was attributed to the reorientation of the VSMCs within the vessel walls compared to normotensive individuals.

Also, we observed a significant impairment in the VSMC endothelial- independent relaxation response of AngII/Scx^{TG} mesenteric arteries following SNP treatment (Fig. 46B). This indicates that AngII treatment and scleraxis over-expression together promote a contractile phenotype characterized by increased contractile capacity of VSMCs, and impaired vasorelaxation in mesenteric arteries.

Finding 4: The role of scleraxis on ECM is cell specific.

We upregulated scleraxis expression in fibroblasts using the TCF21iCre-Scx^{TG} mouse model. The resulting data from this model revealed no significant changes in the structure or the geometry of scleraxis over-expressing aortas (Fig. 12). Also, no geometrical or mechanical alterations were observed in the small resistance arteries of TCF21iCre-Scx^{TG} mice (Fig. 14, 15, respectively). These unexpected findings, concerning the upregulation of scleraxis in the adventitial fibroblasts of the TCF21iCre-Scx^{TG} mice, led to the conclusion that scleraxis

upregulation in vascular fibroblasts does not significantly affect the aortas and mesenteric arteries.

Our unforeseen findings were surprising because our initial research with this line of TCF21iCre mice was based on our lab`s prior work [158]. In that previous study, scleraxis was knocked out using tamoxifen-inducible fibroblast-specific scleraxis knockout (TCF21iCre Scx^{KO}) mice, and we found that scleraxis loss completely attenuated cardiac fibrosis, while significantly improving cardiac systolic function and ventricular remodelling, following TAC. These results were correlated with a reduction in fibroblast activation to myofibroblasts and direct downregulation of ECM gene expression [181]. Our lab's research has shown that scleraxis directly transactivates the expression of several genes associated with the conversion of fibroblasts to myofibroblasts in the heart, including fibronectin, vimentin, and fibrillar collagens col1α1 and col1α2 [143-145]. Initially, we hypothesized that scleraxis upregulation would lead to fibrosis and stiffness in vasculature, similar to our lab's findings in the heart in the TCF21iCre Scx^{KO}- TAC mouse model. However, our findings in TCF21iCre-Scx^{TG} mice have shown that scleraxis upregulation did not result in an increase in profibrotic ECM gene expression in the aortas. Therefore, scleraxis upregulation may exhibit variability in specific cell types depending upon their distinct roles in different tissues. This observation aligns with the effect of scleraxis on αSMA expression in mesangial cells [152] , where scleraxis upregulation reduces the expression of αSMA in diabetic nephropathy thus deactivating the mesangial cell phenotype under diabetic conditions, while it increases the expression of αSMA in cardiac fibroblasts to modulate fibroblast differentiation to myofibroblasts to promote cardiac fibrosis [142].

We also reported that upregulation of scleraxis in the aortas of Myh11Cre-Scx^{TG} mice does not alter the gene expression of specific ECM proteins, including fibronectin and collagens

col1α1 and col1α2. This was confirmed through qPCR analysis and is visually demonstrated in aortic histological sections (Fig. 30 A-E, 31, respectively).

Finding 5: Tamoxifen gavage impacts endothelial relaxation.

Our findings using TCF21iCre-Scx^{TG} and Myh11Cre-Scx^{TG} mice, revealed a significant impairment in mesenteric artery vasorelaxation in response to acetylcholine (Fig. 19A, Fig. 37A, respectively). This effect may be due to tamoxifen gavage rather than changes related to scleraxis gene expression, as this vasorelaxation impairment is similar to what was observed in WT mice treated with tamoxifen (Fig. 27A).

A study that examined the impact of tamoxifen treatment on vascular reactivity in small resistance arteries in rats, found that tamoxifen-treated vessels exhibited decreased responses to acetylcholine and attenuated production of nitric oxide (NO) [193]. In addition, a recent study demonstrated that activation of Cre-ER^{T2} via tamoxifen led to toxicity and damage to endothelial cells in the retinal blood vessels, resulting in impaired angiogenesis [194]. Therefore, the administration of tamoxifen via gavage may have varying effects on different blood vessels, independent of its role in regulating specific transgenes. In our studies, we controlled for the effect of tamoxifen by using WT^{CO} control mice receiving corn oil gavage, and our data show that the endothelial response to Ach is not impaired in corn oil gavage mice, which indicates that endothelial impaired response is due to tamoxifen gavage.

CHAPTER 5: CONCLUSIONS

Scleraxis impacts vascular structure and function. In our study, we induced scleraxis expression in two different layers of the arterial wall and verified its effect within each specific layer. Scleraxis upregulation in the smooth muscle layer induced VSMC proliferation in large arteries and induced vascular stiffness in the small resistance arteries. However, when over-expressed in the adventitial layer, no effect was observed. Conversely, scleraxis deficiency altered the structure, geometry, and mechanics of small and large arteries, characterized by reduced cellularity in large arteries and higher compliance of mesenteric arteries.

An unexpected and novel finding is that scleraxis over-expression triggers VSMC proliferation, with evidence of this effect in both mouse tissues and human cells. This is a critical finding because increased VSMC proliferation correlates with the development of different diseases, such as atherosclerosis and restenosis. We previously showed that scleraxis reduced the proliferation of cardiac fibroblasts [153], thus scleraxis effect on proliferation is cell type specific. On other hand, over-expression of scleraxis in an AngII-induced hypertensive model exacerbated stiffness in small resistance arteries by promoting a VSMC phenotype change to a contractile phenotype as noted in both gene expression and flow cytometry.

In summary, our findings show that both scleraxis over-expression with AngII or AngII infusion alone induces vascular remodeling in mouse arteries. However, vascular stiffness is increased in the AngII+scleraxis model due to cellular phenotype switching to contractile rather than due to ECM accumulation in the blood vessels, which was the hallmark of stiffness induced by AngII infusion alone. Scleraxis thus alters the effect of AngII on vascular remodeling and function. Additionally, scleraxis over-expression alone induces vascular stiffness due to

changing the VSMC phenotype towards proliferation, thus increasing VSMC count which induces vascular stiffness.

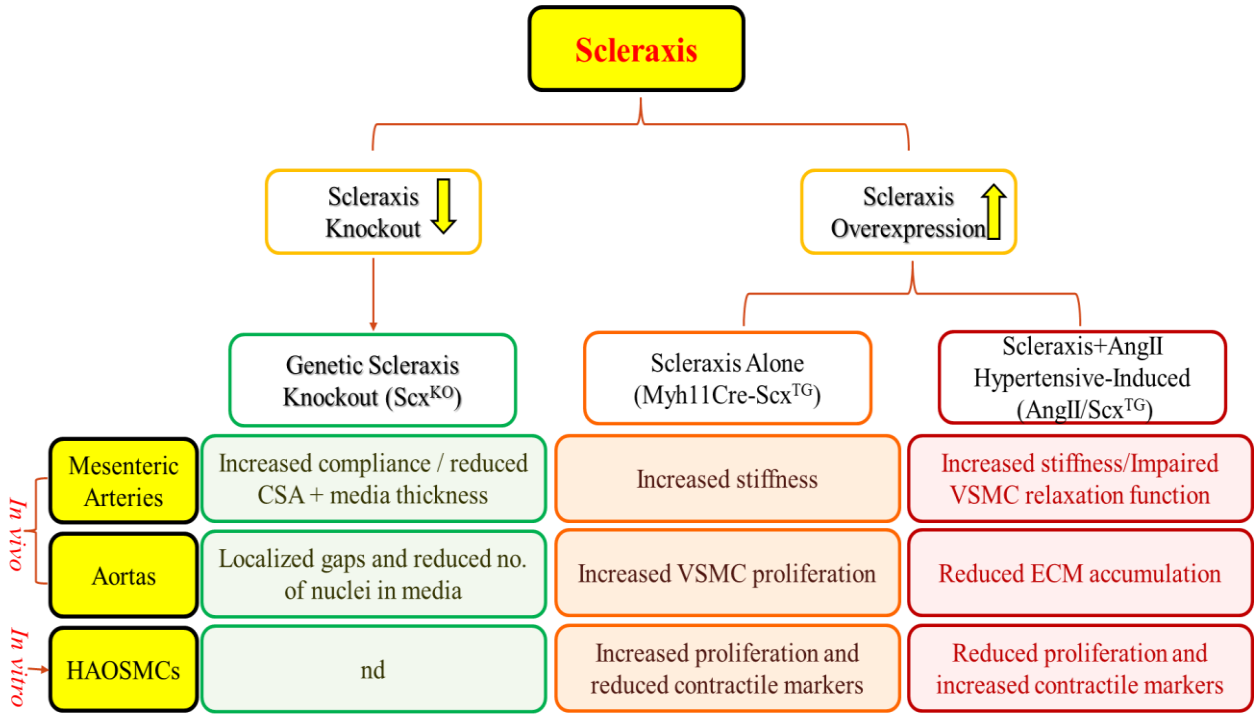

Figure 52. A schematic diagram summarizing the physiological and pathological impacts of scleraxis upregulation or knockout in the arterial wall *in vivo* and HAOSMCs *in vitro*.

This diagram summarizes our study's key findings on the impact of scleraxis expression on arterial structure, mechanics, and function both *in vivo* and in human aortic smooth muscle cells (HAOSMCs) *in vitro*. Using a genetic scleraxis knockout model (Scx^{KO}), we observed that mesenteric arteries demonstrated increased compliance, along with a decrease in cross-sectional area (CSA) and media thickness. Aortas from Scx^{KO} models exhibited localized gaps and a reduced number of nuclei within the media, underscoring alterations in vascular smooth muscle cells (VSMCs) (Green highlight). Scleraxis upregulation in VSMCs, achieved through the physiological Myh11Cre-Scx^{TG} model, resulted in increased VSMC proliferation in large arteries and enhanced vascular stiffness in small resistance arteries. This indicates that scleraxis overexpression promotes

a VSMC proliferative phenotype while reducing contractile marker expression in HAOSMCs (Orange highlight). In the AngII-induced hypertension with scleraxis overexpression model (AngII/Scx^{TG}), there was a significant increase in vascular stiffness in small resistance arteries and an impairment in VSMC relaxation function when infused with sodium nitroprusside (SNP). Additionally, aortas in this model displayed reduced extracellular matrix (ECM) accumulation. HAOSMCs treated with both AngII and scleraxis showed decreased proliferation and an increase in contractile marker expression, suggesting that AngII + Scleraxis induces a contractile phenotype, leading to vascular stiffness (Red highlight).

CHAPTER 6: STUDY PITFALLS AND LIMITATIONS

Sex differences are not accounted for in this study, because a major part of the study includes the Myh11-Cre transgene, which is incorporated into the Y chromosome in this mouse line. This limits the study to using male mice only.

Another limitation of our study is the limited over-expression of scleraxis achieved using the Cre driver B6.FVB-Tg (Myh11-CreER^{T2})1Soff/J. This limitation is related to the potential for CreER^{T2} lines to exhibit a certain degree of tamoxifen-independent, basal Cre activity, as reported in a recent study [195]. The study found that CreERT2 lines may have leaky Cre activity, which can cause background recombination independent of tamoxifen. Therefore, it is possible that our model would have demonstrated more significant effects on PWV and BP measurements if we had achieved higher levels of transgenic scleraxis expression.

In our study, it's important to acknowledge a limitation concerning measuring the protein levels for induced scleraxis upregulation in both the TCF21iCre-Scx^{TG} and Myh11Cre-Scx^{TG} mouse models. We were unable to address this limitation due to the unavailability of a reliable

scleraxis antibody that is effective to use in transgenic mouse tissues. It's worth noting that scleraxis expression in mouse tissues may be relatively low, and the amount of tissue available from the aortas or mesenteries of the mouse models was limited and insufficient for Western Blot analysis, making it more challenging to detect scleraxis protein levels.

Tamoxifen infusion has shown variable effects depending on the tissues being studied. Tamoxifen has been reported to induce coronary ring relaxation [196]. Another study examined the effect of tamoxifen treatment on the vascular reactivity in small resistance arteries in rats and found that tamoxifen-treated vessels had reduced responses to acetylcholine and attenuated formation of NO [193]. A recent study has shown that activation of Cre-ER^{T2} via tamoxifen induces toxicity and endothelial damage in the retinal blood vessels resulting in impaired angiogenesis [194]. Tamoxifen gavage may thus have a number of vascular effects dependent on the vessel in question, and independent of its role in specific transgene regulation.

Our data revealed that endothelial function in mesenteric arteries is altered in response to tamoxifen gavage, which was introduced daily for five consecutive days to induce the transgene overexpression. In the first study, all mice (WT^{TAM}, TCF21iCre-Scx^{TG}, Myh11Cre-Scx^{TG}) were given tamoxifen to activate the transgenes, and they were sacrificed 8 weeks later. Their small mesenteric resistance arteries showed altered dilation when exposed to Ach-infusion because of the tamoxifen treatment. In the second study, after 4 weeks of tamoxifen and pump implantation, the mice were sacrificed. Again, the mesenteric arteries didn't dilate well in response to Ach-infusion. However, in this case, the reason for the impaired endothelial relaxation response was not the tamoxifen but the infusion of AngII in the AngII/Scx^{WT} and AngII/Scx^{TG} mice. Experimental studies using rabbit mesenteric arteries showed that AngII directly attenuates

endothelial relaxation in these vessels [197]. Therefore, the observed changes in endothelial function can be attributed to AngII-infusion rather than the presence or absence of scleraxis.

The data showing the effect of tamoxifen explains why endothelial function could not be fully assessed in scleraxis over-expression mice (TCF21iCre-Scx^{TG} and Myh11Cre-Scx^{TG}). Our data revealed that the endothelial relaxation response is impaired in tamoxifen gavage mice mesenteries in wild-type, TCF21iCre-Scx^{TG}, and Myh11Cre-Scx^{TG} animals. Therefore, the altered vasodilation response to acetylcholine is likely not due to scleraxis over-expression itself, but rather is due to the influence of tamoxifen treatment on endothelial cells over time.

Our findings show that endothelial dependent relaxation is impaired in mesenteric arteries of both AngII/Scx^{WT} and AngII/Scx^{TG} mice following Ach treatment. AngII infusion impairs endothelial relaxation response upon Ach treatment, and this impairment is unrelated to scleraxis expression (Fig. 46A). Experimental studies using rabbit mesenteric arteries showed that AngII directly attenuates endothelial relaxation in these vessels [197]. Therefore, the observed changes in endothelial function can be attributed to AngII-infusion rather than scleraxis.

It is important to note the various challenges that limited the number of animals recruited for the present study. The breeding of all transgenic mice employed in this study was lengthy, particularly Myh11Cre-mice in which we had to use male mice (~50% of total breeding) exclusively for some studies. As a result, only ~15% of the of the total mice that were bred in the colony possessed the correct genotype.

Mice from the Myh11Cre-mice with implanted pumps also had an increased death rate. Animals receiving implantable osmotic mini-pumps experienced multiple stressful operations as

they are involved in a number of subsequent procedures including surgical implantation of a telemetry device, PWV measurements, mini-osmotic pump surgical implantation, and oral gavage. Moreover, a number of these animals were found dead due to strokes, as the catheter of the telemetry device is implanted in one side of the carotid artery, reducing, or blocking the perfusion through it. Poor perfusion from the circle of Willis makes these mice more prone to strokes. This increase in mortality, related only to the procedures themselves rather than to the scientific intervention, limited the total number of mice used in this study.

The duration for which scleraxis is induced in each study can determine the extent of vascular remodeling *in vivo*. For example, after 8 weeks of scleraxis overexpression (Fig. 8A), the compliance of mesenteric arteries is significantly reduced (Fig. 35). However, when using the osmotic pumps and inducing scleraxis overexpression for 4 weeks (Fig. 8B), there was no change in compliance in the mesenteric arteries between Saline/Scx^{TG} compared to Saline/Scx^{WT}, but stiffness was highly exacerbated when challenged with AngII infusion in AngII/Scx^{TG} (Fig. 44). This indicates that a longer duration of scleraxis overexpression, such as 8 weeks, has a noticeable impact on vascular stiffness, whereas a shorter duration of scleraxis overexpression, such as 4 weeks, does not exhibit an effect on vascular stiffness.

CHAPTER 7: FUTURE DIRECTIONS

Our findings from HAOSMC studies show that scleraxis over-expression significantly increases the proliferation rate of these cells after 72 hours. Interestingly, when we examined scleraxis induction through flow cytometry and qPCR studies within a shorter timeframe of 24-48 hours, we didn't observe the same significant effects in modifying smooth muscle proliferation and plasticity. This suggests that additional studies may be required to determine the specific timeframe during which scleraxis can induce changes in VSMCs.

The duration of scleraxis overexpression is important to verify in both *in vitro* as well as in *in vivo* studies. The 8-week study of scleraxis over-expression in Myh11Cre-Scx^{TG} mice showed a significant reduction in compliance in mesenteric resistance arteries. However, in the 4-week study of scleraxis overexpression in Saline/Scx^{TG} mice, there was insufficient evidence to suggest that scleraxis overexpression can induce stiffness in mesenteric resistance arteries, except when scleraxis over-expression is combined with AngII infusion in AngII/Scx^{TG}. This highlights the importance of identifying the duration of scleraxis induction and whether it is being induced alone or in combination with other stressors. The length of overexpression in the AngII study was limited by the ability of the pumps to deliver AngII (4-week maximum).

Our data has verified that vascular compliance is increased in Scx^{KO} mice, and there are notable changes in the geometry and structure of mesenteric arteries in these animals. Therefore, it would be informative to recruit conditional Myh11Cre-Scx^{KO} mice into an AngII infusion pump study. This can help us investigate whether we can target the scleraxis gene as a strategy for lowering vascular stiffness in hypertension.

Our findings show an increase in contractile protein gene expression in scleraxis+AngII-treated HAOSMC. Also, AngII/Scx^{TG} mesenteric arteries show a significant reduction in compliance and increased contractility of mesenteric resistance arteries. This indicates that there might be some internal changes within the VSMC cytoskeleton, contributing to an increase in the overall vascular stiffness. Therefore, employing atomic force microscopy nanoindentation studies to measure the internal stiffnesses of VSMC upon scleraxis over-expression alone or in combination with AngII treatment would be a good future direction to pursue [35, 198].

In the Scx+AngII study, we wanted to investigate the role of scleraxis in a hypertensive model. Therefore, it is recommended to explore whether scleraxis by itself is upregulated in the

arteries of a pathological model, for example, in the spontaneous hypertensive rat (SHR) to correlate with aspects of pathology. Experimental samples have been collected and will be analyzed to examine this possibility.

We found that scleraxis overexpression triggers proliferation in HAOSMCs. Atherosclerosis is a pathological condition triggered by cholesterol accumulation and VSMC proliferation which initiates plaque formation and progression of the atheroma in the wall of blood vessels [199]. Additionally, restenosis is the re-narrowing of arteries which were previously opened surgically by a stent or angioplasty. Restenosis is characterized by platelet aggregation, the release of growth factors, inflammatory cell infiltration, and most importantly VSMC proliferation [200]. Therefore, exploring the role of scleraxis in restenosis or atherosclerosis development and progression might reveal a new area of clinical significance. Hence, targeting scleraxis as a potential anti-proliferative agent in preventing or treating various related vascular pathological conditions such as atherosclerosis or restenosis is an important goal to pursue. Some aortic samples are currently being collected from ApoE-/-LDLR-/- atherosclerotic mice for further investigation.

While our data suggests a minimal role of scleraxis in hypertension, our findings highlight its involvement in inducing VSMC proliferation. This observation could be important in vascular diseases characterized by VSMC proliferation, such as Marfan syndrome. In Marfan syndrome patients with aortic aneurysms, scleraxis is highly expressed in the aortic media [158]. This syndrome is characterized by a notable shift in the phenotype of VSMCs from the contractile to the proliferative state [184] and an increase in vascular stiffness [182, 183]. Therefore, exploring the role of scleraxis in the pathophysiology of Marfan syndrome may provide valuable insights.

Exploring the role of scleraxis in the context of the accelerated Marfan syndrome mouse model described by Cavanaugh et al. offer intriguing insights [201]. This model employs $Fbn1^{C1039G/+}$ heterozygous mice, which carry a mutation in the fibrillin 1 gene, which accelerates the development of aortic aneurysms and dilated cardiomyopathy through daily subcutaneous infusions of Angiotensin II (4.5 mg/kg) via micro-osmotic pumps. The model demonstrates a rapid progression of Marfan syndrome symptoms, with increased mortality rates and significant enlargement of aortic diameters shortly after pump implantation, and increased degree of elastin fragmentation. Investigating the impact of scleraxis knockdown in this model could reveal whether targeting scleraxis could potentially reduce mortality and slow the progression of aneurysms, providing valuable insights into the molecular mechanisms of Marfan syndrome and potential therapeutic targets.

CHAPTER 8: REFERENCES

1. Tucker, W.D., Y. Arora, and K. Mahajan, *Anatomy, Blood Vessels*, in *StatPearls*. 2022: Treasure Island (FL).
2. Wolinsky, H. and S. Glagov, *Nature of species differences in the medial distribution of aortic vasa vasorum in mammals.* Circ Res, 1967. **20**(4): p. 409-21.
3. O'Rourke, M.F. and W.W. Nichols, *Aortic diameter, aortic stiffness, and wave reflection increase with age and isolated systolic hypertension.* Hypertension, 2005. **45**(4): p. 652-8.
4. Azuma, J., et al., *Assessment of elastase-induced murine abdominal aortic aneurysms: comparison of ultrasound imaging with in situ video microscopy.* J Biomed Biotechnol, 2011. **2011**: p. 252141.
5. van der Loop, F.T., et al., *Differentiation of smooth muscle cells in human blood vessels as defined by smoothelin, a novel marker for the contractile phenotype.* Arterioscler Thromb Vasc Biol, 1997. **17**(4): p. 665-71.
6. Steinman, J., et al., *3D morphological analysis of the mouse cerebral vasculature: Comparison of in vivo and ex vivo methods.* PLoS One, 2017. **12**(10): p. e0186676.
7. Wenceslau, C.F., et al., *Guidelines for the measurement of vascular function and structure in isolated arteries and veins.* Am J Physiol Heart Circ Physiol, 2021. **321**(1): p. H77-H111.
8. Martinez-Lemus, L.A., *The dynamic structure of arterioles.* Basic Clin Pharmacol Toxicol, 2012. **110**(1): p. 5-11.
9. Schiffrin, E.L., *Reactivity of small blood vessels in hypertension: relation with structural changes. State of the art lecture.* Hypertension, 1992. **19**(2 Suppl): p. II1-9.
10. Hill, L.K., J.J. Sollers Iii, and J.F. Thayer, *Resistance reconstructed estimation of total peripheral resistance from computationally derived cardiac output - biomed 2013.* Biomed Sci Instrum, 2013. **49**: p. 216-23.
11. Dobrin, P.B., *Mechanical properties of arteries.* Physiol Rev, 1978. **58**(2): p. 397-460.
12. Belz, G.G., *Elastic properties and Windkessel function of the human aorta.* Cardiovasc Drugs Ther, 1995. **9**(1): p. 73-83.
13. van Popele, N.M., et al., *Association between arterial stiffness and atherosclerosis: the Rotterdam Study.* Stroke, 2001. **32**(2): p. 454-60.
14. Safar, M.E., B.I. Levy, and H. Struijker-Boudier, *Current perspectives on arterial stiffness and pulse pressure in hypertension and cardiovascular diseases.* Circulation, 2003. **107**(22): p. 2864-9.
15. WOLINSKY, H. and S. GLAGOV, *STRUCTURAL BASIS FOR THE STATIC MECHANICAL PROPERTIES OF THE AORTIC MEDIA.* Circ Res, 1964. **14**: p. 400-13.
16. Davis, E.C., *Smooth muscle cell to elastic lamina connections in developing mouse aorta. Role in aortic medial organization.* Lab Invest, 1993. **68**(1): p. 89-99.
17. Intengan, H.D. and E.L. Schiffrin, *Structure and mechanical properties of resistance arteries in hypertension: role of adhesion molecules and extracellular matrix determinants.* Hypertension, 2000. **36**(3): p. 312-8.
18. Sun, Z., et al., *Extracellular matrix-specific focal adhesions in vascular smooth muscle produce mechanically active adhesion sites.* Am J Physiol Cell Physiol, 2008. **295**(1): p. C268-78.
19. Bell, J.S., et al., *Microstructure and mechanics of human resistance arteries.* Am J Physiol Heart Circ Physiol, 2016. **311**(6): p. H1560-H1568.
20. Clifford, P.S., et al., *Spatial distribution and mechanical function of elastin in resistance arteries: a role in bearing longitudinal stress.* Arterioscler Thromb Vasc Biol, 2011. **31**(12): p. 2889-96.
21. Schiffrin, E.L., *The endothelium of resistance arteries: physiology and role in hypertension.* Prostaglandins Leukot Essent Fatty Acids, 1996. **54**(1): p. 17-25.
22. Masi, S., et al., *The importance of endothelial dysfunction in resistance artery remodelling and cardiovascular risk.* Cardiovasc Res, 2020. **116**(2): p. 429-437.

23. Furchgott, R.F. and J.V. Zawadzki, *The obligatory role of endothelial cells in the relaxation of arterial smooth muscle by acetylcholine.* Nature, 1980. **288**(5789): p. 373-6.
24. Palmer, R.M., A.G. Ferrige, and S. Moncada, *Nitric oxide release accounts for the biological activity of endothelium-derived relaxing factor.* Nature, 1987. **327**(6122): p. 524-6.
25. Fitridge, R. and M. Thompson, *Mechanisms of Vascular Disease: A Reference Book for Vascular Specialists*. 2011.
26. Iyemere, V.P., et al., *Vascular smooth muscle cell phenotypic plasticity and the regulation of vascular calcification.* J Intern Med, 2006. **260**(3): p. 192-210.
27. Frismantiene, A., et al., *Smooth muscle cell-driven vascular diseases and molecular mechanisms of VSMC plasticity.* Cell Signal, 2018. **52**: p. 48-64.
28. Rensen, S.S., P.A. Doevendans, and G.J. van Eys, *Regulation and characteristics of vascular smooth muscle cell phenotypic diversity.* Neth Heart J, 2007. **15**(3): p. 100-8.
29. Winder, S.J. and M.P. Walsh, *Smooth muscle calponin. Inhibition of actomyosin MgATPase and regulation by phosphorylation.* J Biol Chem, 1990. **265**(17): p. 10148-55.
30. Je, H.D. and U.D. Sohn, *SM22alpha is required for agonist-induced regulation of contractility: evidence from SM22alpha knockout mice.* Mol Cells, 2007. **23**(2): p. 175-81.
31. Miano, J.M., et al., *Smooth muscle myosin heavy chain exclusively marks the smooth muscle lineage during mouse embryogenesis.* Circ Res, 1994. **75**(5): p. 803-12.
32. Kim, H.R., et al., *Cytoskeletal remodeling in differentiated vascular smooth muscle is actin isoform dependent and stimulus dependent.* Am J Physiol Cell Physiol, 2008. **295**(3): p. C768-78.
33. Campbell, G.R. and J.H. Campbell, *The phenotypes of smooth muscle expressed in human atheroma.* Ann N Y Acad Sci, 1990. **598**: p. 143-58.
34. Contard, F., et al., *Arterial smooth muscle cell phenotype in stroke-prone spontaneously hypertensive rats.* Hypertension, 1993. **22**(5): p. 665-76.
35. Sehgel, N.L., et al., *Increased vascular smooth muscle cell stiffness: a novel mechanism for aortic stiffness in hypertension.* Am J Physiol Heart Circ Physiol, 2013. **305**(9): p. H1281-7.
36. Kreye, V.A., et al., *Mode of action of sodium nitroprusside on vascular smooth muscle.* Naunyn Schmiedebergs Arch Pharmacol, 1975. **288**(4): p. 381-402.
37. *StatPearls*. 2022.
38. Rapoport, R.M., M.B. Draznin, and F. Murad, *Endothelium-dependent relaxation in rat aorta may be mediated through cyclic GMP-dependent protein phosphorylation.* Nature, 1983. **306**(5939): p. 174-6.
39. Heistad, D.D., et al., *Role of vasa vasorum in nourishment of the aortic wall.* Am J Physiol, 1981. **240**(5): p. H781-7.
40. Mulligan-Kehoe, M.J., *The vasa vasorum in diseased and nondiseased arteries.* Am J Physiol Heart Circ Physiol, 2010. **298**(2): p. H295-305.
41. Williams, J.K., M.L. Armstrong, and D.D. Heistad, *Blood flow through new microvessels: factors that affect regrowth of vasa vasorum.* Am J Physiol, 1988. **254**(1 Pt 2): p. H126-32.
42. Ohhira, A. and T. Ohhashi, *Effects of aortic pressure and vasoactive agents on the vascular resistance of the vasa vasorum in canine isolated thoracic aorta.* J Physiol, 1992. **453**: p. 233-45.
43. Scotland, R.S., P.J. Vallance, and A. Ahluwalia, *Endogenous factors involved in regulation of tone of arterial vasa vasorum: implications for conduit vessel physiology.* Cardiovasc Res, 2000. **46**(3): p. 403-11.
44. Nakata, Y. and S. Shionoya, *Vascular lesions due to obstruction of the vasa vasorum.* Nature, 1966. **212**(5067): p. 1258-9.
45. Barger, A.C., et al., *Hypothesis: vasa vasorum and neovascularization of human coronary arteries. A possible role in the pathophysiology of atherosclerosis.* N Engl J Med, 1984. **310**(3): p. 175-7.

46. Zhang, Y., et al., *Immunohistochemical study of intimal microvessels in coronary atherosclerosis.* Am J Pathol, 1993. **143**(1): p. 164-72.
47. Xu, J., X. Lu, and G.P. Shi, *Vasa vasorum in atherosclerosis and clinical significance.* Int J Mol Sci, 2015. **16**(5): p. 11574-608.
48. Secomb, T.W., *Hemodynamics.* Compr Physiol, 2016. **6**(2): p. 975-1003.
49. Eigenbrodt, M.L., et al., *Mathematical estimation of the potential effect of vascular remodelling/dilatation on B-mode ultrasound intima-medial thickness.* QJM, 2004. **97**(11): p. 729-37.
50. *StatPearls*. 2023.
51. Bots, M.L., et al., *Isolated systolic hypertension and vessel wall thickness of the carotid artery. The Rotterdam Elderly Study.* Arterioscler Thromb, 1993. **13**(1): p. 64-9.
52. Camasão, D.B. and D. Mantovani, *The mechanical characterization of blood vessels and their substitutes in the continuous quest for physiological-relevant performances. A critical review.* Mater Today Bio, 2021. **10**: p. 100106.
53. Jacobsen, J.C. and N.H. Holstein-Rathlou, *A life under pressure: circumferential stress in the microvascular wall.* Basic Clin Pharmacol Toxicol, 2012. **110**(1): p. 26-34.
54. Gimbrone, M.A., et al., *Special communicationthe critical role of mechanical forces in blood vessel development, physiology and pathology.* J Vasc Surg, 1999. **29**(6): p. 1104-51.
55. Cheng, G.C., et al., *Distribution of circumferential stress in ruptured and stable atherosclerotic lesions. A structural analysis with histopathological correlation.* Circulation, 1993. **87**(4): p. 1179-87.
56. Vorp, D.A., *Biomechanics of abdominal aortic aneurysm.* J Biomech, 2007. **40**(9): p. 1887-902.
57. Mishani, S., et al., *Stress distribution in the walls of major arteries: implications for atherogenesis.* Quant Imaging Med Surg, 2021. **11**(8): p. 3494-3505.
58. Paszkowiak, J.J. and A. Dardik, *Arterial wall shear stress: observations from the bench to the bedside.* Vasc Endovascular Surg, 2003. **37**(1): p. 47-57.
59. Lu, D. and G.S. Kassab, *Role of shear stress and stretch in vascular mechanobiology.* J R Soc Interface, 2011. **8**(63): p. 1379-85.
60. Cunningham, K.S. and A.I. Gotlieb, *The role of shear stress in the pathogenesis of atherosclerosis.* Lab Invest, 2005. **85**(1): p. 9-23.
61. Shadwick, R.E., *Mechanical design in arteries.* J Exp Biol, 1999. **202**(Pt 23): p. 3305-13.
62. Isnard, R.N., et al., *Pulsatile diameter and elastic modulus of the aortic arch in essential hypertension: a noninvasive study.* J Am Coll Cardiol, 1989. **13**(2): p. 399-405.
63. Lehmann, E.D., *Terminology for the definition of arterial elastic properties.* Pathol Biol (Paris), 1999. **47**(6): p. 656-64.
64. Silver, F.H., P.B. Snowhill, and D.J. Foran, *Mechanical behavior of vessel wall: a comparative study of aorta, vena cava, and carotid artery.* Ann Biomed Eng, 2003. **31**(7): p. 793-803.
65. Shirwany, N.A. and M.H. Zou, *Arterial stiffness: a brief review.* Acta Pharmacol Sin, 2010. **31**(10): p. 1267-76.
66. Lacolley, P., V. Regnault, and S. Laurent, *Mechanisms of Arterial Stiffening: From Mechanotransduction to Epigenetics.* Arterioscler Thromb Vasc Biol, 2020. **40**(5): p. 1055-1062.
67. Stehouwer, C.D., R.M. Henry, and I. Ferreira, *Arterial stiffness in diabetes and the metabolic syndrome: a pathway to cardiovascular disease.* Diabetologia, 2008. **51**(4): p. 527-39.
68. Ponticos, M. and B.D. Smith, *Extracellular matrix synthesis in vascular disease: hypertension, and atherosclerosis.* J Biomed Res, 2014. **28**(1): p. 25-39.
69. Whelton, P.K., et al., *2017 ACC/AHA/AAPA/ABC/ACPM/AGS/APhA/ASH/ASPC/NMA/PCNA Guideline for the Prevention, Detection, Evaluation, and Management of High Blood Pressure in*

Adults: A Report of the American College of Cardiology/American Heart Association Task Force on Clinical Practice Guidelines. Hypertension, 2018. **71**(6): p. e13-e115.
70. Townsend, R.R., et al., *Recommendations for Improving and Standardizing Vascular Research on Arterial Stiffness: A Scientific Statement From the American Heart Association.* Hypertension, 2015. **66**(3): p. 698-722.
71. Vlachopoulos, C., et al., *The role of vascular biomarkers for primary and secondary prevention. A position paper from the European Society of Cardiology Working Group on peripheral circulation: Endorsed by the Association for Research into Arterial Structure and Physiology (ARTERY) Society.* Atherosclerosis, 2015. **241**(2): p. 507-32.
72. Laurent, S., *Aortic, carotid and femoral stiffness: how do they relate? Towards reference values.* J Hypertens, 2008. **26**(7): p. 1305-6.
73. Chirinos, J.A., *Arterial stiffness: basic concepts and measurement techniques.* J Cardiovasc Transl Res, 2012. **5**(3): p. 243-55.
74. Sun, J., et al., *Isometric Contractility Measurement of the Mouse Mesenteric Artery Using Wire Myography.* J Vis Exp, 2018(138).
75. del Campo, L. and M. Ferrer, *Wire Myography to Study Vascular Tone and Vascular Structure of Isolated Mouse Arteries.* Methods Mol Biol, 2015. **1339**: p. 255-76.
76. Shahid, M. and E.S. Buys, *Assessing murine resistance artery function using pressure myography.* J Vis Exp, 2013(76).
77. Falloon, B.J., et al., *Comparison of small artery sensitivity and morphology in pressurized and wire-mounted preparations.* Am J Physiol, 1995. **268**(2 Pt 2): p. H670-8.
78. Dunn, W.R., G.C. Wellman, and J.A. Bevan, *Enhanced resistance artery sensitivity to agonists under isobaric compared with isometric conditions.* Am J Physiol, 1994. **266**(1 Pt 2): p. H147-55.
79. Rabi, D.M., et al., *Hypertension Canada's 2020 Comprehensive Guidelines for the Prevention, Diagnosis, Risk Assessment, and Treatment of Hypertension in Adults and Children.* Can J Cardiol, 2020. **36**(5): p. 596-624.
80. (NCD-RisC), N.R.F.C., *Worldwide trends in blood pressure from 1975 to 2015: a pooled analysis of 1479 population-based measurement studies with 19·1 million participants.* Lancet, 2017. **389**(10064): p. 37-55.
81. Padwal, R.S., et al., *Epidemiology of Hypertension in Canada: An Update.* Can J Cardiol, 2016. **32**(5): p. 687-94.
82. Carretero, O.A. and S. Oparil, *Essential hypertension. Part I: definition and etiology.* Circulation, 2000. **101**(3): p. 329-35.
83. Sever, P.S. and N.R. Poulter, *A hypothesis for the pathogenesis of essential hypertension: the initiating factors.* J Hypertens Suppl, 1989. **7**(1): p. S9-12.
84. Laghlam, D., M. Jozwiak, and L.S. Nguyen, *Renin-Angiotensin-Aldosterone System and Immunomodulation: A State-of-the-Art Review.* Cells, 2021. **10**(7).
85. Bernstein, K.E., et al., *Angiotensin-converting enzyme in innate and adaptive immunity.* Nat Rev Nephrol, 2018. **14**(5): p. 325-336.
86. Harrison-Bernard, L.M., *The renal renin-angiotensin system.* Adv Physiol Educ, 2009. **33**(4): p. 270-4.
87. Chiong, M., et al., *Mitochondrial metabolism and the control of vascular smooth muscle cell proliferation.* Front Cell Dev Biol, 2014. **2**: p. 72.
88. Ruiz-Ortega, M., et al., *Molecular mechanisms of angiotensin II-induced vascular injury.* Curr Hypertens Rep, 2003. **5**(1): p. 73-9.
89. Kaufman, M.B., *Pharmaceutical Approval Update.* P T, 2018. **43**(3): p. 141-170.
90. Paquet, J.L., et al., *Angiotensin II-induced proliferation of aortic myocytes in spontaneously hypertensive rats.* J Hypertens, 1990. **8**(6): p. 565-72.

91. Geisterfer, A.A., M.J. Peach, and G.K. Owens, *Angiotensin II induces hypertrophy, not hyperplasia, of cultured rat aortic smooth muscle cells.* Circ Res, 1988. **62**(4): p. 749-56.
92. Touyz, R.M. and E.L. Schiffrin, *Signal transduction mechanisms mediating the physiological and pathophysiological actions of angiotensin II in vascular smooth muscle cells.* Pharmacol Rev, 2000. **52**(4): p. 639-72.
93. Ushio-Fukai, M., et al., *p38 Mitogen-activated protein kinase is a critical component of the redox-sensitive signaling pathways activated by angiotensin II. Role in vascular smooth muscle cell hypertrophy.* J Biol Chem, 1998. **273**(24): p. 15022-9.
94. Itoh, H., et al., *Multiple autocrine growth factors modulate vascular smooth muscle cell growth response to angiotensin II.* J Clin Invest, 1993. **91**(5): p. 2268-74.
95. Saward, L. and P. Zahradka, *Angiotensin II activates phosphatidylinositol 3-kinase in vascular smooth muscle cells.* Circ Res, 1997. **81**(2): p. 249-57.
96. Ushio-Fukai, M., et al., *Reactive oxygen species mediate the activation of Akt/protein kinase B by angiotensin II in vascular smooth muscle cells.* J Biol Chem, 1999. **274**(32): p. 22699-704.
97. Dasgupta, C. and L. Zhang, *Angiotensin II receptors and drug discovery in cardiovascular disease.* Drug Discov Today, 2011. **16**(1-2): p. 22-34.
98. Pueyo, M.E., N. N'Diaye, and J.B. Michel, *Angiotensin II-elicited signal transduction via AT1 receptors in endothelial cells.* Br J Pharmacol, 1996. **118**(1): p. 79-84.
99. Schena, M., et al., *Vasoactive hormones induce nitric oxide synthase mRNA expression and nitric oxide production in human endothelial cells and monocytes.* Am J Hypertens, 1999. **12**(4 Pt 1): p. 388-97.
100. Kaschina, E., P. Namsolleck, and T. Unger, *AT2 receptors in cardiovascular and renal diseases.* Pharmacol Res, 2017. **125**(Pt A): p. 39-47.
101. Yang, Z., et al., *Angiotensin II type 2 receptor overexpression preserves left ventricular function after myocardial infarction.* Circulation, 2002. **106**(1): p. 106-11.
102. Oishi, Y., et al., *Cardioprotective role of AT2 receptor in postinfarction left ventricular remodeling.* Hypertension, 2003. **41**(3 Pt 2): p. 814-8.
103. Adachi, Y., et al., *Angiotensin II type 2 receptor deficiency exacerbates heart failure and reduces survival after acute myocardial infarction in mice.* Circulation, 2003. **107**(19): p. 2406-8.
104. Katada, J. and M. Majima, *AT(2) receptor-dependent vasodilation is mediated by activation of vascular kinin generation under flow conditions.* Br J Pharmacol, 2002. **136**(4): p. 484-91.
105. Tsutsumi, Y., et al., *Angiotensin II type 2 receptor overexpression activates the vascular kinin system and causes vasodilation.* J Clin Invest, 1999. **104**(7): p. 925-35.
106. Emathinger, J.M., J.W. Nelson, and S.B. Gurley, *Advances in use of mouse models to study the renin-angiotensin system.* Mol Cell Endocrinol, 2021. **529**: p. 111255.
107. Kim, H.S., et al., *Genetic control of blood pressure and the angiotensinogen locus.* Proc Natl Acad Sci U S A, 1995. **92**(7): p. 2735-9.
108. Tanimoto, K., et al., *Angiotensinogen-deficient mice with hypotension.* J Biol Chem, 1994. **269**(50): p. 31334-7.
109. Caron, K.M., et al., *A genetically clamped renin transgene for the induction of hypertension.* Proc Natl Acad Sci U S A, 2002. **99**(12): p. 8248-52.
110. Sharp, M.G., et al., *Targeted inactivation of the Ren-2 gene in mice.* Hypertension, 1996. **28**(6): p. 1126-31.
111. Paradis, P., et al., *Overexpression of angiotensin II type I receptor in cardiomyocytes induces cardiac hypertrophy and remodeling.* Proc Natl Acad Sci U S A, 2000. **97**(2): p. 931-6.
112. Ito, M., et al., *Regulation of blood pressure by the type 1A angiotensin II receptor gene.* Proc Natl Acad Sci U S A, 1995. **92**(8): p. 3521-5.

113. Krege, J.H., et al., *Angiotensin-converting enzyme gene mutations, blood pressures, and cardiovascular homeostasis.* Hypertension, 1997. **29**(1 Pt 2): p. 150-7.
114. Esther, C.R., et al., *Mice lacking angiotensin-converting enzyme have low blood pressure, renal pathology, and reduced male fertility.* Lab Invest, 1996. **74**(5): p. 953-65.
115. Mulvany, M.J., et al., *Vascular remodeling.* Hypertension, 1996. **28**(3): p. 505-6.
116. Korsgaard, N., et al., *Histology of subcutaneous small arteries from patients with essential hypertension.* Hypertension, 1993. **22**(4): p. 523-6.
117. Deng, L.Y. and E.L. Schiffrin, *Effects of endothelin-1 and vasopressin on resistance arteries of spontaneously hypertensive rats.* Am J Hypertens, 1992. **5**(11): p. 817-22.
118. Rizzoni, D., et al., *Vascular hypertrophy and remodeling in secondary hypertension.* Hypertension, 1996. **28**(5): p. 785-90.
119. Deng, L.Y. and E.L. Schiffrin, *Effects of endothelin on resistance arteries of DOCA-salt hypertensive rats.* Am J Physiol, 1992. **262**(6 Pt 2): p. H1782-7.
120. Roman, M.J., et al., *Parallel cardiac and vascular adaptation in hypertension.* Circulation, 1992. **86**(6): p. 1909-18.
121. Laurent, S. and P. Boutouyrie, *The structural factor of hypertension: large and small artery alterations.* Circ Res, 2015. **116**(6): p. 1007-21.
122. Bache, R.J., *Vasodilator reserve: a functional assessment of coronary health.* Circulation, 1998. **98**(13): p. 1257-60.
123. Izzard, A.S., et al., *Small artery structure and hypertension: adaptive changes and target organ damage.* J Hypertens, 2005. **23**(2): p. 247-50.
124. FOLKOW, B., G. GRIMBY, and O. THULESIUS, *Adaptive structural changes of the vascular walls in hypertension and their relation to the control of the peripheral resistance.* Acta Physiol Scand, 1958. **44**(3-4): p. 255-72.
125. Aalkjaer, C., et al., *Evidence for increased media thickness, increased neuronal amine uptake, and depressed excitation--contraction coupling in isolated resistance vessels from essential hypertensives.* Circ Res, 1987. **61**(2): p. 181-6.
126. Sugiyama, T., et al., *The elevation of the cytoplasmic calcium ions in vascular smooth muscle cells in SHR--measurement of the free calcium ions in single living cells by lasermicrofluorospectrometry.* Biochem Biophys Res Commun, 1986. **141**(1): p. 340-5.
127. Crews, J.K., J.G. Murphy, and R.A. Khalil, *Gender differences in Ca(2+) entry mechanisms of vasoconstriction in Wistar-Kyoto and spontaneously hypertensive rats.* Hypertension, 1999. **34**(4 Pt 2): p. 931-6.
128. Neves, M.F., et al., *Vascular dysfunction as target organ damage in animal models of hypertension.* Int J Hypertens, 2012. **2012**: p. 187526.
129. Park, J.B. and E.L. Schiffrin, *Small artery remodeling is the most prevalent (earliest?) form of target organ damage in mild essential hypertension.* J Hypertens, 2001. **19**(5): p. 921-30.
130. Panza, J.A., *Endothelial dysfunction in essential hypertension.* Clin Cardiol, 1997. **20**(11 Suppl 2): p. II-26-33.
131. Endemann, D.H. and E.L. Schiffrin, *Endothelial dysfunction.* J Am Soc Nephrol, 2004. **15**(8): p. 1983-92.
132. Laurent, S. and P. Boutouyrie, *Arterial Stiffness and Hypertension in the Elderly.* Front Cardiovasc Med, 2020. **7**: p. 544302.
133. Dao, H.H., et al., *Evolution and modulation of age-related medial elastocalcinosis: impact on large artery stiffness and isolated systolic hypertension.* Cardiovasc Res, 2005. **66**(2): p. 307-17.
134. Wallace, S.M., et al., *Isolated systolic hypertension is characterized by increased aortic stiffness and endothelial dysfunction.* Hypertension, 2007. **50**(1): p. 228-33.

135. Franklin, S.S., et al., *Hemodynamic patterns of age-related changes in blood pressure. The Framingham Heart Study.* Circulation, 1997. **96**(1): p. 308-15.
136. Lerman, L.O., et al., *Animal Models of Hypertension: A Scientific Statement From the American Heart Association.* Hypertension, 2019. **73**(6): p. e87-e120.
137. Basting, T. and E. Lazartigues, *DOCA-Salt Hypertension: an Update.* Curr Hypertens Rep, 2017. **19**(4): p. 32.
138. Sawamura, T. and T. Nakada, *Role of dopamine in the striatum, renin-angiotensin system and renal sympathetic nerve on the development of two-kidney, one-clip Goldblatt hypertension.* J Urol, 1996. **155**(3): p. 1108-11.
139. Cserjesi, P., et al., *Scleraxis: a basic helix-loop-helix protein that prefigures skeletal formation during mouse embryogenesis.* Development, 1995. **121**(4): p. 1099-110.
140. Kadesch, T., *Consequences of heteromeric interactions among helix-loop-helix proteins.* Cell Growth Differ, 1993. **4**(1): p. 49-55.
141. Wilson-Rawls, J., J.M. Rhee, and A. Rawls, *Paraxis is a basic helix-loop-helix protein that positively regulates transcription through binding to specific E-box elements.* J Biol Chem, 2004. **279**(36): p. 37685-92.
142. Bagchi, R.A., et al., *The transcription factor scleraxis is a critical regulator of cardiac fibroblast phenotype.* BMC Biol, 2016. **14**: p. 21.
143. Nagalingam, R.S., et al., *Regulation of cardiac fibroblast MMP2 gene expression by scleraxis.* J Mol Cell Cardiol, 2018. **120**: p. 64-73.
144. Bagchi, R.A., et al., *Regulation of fibronectin gene expression in cardiac fibroblasts by scleraxis.* Cell Tissue Res, 2016. **366**(2): p. 381-391.
145. Espira, L., et al., *The basic helix-loop-helix transcription factor scleraxis regulates fibroblast collagen synthesis.* J Mol Cell Cardiol, 2009. **47**(2): p. 188-95.
146. Al-Hattab, D.S., et al., *Scleraxis regulates Twist1 and Snai1 expression in the epithelial-to-mesenchymal transition.* Am J Physiol Heart Circ Physiol, 2018. **315**(3): p. H658-H668.
147. Tran, D.D., et al., *Temporal and spatial cooperation of Snail1 and Twist1 during epithelial-mesenchymal transition predicts for human breast cancer recurrence.* Mol Cancer Res, 2011. **9**(12): p. 1644-57.
148. Leptin, M., *twist and snail as positive and negative regulators during Drosophila mesoderm development.* Genes Dev, 1991. **5**(9): p. 1568-76.
149. Schweitzer, R., et al., *Analysis of the tendon cell fate using Scleraxis, a specific marker for tendons and ligaments.* Development, 2001. **128**(19): p. 3855-66.
150. Liu, H., et al., *The Scleraxis Transcription Factor Directly Regulates Multiple Distinct Molecular and Cellular Processes During Early Tendon Cell Differentiation.* Front Cell Dev Biol, 2021. **9**: p. 654397.
151. Murchison, N.D., et al., *Regulation of tendon differentiation by scleraxis distinguishes force-transmitting tendons from muscle-anchoring tendons.* Development, 2007. **134**(14): p. 2697-708.
152. Abe, H., et al., *Scleraxis modulates bone morphogenetic protein 4 (BMP4)-Smad1 protein-smooth muscle α-actin (SMA) signal transduction in diabetic nephropathy.* J Biol Chem, 2012. **287**(24): p. 20430-42.
153. Roche, P.L., et al., *Role of scleraxis in mechanical stretch-mediated regulation of cardiac myofibroblast phenotype.* Am J Physiol Cell Physiol, 2016. **311**(2): p. C297-307.
154. Scott, A., et al., *Mechanical force modulates scleraxis expression in bioartificial tendons.* J Musculoskelet Neuronal Interact, 2011. **11**(2): p. 124-32.
155. Muhl, L., et al., *A single-cell transcriptomic inventory of murine smooth muscle cells.* Dev Cell, 2022. **57**(20): p. 2426-2443.e6.

156. Chen, K., X. Zhou, and Z. Sun, *Haplodeficiency of Klotho Gene Causes Arterial Stiffening via Upregulation of Scleraxis Expression and Induction of Autophagy.* Hypertension, 2015. **66**(5): p. 1006-13.
157. Bagchi, R.A. and M.P. Czubryt, *Synergistic roles of scleraxis and Smads in the regulation of collagen 1α2 gene expression.* Biochim Biophys Acta, 2012. **1823**(10): p. 1936-44.
158. Verhagen, J.M.A., et al., *Multi-Omics Profiling in Marfan Syndrome: Further Insights into the Molecular Mechanisms Involved in Aortic Disease.* Int J Mol Sci, 2021. **23**(1).
159. Garvin, A.M., et al., *RAS inhibition in resident fibroblast biology.* Cell Signal, 2021. **80**: p. 109903.
160. Wang, W., et al., *Essential role of Smad3 in angiotensin II-induced vascular fibrosis.* Circ Res, 2006. **98**(8): p. 1032-9.
161. Lim, D.S., et al., *Angiotensin II blockade reverses myocardial fibrosis in a transgenic mouse model of human hypertrophic cardiomyopathy.* Circulation, 2001. **103**(6): p. 789-91.
162. Zhu, A., et al., *Scleraxis as a prognostic marker of myocardial fibrosis in hypertrophic cardiomyopathy (SPARC) study.* Can J Physiol Pharmacol, 2020. **98**(7): p. 459-465.
163. Brown, D., et al., *Dual role of the basic helix-loop-helix transcription factor scleraxis in mesoderm formation and chondrogenesis during mouse embryogenesis.* Development, 1999. **126**(19): p. 4317-29.
164. Czubryt, M.P., *A tale of 2 tissues: the overlapping role of scleraxis in tendons and the heart.* Can J Physiol Pharmacol, 2014. **92**(9): p. 707-12.
165. Levay, A.K., et al., *Scleraxis is required for cell lineage differentiation and extracellular matrix remodeling during murine heart valve formation in vivo.* Circ Res, 2008. **103**(9): p. 948-56.
166. *StatPearls*. 2024.
167. Ammash, N.M., T.M. Sundt, and H.M. Connolly, *Marfan syndrome-diagnosis and management.* Curr Probl Cardiol, 2008. **33**(1): p. 7-39.
168. Yuan, S.M., et al., *Transforming growth factor-β signaling pathway in Marfan's syndrome: a preliminary histopathological study.* Vasa, 2011. **40**(5): p. 369-74.
169. Xiong, W., et al., *MMP-2 regulates Erk1/2 phosphorylation and aortic dilatation in Marfan syndrome.* Circ Res, 2012. **110**(12): p. e92-e101.
170. Hoffjan, S., *Genetic dissection of marfan syndrome and related connective tissue disorders: an update 2012.* Mol Syndromol, 2012. **3**(2): p. 47-58.
171. Lazea, C., et al., *Cardiovascular manifestations in Marfan syndrome.* Med Pharm Rep, 2021. **94**(Suppl No 1): p. S25-S27.
172. Zeigler, S.M., B. Sloan, and J.A. Jones, *Pathophysiology and Pathogenesis of Marfan Syndrome.* Adv Exp Med Biol, 2021. **1348**: p. 185-206.
173. Weyman, A.E. and M. Scherrer-Crosbie, *Marfan syndrome and mitral valve prolapse.* J Clin Invest, 2004. **114**(11): p. 1543-6.
174. Barnette, D.N., et al., *Tgfβ-Smad and MAPK signaling mediate scleraxis and proteoglycan expression in heart valves.* J Mol Cell Cardiol, 2013. **65**: p. 137-46.
175. Barnette, D.N., et al., *RNA-seq analysis to identify novel roles of scleraxis during embryonic mouse heart valve remodeling.* PLoS One, 2014. **9**(7): p. e101425.
176. Benke, K., et al., *The role of transforming growth factor-beta in Marfan syndrome.* Cardiol J, 2013. **20**(3): p. 227-34.
177. Acharya, A., et al., *Efficient inducible Cre-mediated recombination in Tcf21 cell lineages in the heart and kidney.* Genesis, 2011. **49**(11): p. 870-7.
178. Wirth, A., et al., *G12-G13-LARG-mediated signaling in vascular smooth muscle is required for salt-induced hypertension.* Nat Med, 2008. **14**(1): p. 64-8.
179. Jadeja, R.N., et al., *Assessing Myogenic Response and Vasoactivity In Resistance Mesenteric Arteries Using Pressure Myography.* J Vis Exp, 2015(101): p. e50997.

180. Acharya, A., et al., *The bHLH transcription factor Tcf21 is required for lineage-specific EMT of cardiac fibroblast progenitors.* Development, 2012. **139**(12): p. 2139-49.
181. Nagalingam, R.S., et al., *Scleraxis and fibrosis in the pressure-overloaded heart.* Eur Heart J, 2022. **43**(45): p. 4739-4750.
182. Selamet Tierney, E.S., et al., *Influence of Aortic Stiffness on Aortic-Root Growth Rate and Outcome in Patients With the Marfan Syndrome.* Am J Cardiol, 2018. **121**(9): p. 1094-1101.
183. Syyong, H.T., et al., *Dysfunction of endothelial and smooth muscle cells in small arteries of a mouse model of Marfan syndrome.* Br J Pharmacol, 2009. **158**(6): p. 1597-608.
184. Zhang, J., et al., *Smooth muscle cell phenotypic diversity between dissected and unaffected thoracic aortic media.* J Cardiovasc Surg (Torino), 2013. **54**(4): p. 511-21.
185. Clarke, M.C., et al., *Chronic apoptosis of vascular smooth muscle cells accelerates atherosclerosis and promotes calcification and medial degeneration.* Circ Res, 2008. **102**(12): p. 1529-38.
186. Tham, D.M., et al., *Angiotensin II injures the arterial wall causing increased aortic stiffening in apolipoprotein E-deficient mice.* Am J Physiol Regul Integr Comp Physiol, 2002. **283**(6): p. R1442-9.
187. Wang, H.D., et al., *Role of NADPH oxidase in the vascular hypertrophic and oxidative stress response to angiotensin II in mice.* Circ Res, 2001. **88**(9): p. 947-53.
188. Lu, H., et al., *Subcutaneous Angiotensin II Infusion using Osmotic Pumps Induces Aortic Aneurysms in Mice.* J Vis Exp, 2015(103).
189. Branchetti, E., et al., *Oxidative stress modulates vascular smooth muscle cell phenotype via CTGF in thoracic aortic aneurysm.* Cardiovasc Res, 2013. **100**(2): p. 316-24.
190. Leone, O., et al., *The complex interplay among atherosclerosis, inflammation, and degeneration in ascending thoracic aortic aneurysms.* J Thorac Cardiovasc Surg, 2020. **160**(6): p. 1434-1443.e6.
191. Qiu, H., et al., *Short communication: vascular smooth muscle cell stiffness as a mechanism for increased aortic stiffness with aging.* Circ Res, 2010. **107**(5): p. 615-9.
192. Ye, G.J., A.P. Nesmith, and K.K. Parker, *The role of mechanotransduction on vascular smooth muscle myocytes' [corrected] cytoskeleton and contractile function.* Anat Rec (Hoboken), 2014. **297**(9): p. 1758-69.
193. Montenegro, M.F., et al., *Assessment of vascular effects of tamoxifen and its metabolites on the rat perfused hindquarter vascular bed.* Basic Clin Pharmacol Toxicol, 2009. **104**(5): p. 400-7.
194. Brash, J.T., et al., *Tamoxifen-Activated CreERT Impairs Retinal Angiogenesis Independently of Gene Deletion.* Circ Res, 2020. **127**(6): p. 849-850.
195. Álvarez-Aznar, A., et al., *Tamoxifen-independent recombination of reporter genes limits lineage tracing and mosaic analysis using CreER.* Transgenic Res, 2020. **29**(1): p. 53-68.
196. Figtree, G.A., C.M. Webb, and P. Collins, *Tamoxifen acutely relaxes coronary arteries by an endothelium-, nitric oxide-, and estrogen receptor-dependent mechanism.* J Pharmacol Exp Ther, 2000. **295**(2): p. 519-23.
197. Itoh, T., et al., *Angiotensin II-induced modulation of endothelium-dependent relaxation in rabbit mesenteric resistance arteries.* J Physiol, 2003. **548**(Pt 3): p. 893-906.
198. Sehgel, N.L., et al., *Augmented vascular smooth muscle cell stiffness and adhesion when hypertension is superimposed on aging.* Hypertension, 2015. **65**(2): p. 370-7.
199. Bennett, M.R., S. Sinha, and G.K. Owens, *Vascular Smooth Muscle Cells in Atherosclerosis.* Circ Res, 2016. **118**(4): p. 692-702.
200. Marx, S.O., H. Totary-Jain, and A.R. Marks, *Vascular smooth muscle cell proliferation in restenosis.* Circ Cardiovasc Interv, 2011. **4**(1): p. 104-11.
201. Cavanaugh, N.B., et al., *A Novel Murine Model of Marfan Syndrome Accelerates Aortopathy and Cardiomyopathy.* Ann Thorac Surg, 2017. **104**(2): p. 657-665.